Norwegian University of Life Sciences

Master's Thesis 2018 30 ECTS

Faculty of Science and Technology
Petter Heyerdahl

An Independent Solar Energy Community in Longyearbyen by use of Borehole Thermal Energy Storage in Permafrost - A feasibility study.

Morten Hustad Kleven
Industrial Economics
Faculty of Science and Technology

Preface

First I would like to thank my supervisor Petter Heyerdahl for presenting me with a fascinating task, he has been outstanding in presenting valuable ideas and engaged himself in the project. In addition, he has been both positive and supportive during the up and downs through this six months of work. I would also like to thank outsiders contributing with valuble information, a special thanks to Kjell Ivar Kasin which has sacrificed time on his travels in Asia to provide me with the best possible information about Microwave Assisted Pyrolisys.

I would like to thank my family and friends who have sacrificed time for proofreading the thesis, as well as helped in calculations of heat losses.

Abstract

This thesis proposes an assemblage of comprehensive recommendations to the Longyearbyen community council with regard to the avalanche and energy challenges they face today.

Foremost, we suggest an 30000m^2 heated hall which can contain an all year heated indoor society at Svalbard. This recommendation is derived via our calculations, which prove that clean solar thermal energy and microwave assisted pyrolysis (MAP) in combination with Borehole Thermal Energy Storage (BTES) makes it possible to maintain a 17°C constant temperature all year around. A construction of living areas within the heated indoor society would vacate the avalanche prone settlements.

However, to secure the electrical demand of the 30000m^2 heated hall remains a challenge. The biggest and most reliable contributor of electrical energy production is MAP of waste materials. Photovoltaic cells (PV cells), bioreactors and wind energy in combination with hydrogen production and storage have been examined to some extent to calculate a secure electrical energy supply to the hall.

Wind energy is necessary to secure the hall electrical demands. Wind, however could turn out to be a sub-optimal solution due to high installation cost. PV cells and bioreactors are too inefficient to be able to supply the necessary electrical demand through the Polar Night. However, a more detailed analysis of the waste composition may prove a higher production yield for the MAP (cf. table 6).

Currently, a heat demand of 2.5GWh is requested from the BTES by the 30000m^2 hall. The heat delivered by solar collectors and MAP to the BTES equals approximately 8GWh, which creates a 2.9GWh surplus of heat assuming an 80% BTES efficiency. Electricity consumption, on the other hand, is very uncertain and sums up to 3.1 GWh. The values of electricity consumption were retrieved from the Norwgian Standard, NS3031, and vary depending on the use of the building. Without wind

power generation the expected shortage of electrical supply sums up to 0.8GWh. Wind power looks promising at Svalbard with a production yield of 42%.

Based on our analysis, a closer examination of the heated hall electrical demand must be completed when the intended use is decided. This also applies to the heat loss calculations after the architects change layouts and the use of the construction material is decided. However, a heat surplus of 2.9GWh is a pleasant result to conclude that the heated hall can maintain 17℃ all year.

Sammendrag

Denne oppgaven foreslår en samling av omfattende anbefalinger til Longyearbyen lokalstyre med hensyn til de utfordringene lokalstyret møter ved skredfare og energiomlegging.

Vi foreslår en oppvarmet hall på 30000m2 som kan fasilitere et oppvarmet innendørs miljø på Svalbard. Denne anbefalingen er utledet gjennom våre beregninger, som viser at ren solvarmeenergi og mikrobølgeassistert pyrolyse (MAP) i kombinasjon med termisk borrehullslagring (BTES) gjør det mulig å opprettholde en konstant temperatur på 17 ℃ året rundt. En konstruksjon av boareal i det oppvarmede innemiljøet vil føre til en fraflytning av skredutsatte hjem.

En løsning på den elektriske etterspørselen til den 30000m2 oppvarmede hallen er fortsatt en utfordring. Den største og mest pålitelige bidragsyteren til elektrisk kraftproduksjon er MAP av avfallsmaterialer. Fotovoltaiske celler (PV-celler), bioreaktorer og vindenergi i kombinasjon med hydrogenproduksjon og -lagring har til en viss grad blitt undersøkt for å beregne en sikker elektrisk energiforsyning til hallen.

For å sikre den nødvendige elektriske forsyningen til hallen må vindkraftproduksjon medregnes. Vindkraft for å støtte samfunnsbehovet kan være en suboptimal løsning på grunn av ukjente høye installasjonskostnader. PV-celler og bioreaktorer er for ineffektive for å kunne levere den nødvendige elektriske etterspørselen gjennom Polar Night. En mer detaljert analyse av avfallssammensetningen kan imidlertid vise et høyere produksjonsutbytte for MAP (jf tabell 6).

Hallen har et netto varmebehov på 2,5 GWh fra BTES. Varmen som leveres av solfangere og MAP til BTES er omtrent 8GWh, noe som skaper et 2,9GWh overskudd av varme med en 80% BTES effektivitet. Det elektriske forbruk er derimot svært usikkert men er kalkulert til 3,1 GWh. Verdiene for strømforbruk ble hentet fra Norsk Standard, NS3031, og varierer avhengig av bruken av hallen. Uten vindkraftproduksjon oppstår forventet mangel på strømforsyning opp til 0,8 GWh. Vindkraft ser lovende ut på Svalbard med et produksjonsutbytte på 42%.

Basert på analysen, må en nærmere undersøkelse av den oppvarmede hallenes elektriske etterspørsel fylles ut når den tilsiktede bruken avgjøres. Dette gjelder også varmetabsberegningene etter at arkitektene har endret layout og bestemt byggematerialet. Imidlertid er et varmeoverskudd på 2,9

GWh et romslig resultat for å konkludere med at den oppvarmede hallen kan opprettholde 17 °C hele året.

Symbol list

Symbol	Explanation	Unit
P_{cd}	Conductive power	W
k	Conductivity	W/mK
A_s	Area of surface	m^2
T	Temperature	K
x	Distance	m
P_{conv}	Convective Power	W
h	Convective heat transfer coefficient	W/m^2K
T_s	Temperature surface	K
T_m	Temperature medium	K
ε	Emissivity	-
σ	Stefan-Boltzmann constant	$5.67x10^{-8}$ W/m^2K^4
P_E	Power on earth atmosphere	W
H_0	Solar radiation Intensity	W/m^2
R_{SE}	Distance from centre of sun to centre of earth	$1.5x10^8$ ±1.7% km
H_p	Planck constant	$6.415x10^{-34}$ W
c	Speed of light in vacuum	$2.998x10^8$ m/s
λ	Wavelength	m
k_b	Boltzman constant	$1.38x10^{-23}$ J/K
R_{sun}	Radius of the sun	$695\ 508x10^3$ m
D	Distance	m
AM	Air mass	-
θ	Angle form zenith angle	-
δ	Tilt angle of the earth	-
α	Elevation angle of the sun	-
φ	Latitude degree	-
d	days	-

P_u	Power output of solar collector	W
A_{sc}	Area of solar collector	m^2
q_u	Power absorbed per unit area and delivered to medium	W/m^2
η	Solar collector efficiency	-
G	Power irradiance from sun	W/m^2
η_{rp}	Efficiency of solar collector absorption plate	-
η_{pm}	Efficiency of heat transfer from collector plate to medium	-
τ_{cov}	Transmittance coefficient of plate cover	-
α_p	Absorption coefficient of collector	-
U_L	U-value of the plate collector	W/m^2K
T_p	Average temperature of collector	K
T_a	Ambient temperature	K
η_o	Optical efficiency	-
a_1	linear heat loss coefficient	W/m^2K
a_2	quadratic heat loss coefficient	W/m^2K
I_D	Irradiation intensity on the earth surface	W/m^2
h	Hight above ground	km
P_{sc}	Power incident on solar collector	W
β	Tilt angle of solar collector	-
u	Wind speed	m/s
E_{kw}	Kinetic energy of wind	J
C_{tp}	Maximum theoretical power coefficient for wind turbine	59.3%
ρ	Density	kg/m^3
A_w	Turbine sweeping area	m^2
v_2	Wind speed at height 2	m/s
v_1	Wind speed at height 1	m/s
h_2	Height 2	m
h_1	Height 1	m
z_0	Ground roughness factor	m
η	Boiler efficiency	-
H_b	Heat of combustion per unit volume biogas	J/m^3
V_b	Volume of biogas	m^3
H_m	Heat of combustion methane	J/m^3
f_m	Fraction of methane	-
c	Biogas yield per unit dry mass	m^3/kg

m_o	Dry mass	kg
V_f	Volume of digester fluid	m^3
ρ_m	Density of dry mass	kg/m^3
V_d	Total volume of digester	m^3
t	Retention time of organic matter in digester	day
H	Total power of heat loss per K	W/K
H_D	Transmission loss through buildings wall and roof	W/K
H_U	Heat loss to unheated building parts	W/K
H_G	Heat loss to the ground	W/K
H_V	Heat loss through the ventilation	W/K
H_{inf}	Heat loss through infiltration	W/K
U_i	U-value of element i	W/m^2K
A_i	Area of element i	m^2
ψ_k	Thermal bridge value of element k	W/mK
l_k	Length of element k	m
χ	Specifick thermal bridge values	W/K
$\dot{V}$	Average ventilated air supply	m^3/h
η_T	Temperature of heat recovery unit	-
V	Total heated volume	m^3
n_{inf}	Air substitution factor infiltration	h^{-1}
n_{50}	Air substitution factor 50Pa	h^{-1}
e	terrain coefficient	-
f	terrain coefficient	-
V_1	Supplied air	m^3/h
V_2	Extracted air	m^3/h
Q_t	Transmission heat loss	Wh
G	Degree day figure	Kd
Q_{HS}	Heat supplements	Wh
Q_{sun}	Heat supplied by sun through windows	Wh
Q_{int}	Heat supplied by internal sources	Wh
q_{light}	heat supplied by electrical lights	W/m^2
q_{equ}	heat supplied by various equipment	W/m^2
q_{per}	Heat supplied by persons	W/m^2
q_{fan}	Heat supplied by ventilation fans	W/m^2
A_{fl}	Area floor	m^2

$\Delta\theta_1$	Temperature increase over fan one	K
$\Delta\theta_2$	Temperature increase over fan two	K
$\Delta\theta_3$	Temperature increase over fan three	K
E_{fan}	Electrical energy demand ventilation unit	kWh
SFP	Specific fan power	KW/m^3sec
t	time	hour
E_p	Electrical energy demand pump	kWh
SPP	Specific pump power	kW/l/sec
t_{dr}	Time of operation for heating/cooling distribution system	hour
Q	Heat demand	kWh
$\Delta\theta$	Temperature difference of supplied and extracted water in heating/cooling distribution system	K
C_p	Specific heat capacity	kJ/kgK
$E_{del,el}$	Electrical demand for building	kWh
$E_{del,spes-el}$	Specific electrical demands	kWh
E_l	Electrical demand lighting	kWh
E_{eq}	Electrical deman various equipment	kWh
k_{eff}	Effective thermal conductivity	W/mK
k_l	Conductivity liquid	W/mK
k_s	Conductivity solid	W/mK
n	Share of liquid saturation	-
k_T	Conductivity of unknown temperature	W/mK
k_k	Known conductivity	W/mK
T	Unknown temperature	K
$\Delta G°$	Change in Gibbs free energy	kJ
$\Delta H°$	Enthalpy change	kJ/mol
ΔS	Entropy change	kJ/molK
P	Pressure	Pa
V	Volume	m^3
n	Amount of gas	mol
R	Ideal gas constant	8.3145 J/molK
T	Temperature	K
a	Van der Waal constant	Jm^3/mol^2
b	Van der Waal constant	m^3/mol
A_{cyl}	Surface area of cylinder	m^2

V_{cyl}	Volume of cylinder	m^3
r	radius	m

Figure list

Table of Contents

1. Introduction

1.1 Background and motivation for master thesis

Svalbard is a group of islands located between 74º and 81º N latitude and 10º to 35º E longitude. The islands are a part of the Norwegian Kingdom, but not all of Norway's laws apply in the archipelago. On Svalbard's main island, Spitsbergen, there are both Norwegian and Russian settlements with a total population of 2583 people registered in 2017. Almost two-thirds of the population is located in Longyearbyen, while 428 Russians and Ukrainians resides in Barentsburg. The rest of the population is distributed among the research settlements Ny-Ålesund and Hornsund. (Barr, 2018)

Figure 1: Map of Svalbard geography.

Longyearbyen is located inside “Adventsfjord,” a branch of the bigger fjord “Isfjorden.” In recent years, due to global warming there has been an increase in temperature. Consequently, the permafrost is thawing which has developed unforeseen challenges for the society in Longyearbyen.

One of the challenges is that settlements at Svalbard are built on piles anchored in the permafrost, and as the ground thaws the piles lose their structural stability. The problem is increasing as the temperature, and active layer increases every year. (fig.2 and 3)

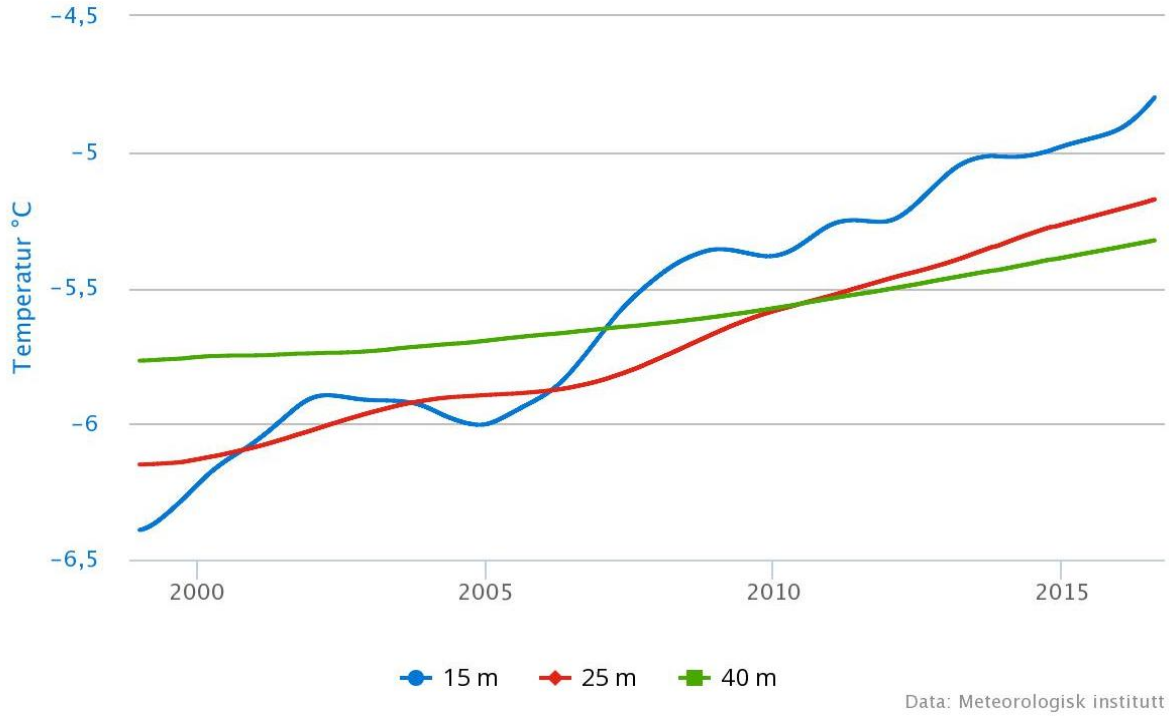

Figure 2: Permafrost temperature may vary from one year to the next, but the inclination is quite clear the last 20 years.
Source: Norwegian Meteorological Institute

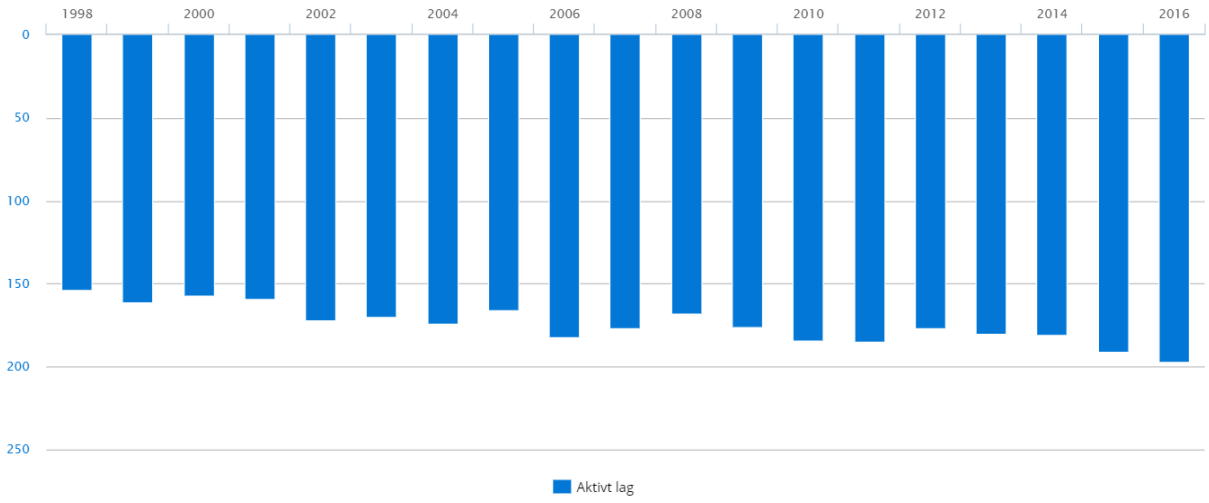

Figure 3: Shows an increasing depth in the active permafrost layer. [cm]
Source: Norwegian Meteorological Institute

The increase in temperature creates other issues as well. Usually, in areas with permafrost, the layer of sediments creates sturdy bindings of ice structures keeping the layer together. As the layer defrosts, the binding structures caused by the ice dissolves, also, the temperature increase accelerate the snow melting causing the thawed ground to saturate quicker with water. Underneath the saturated soil, the deeper layer of permafrost acts as a gliding layer. These events create ideal conditions for mud slides. (Hannus, 2016).

It is likely that mud slides will intensify. Climate simulations published in 2017 expect a yearly increase in seasonal precipitation. Up to now the yearly increase in precipitation has averaged 2% per decade since 1912, but scientists predicts a further increase of 20, 30 or 40% toward 2100 pending on the pollution scenarios RCP2.6, RCP4.5 and RCP8.5. These are pollution scenarios developed by IPCC. (Isaksen, 2017).

Today the area around Longyearbyen is matches the definition for dessert as the yearly precipitation in the region is less than 250mm per year(Isaksen, 2017). However, the area is cold and receives most of its precipitation as snow, the combination of wind and snow as makes it hard to get accurate readings of the precipitation as it blows out of the measurement instruments (Isaksen, 2017). The combined factors of a cold climate, strong and steady directional wind, and snow, creates dangerous avalanche prone areas as wind transported snow builds up in leeward mountainsides (Hannus, 2016). In addition, increased frequency of precipitation as rain during the winter creates ice which are an excellent sliding layer for avalanches.

In the winter of 2015, Longyearbyen suffered a natural catastrophe when a snow avalanche slid into ten houses. As a consequence, it killed a 42-year-old man and a little girl. This event launched an evaluation of the avalanche danger in and around Longyearbyen. NVE (The Norwegian Water Resources and Energy Directorate) in collaboration with Multiconsult published a report the following summer 2016. The report revealed critical information about houses within an unacceptable risk of avalanches (see fig. 4, 5 and 6). Because of the findings, NVE is now in charge of local avalanche risk forecasts, and the mountainsides are kept under close supervision to alarm the exposed households (Damkås. J., 2017). However, this should be a temporary solution in anticipation of a permanent one as the uncertainty and constant evacuations aggravates additional strain to families and individuals. In addition, on the 21.feb 2017 a snow avalanche slid towards two houses that were not evacuated even though the avalanche risk had been evaluated (Landrø, 2017). The report published by NVE after this incident concludes that the local alert should have greater margins for uncertainties in data and personal assessments. Such a measure would intensify the number of evacuation during the year causing extra strain to residents in avalanche-prone settlements.

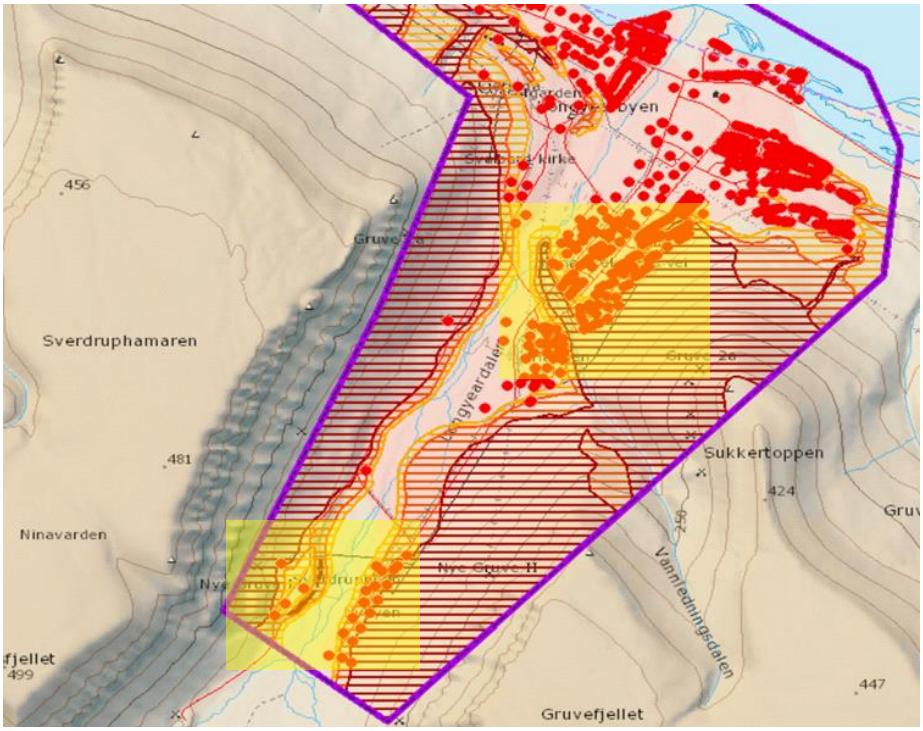

Figure 4: Illustrates the avalanche risk areas. Dark red indicates an avalanche once every 100-year, orange every 1000 year, and yellow every 5000 year. The two areas marked in yellow are of interest, the one on the top right is where the tragic accident occurred December 2015. Source: (The Norwegian Water Resources and Energy Directorate, n.d.)

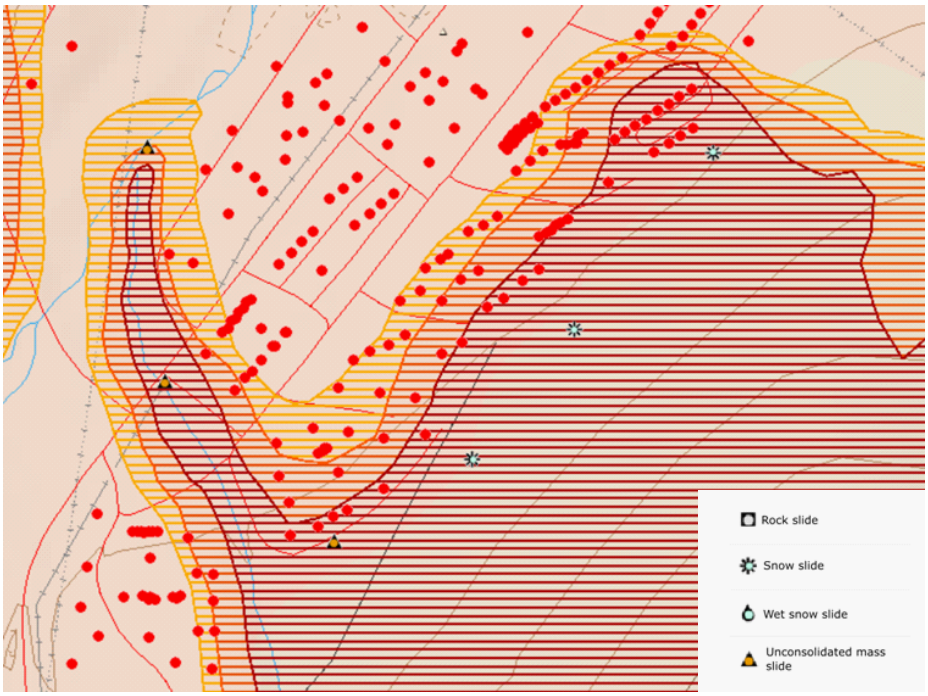

Figure 5: Illustrates that there are settlements (red dots) within the 100-year boarder of avalanches. Top right corner is the houses hit in 2015.

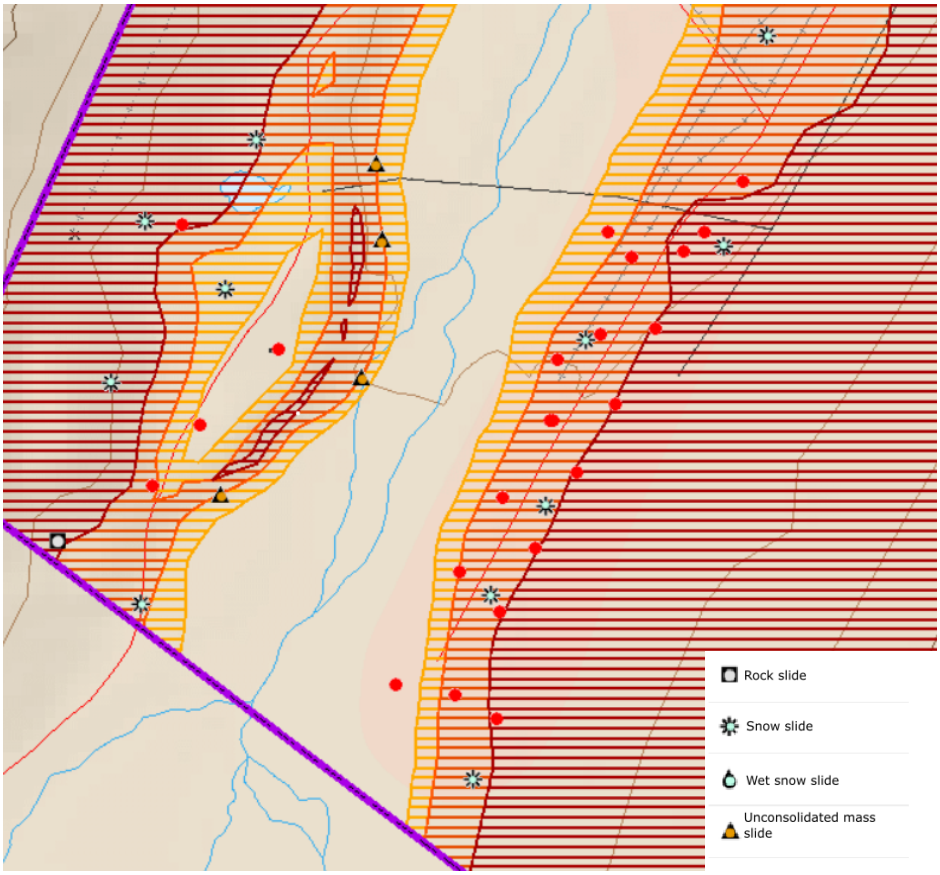

Figure 6: Some of the settlements in the "student city" are within the 100-year risk zone.

On the 18.01.2018 the Ministry of Petroleum and Energy issued a survey, requesting an energy solution at Svalbard. The survey should contain a technical-economic analysis which contains all realistic alternatives within the timeline of phasing out coal energy production. It should also consider global warming emissions, cost effectivity, supply guarantee, and sustainability (Olje- og energidepartementet, 2018). This request also points to the proposition 129 S containing additional appropriations and re-priorities in the state budget 2017. The proposition determined a 28 MNOK fund for geological surveys, and underlines the importance of securing energy supply to the island.(Prop. 129 S (2016-2017))

1.2 Description of the project

The initial focus of this master thesis was a technical-economic analysis of an all year-round heated hall in Longyearbyen. But due to discretion around the idea, it proved extremely difficult to get necessary information to do an economic analysis, it has also limited the certainty in the physical study. Consequently, the thesis became more focused on whether a construction of these dimension is feasible and the social benefits it could provide the arctic society of Longyearbyen.

The hall would stand on piles the same way as the rest of the settlements in Longyearbyen. The main difference is that it will be built on a borehole thermal energy storage (BTES), charged mainly by solar

energy. By doing so, the piles cannot be anchored in the permafrost but must be anchored in the solid rock beneath the sediments. This can be done by drilling holes of bigger dimension than the actual well. E.g. picture a 160mm drill bit, anchored to the drill bit is a 160mm outer diameter steel tube with a 140mm inner dimension, when the depth of the anchor (steel tube) is sufficient the drill bit is pulled back up leaving the steel tube in place. It is then possible to drill the rest of the collector by changing the drill bit to 140mm diameter and continue through the bedrock for another 60-100m. The structure can then be built on 200-500 secure and stable pillars depending on the distance between the collectors. This has been done several places in the world, only difference is that the SLSC (Svalbard Longyearbyen Solar Community) combines the technology with BTES. (Garathun. M.G, 2014)

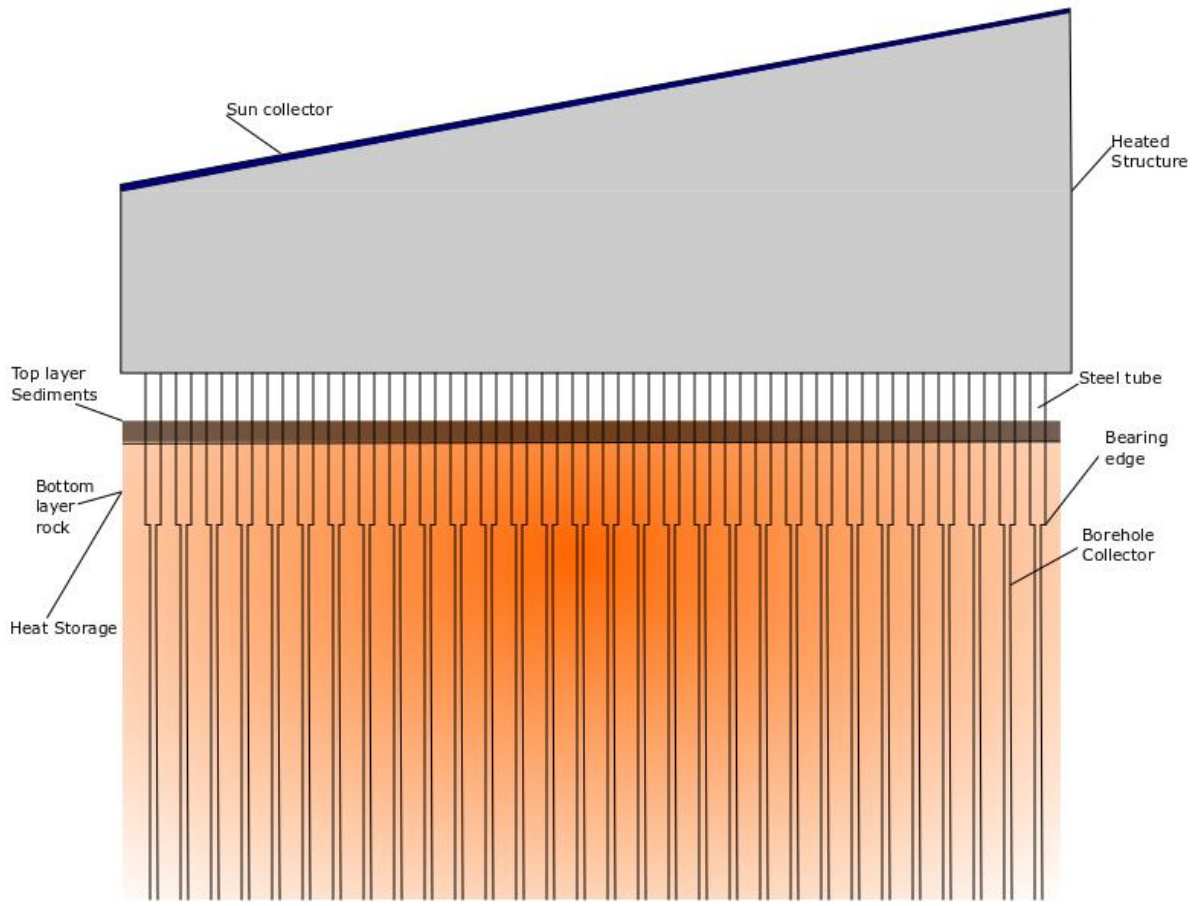

Figure 7. Shows an example draft of the construction from east. The illustration is not to scale.

Furthermore, the heated storage and indoor area require some electrical energy for different purposes, e.g. ventilation, lights, heated water, electrical equipment, and pumps for circulation of the medium in solar collectors and heating applications. To be certain not to underestimate the demand, the project is based on TEK 17 standards and NS3031:2014 (The Norwegian Standard for calculating the energy performance of buildings).

Today Longyearbyen is powered by coal energy production, but the Norwegian government decided in 2018 to liquidate all coal production in Lunckfjell- and Svea mines. Based on this decision, the thesis has liberated itself from a coal energy future on Svalbard (Prop. 1 S (2017-2018)).

To resolve the issue of a safe energy supply, the energy must be supplied by several independent production methods. The thesis examines microwave assisted pyrolysis (MAP), Photovoltaic sun cells (PV), Wind turbines, and biogas reactor as providers of electrical energy to the heated indoor society. Concerning the unregulated energy sources, such as wind and PV, an energy carrier in form of Hydrogen has been evaluated in depth as a viable option for the future.

The goal of this master thesis is to present a suggestion on how to resolve some of the challenges Longyearbyen faces today. How to resolve the energy challenge as well as the problems connected to the avalanche prone households. If this building proves to be feasible, it presents additional opertunities besides living areas for the society further discussed in chapter 6.

2. Theory

2.1 Fundamental Thermodynamics

Thermodynamics is the study of relations between heat, temperature, work, and energy. In general, thermodynamics deals with energy transfers from one form to another. (Drake, 2017)

In thermodynamics, it is crucial to define the system and the system boundaries. The defined volume examined is called a control volume. This volume is separated from the surroundings by a control surface. The surface is either closed or open to mass transportation and may or may not have energy flowing through in form of heat and work. In cases where the control volume is sealed off for mass transportation, it is called a control mass and contains the same amount of matter at all times. (Borgnakke, 2009)

2.1.1 Three fundamental laws compile thermodynamics.

The first law of thermodynamics states that the change in internal energy of a system must equal energy transferred to the system by heat and work. Consequently, energy can only change form and not be created, meaning that the change in internal energy must equal the work and heat going in or out of the control volume. (Tipler, 1996)

The second law of thermodynamics is recited in two ways. The Kelvin statement: No system can absorb heat from a single reservoir and convert it entirely into work without additional net changes in the system or its surroundings. The Clausius statement: A process whose only net result is to absorb heat from a cold reservoir and release the same amount of heat to a hot reservoir is impossible. In short, the second law of thermodynamics states that when energy transfers or transforms, it decreases in quality. (Tipler, 1996)

The third law states merely that the entropy of a perfect crystal at absolute zero temperature, is zero.

2.1.2 Thermal properties and processes.

There are three forms in which heat transfers from one reservoir to another. They are conductive heat transfer, convective heat transfer, and transfer by thermal radiation.

Conductive heat transfer is transfer by interactions/collisions between molecules. Energy in molecules of matter has translational(kinetic), rotational and vibrational energy. When colliding with molecules of different internal energy the substances exchange energy with each other and comes closer to thermal equilibrium. This power transfer called conductive heat transfer are expressed in Fourier's law of conduction:

$$P_{cd} = -kA_s \frac{dT}{dx} \tag{1}$$

Where P_{cd} is the power of the heat transfer, k is the substance conductivity, A_s is the area in contact and dT/dx is the temperature gradient. In some cases, when numerical solutions are problematic to obtain, the equation gets simplified by dividing the temperature by distance. (Cengel, 2005)

Convective heat is heat transfer caused by a medium drifting over a surface of dissimilar temperature. When a medium drift over a surface, new sets of molecules absorbs/exudes heat from/to that contact surface. The temperature difference is higher compared to conductive heat transfer, which contribute to a more effective heat transfer. The overall heat transfer closely correlates with Newton's cooling law. The equation looks simple, but the convection heat transfer coefficient is quite complex and is best found by empirical testing. Newton's cooling law is stated as:

$$P_{conv} = hA_S(T_s - T_m) \tag{2}$$

Where

h = convection heat transfer coefficient, W/m^2K

A_s = heat transfer surface area, m^2

T_s = Temperature of the surface, K

T_m = Temperature of the medium, K

Note that the temperature of the medium needs to be measured far enough from the surface area to give a correct representation of the temperature due to the no-slip condition. (Cengel, 2005)

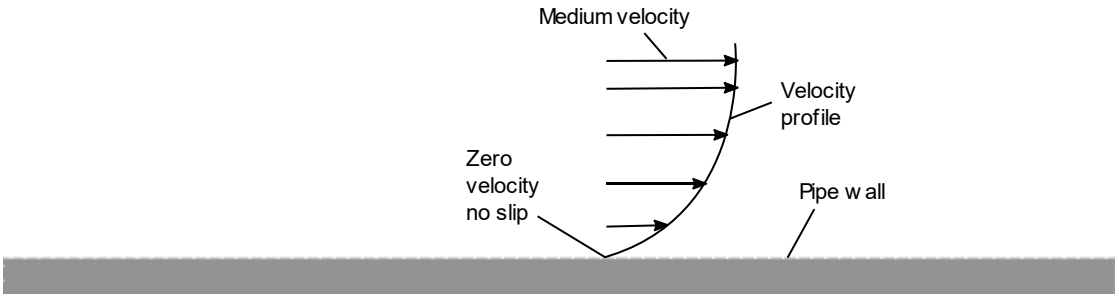

Figure 8: Representation of the no-slip condition, The molecules closest to the pipe wall does not slip. These molecules will therefore not represent the average heat in the medium. The velocity of the medium is also not representative close to the wall. The size of

Thermal radiation is heat transferred by electromagnetic waves. All objects can absorb and emit electromagnetic radiation. This way of transmitting heat does not require any matter to be present except when absorbing or emitting radiation. The power radiated is expressed by Stefan-Boltzmann law:

$$P_r = \varepsilon \sigma A_s T_s^4 \tag{3}$$

Where ε is the substance emissivity, σ is the Stefan-Boltzmann constant, A_s is the surface area and T_s is the temperature of the surface. (Cengel, 2005)

2.2 Solar radiation

The sun is a hot sphere of gas that uses nuclear fusion reaction to keep its core temperature above 20.000.000 K. At this temperature and pressure, two nuclei can possess enough energy to overcome the Coulomb repulsion hump, when they do, they penetrate the repulsion barrier, a phenomenon is called tunnelling. Penetration of the repulsion barrier happens when the strong nuclei force overcomes the separation force.

The temperature on the sun's surface, also known as the photosphere, is roughly said to be about 6000-degrees Kelvin for simplicity in calculations. However, more accurate values exist today as a more accurate fit to the suns spectrum. These values were proposed by Backus in 1976 and Parrot in 1993, suggesting 5762±50 K and 5730±90 K.(Bowden. S. & Honsberg. C., n.d.-b)

The sun radiates its power in a sphere. Therefore, only a fraction of the total power emitted by the sun is received by the earth. The irradiance received on the earth atmosphere is called the solar irradiance and has a power density factor presented as:

$$P_E = \frac{H_0}{4\pi R_{SE}^2} \tag{4}$$

Where P_E is the power radiated on the earth atmosphere, H_0 is the solar radiation intensity, and R_{SE} is the distance between the sun and the earth centre. (Bowden. S. & Honsberg. C., n.d.-a)

The sun is often considered as a black body object. It is a perfect absorber and emitter of thermal radiation; which means that the emissivity from equation 3 equals one. The blackbody power density is therefore very easy to calculate and is given by the Stefan-Boltzmann law.

$$H = \sigma * T_S^4 \tag{5}$$

There H is the blackbody power density, σ is the Stefan-Boltzmann constant and T_s is the surface temperature of the radiating object.

A blackbody source radiates its energy through a wide range of wavelengths. This spectral is distributed as shown in Planck's Radiation Law.

$$F(\lambda) = \frac{2\pi h_P c^2}{\lambda^5 \left(\exp\left(\left(\frac{h_P c}{k_B \lambda T} \right) \right) - 1 \right)} \tag{6}$$

Where h_P is Planck's constant, k_B is Boltzmann's constant, c is the speed of light in vacuum, and λ is the wavelength. The figure below graphs the suns radiation spectrum based on Planck's radiation law. It shows three different temperature based on Backus 1976 as a more accurate fit to the suns actual spectrum. By differentiating equation 6 with respect to λ the peak wavelength can be obtained by solving $\frac{dF}{d\lambda} = 0$.

By integrating equation 6 over all wavelengths λ, the solution becomes the Stefan-Boltzmann law.

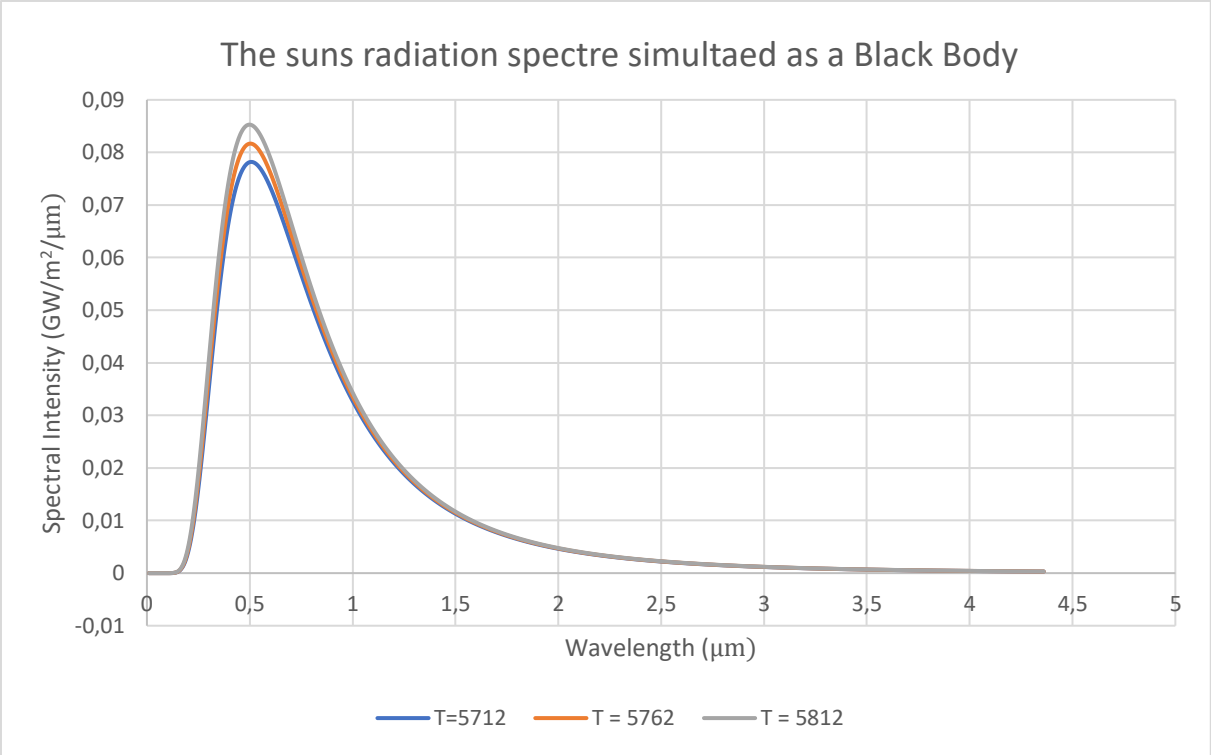

Figure 9: Graphs the radiation spectre of a blackbody object, in this case, the sun. The different surface temperatures of the sun are based on Backus's observations 1976 as a more accurate fit to the suns spectrum. Note as the temperature rises the peak wavelength shifts left.

The solar radiation intensity recived on a surface at a given distance from the sun is expressed by equation:

$$H_0 = \frac{R_{sun}^2}{D^2} * H_{sun} \tag{7}$$

Where H_0 is the suns radiation intensity at an assumed distance from the sun, R_{sun} is the radius of the sun and D is the given distance from centre of the sun. However, because the earth orbit around the sun is elliptical, and not circular, the parameter representing the distance is not constant. On an average, this causes the power radiant on earth atmosphere to vary around 3,4% per year. The highest power radiation is received in January when the earth is closest to the sun. Power received on the earth atmosphere is graphed in figure 10 based on equation 9.

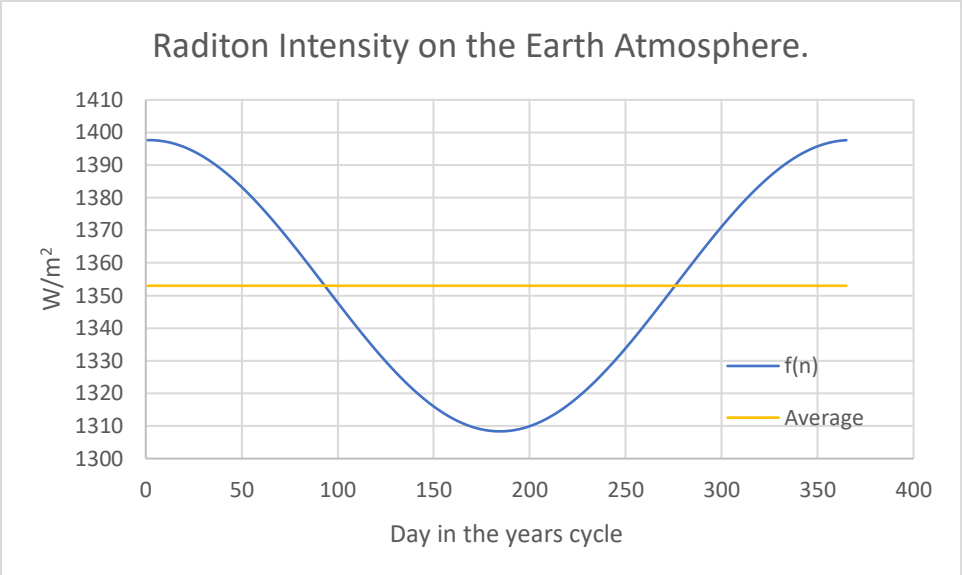

Figure 10: Illustrates how the suns radiation on the earth atmosphere changes due to the earth's spherical orbit around the sun, in most calculations the solar constant is used. The solar constant is an average of the solar radiation.

2.3 Solar power on the earth's surface

As mentioned in the chapter above, the radiation on the earth's atmosphere is relatively constant with a deviation ±3,4% from the average power density. Solar radiation reaching the earth's surface however are divided into two categories, diffuse and direct radiation. The amount of radiation from the two categories reaching the earth's surface varies due to a wide range of atmospheric effects causing absorption and scattering of radiation. The atmospheric effects are often local effects such as clouds and aerosols (pollution). However, latitude of the location and season of the year also affect the radiation intensity as described in the next paragraph. (Honsberg, 2018)

A way to measure how much of the sun's radiation that reaches the earth's surface on a cloudless day is by calculating what is called airmass (henceforth called AM). The AM is the length in which the radiation travels through the atmosphere compared to the shortest possible length. When the radiation travels for longer distance, more of it will be absorbed and scattered by air molecules and dust. Air mass is expressed in the equation below.

$$AM = \frac{1}{\cos\left(\frac{1}{\theta}\right)} \tag{8}$$

There θ is the angle from the zenith angle shown in the figure below.

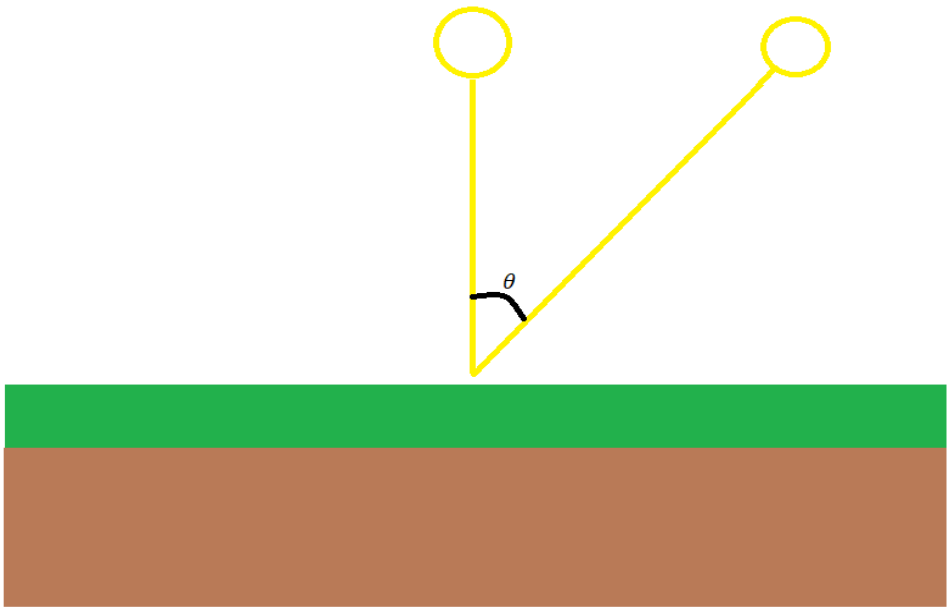

Figure 11: illustrates how sunrays travel longer through the atmosphere when the sun is in lower orbit

AM describes how the radiation intensity varies depending on the suns positioning on the hemisphere. The location on earth determines how the sun moves over the sky during the day and the angle of the earth tilt towards the sun during the summer and winter. In general, higher latitudes indicates lower sun orbit and therefore a lower radiation intensity (eq.11). The variation in suns angle can be described by the earth tilt towards the sun and the elevation angle provided by equation 9 and 10:

$$\delta = 23.45 \sin\left(\frac{360}{365}(284 + d)\right) \tag{9}$$

$$\alpha = 90 - \phi + \delta \tag{10}$$

where δ is the tilt angle of the earth angle towards the sun, d is the day of the year, α is the suns elevation angle and φ is the latitude degree. The radiation intensity at a certain hight above ground can then be calculated as:

$$I_D = 1.353 * [(1 - 0.14h) * 0.7^{AM^{0,678}} + 0.14h] \tag{11}$$

Where h is the height in km. (Bowden. S. & Honsberg. C., n.d.-c)

2.4 Sun collector

There are several different types of sun collectors with a wide range of complexity. A sun collector heats water from the sun and ranges between a black barrel baking in the sun to parabolic sun collectors. This chapter will explain the physical laws behind flat metal plate sun collectors with moving fluids. These collectors collect the suns radiation on a selective surface, a surface that specialize in absorbing as much of the radiation as possible by using materials of unique chemical compositions. These collectors possess excellent heat conductivity while designed to minimise the thermal and optical heat losses to the surroundings. By absorbing radiation from the sun, molecules will increase their kinetic energy and the material will get warm. By using a medium circulating through the sun collector the heat can be transported to storage or utilized in heat applications.

A sun collector of area A_{sc} that is exposed to irradiance G from the sun gives a useful power output of:

$$\mathrm{P_u} = \mathrm{A_{sc}} q_u = \eta_{sc} A_{sc} G \tag{12}$$

Where q_u is the power per unit area absorbed and transported out of the system/collector. η_{sc} is the solar collector efficiency. The solar collector efficiency is dependent on how efficient the collector absorbs the radiation and how quickly it can pass that heat through to the flowing medium. η_{sc} is therefore represented by:

$$\eta_{sc} = \eta_{rp} \eta_{pm} \tag{13}$$

Where η_{rp} is the efficiency in which the plate absorbs the suns radiation and η_{pm} is the efficiency in which the heat is transported from the plate to the flowing medium. The absorption abilities of the sun collector can be given as:

$$n_{rp} = \tau_{cov} \alpha_p - \frac{U_L (T_p - T_a)}{G} \tag{14}$$

Where τ_{cov} is the transmittance coefficient of the glass cover, α_p is the absorbance ratio of the plate collector, U_L is the heat loss coefficient of the sun collector housing, T_p is the plate average temperature, T_a the ambient air temperature, and G is the insolation.

Volker-Quashning has derived a more empirical equation of the solar collector efficiency including the η_{pm} efficiency as well. The equation is given as:

$$\eta_{sc} = \eta_0 - \frac{a_1 * (T_p - T_a) + a_2 * (T_p - T_a)^2}{G} \tag{15}$$

There η_0 is the optical efficiency, a_1 is the linear heat loss coefficient, and a_2 are the quadric heat loss coefficient. These values are individual for each solar collector and are presented by the manufacturer. This equation and these experimentally obtained factors correct several factors not comprehended by theoretical equations. E.g. the resistance decreases with temperature which implicates that U_L (=1/R) does not vary in a linear matter as assumed in equation 14.

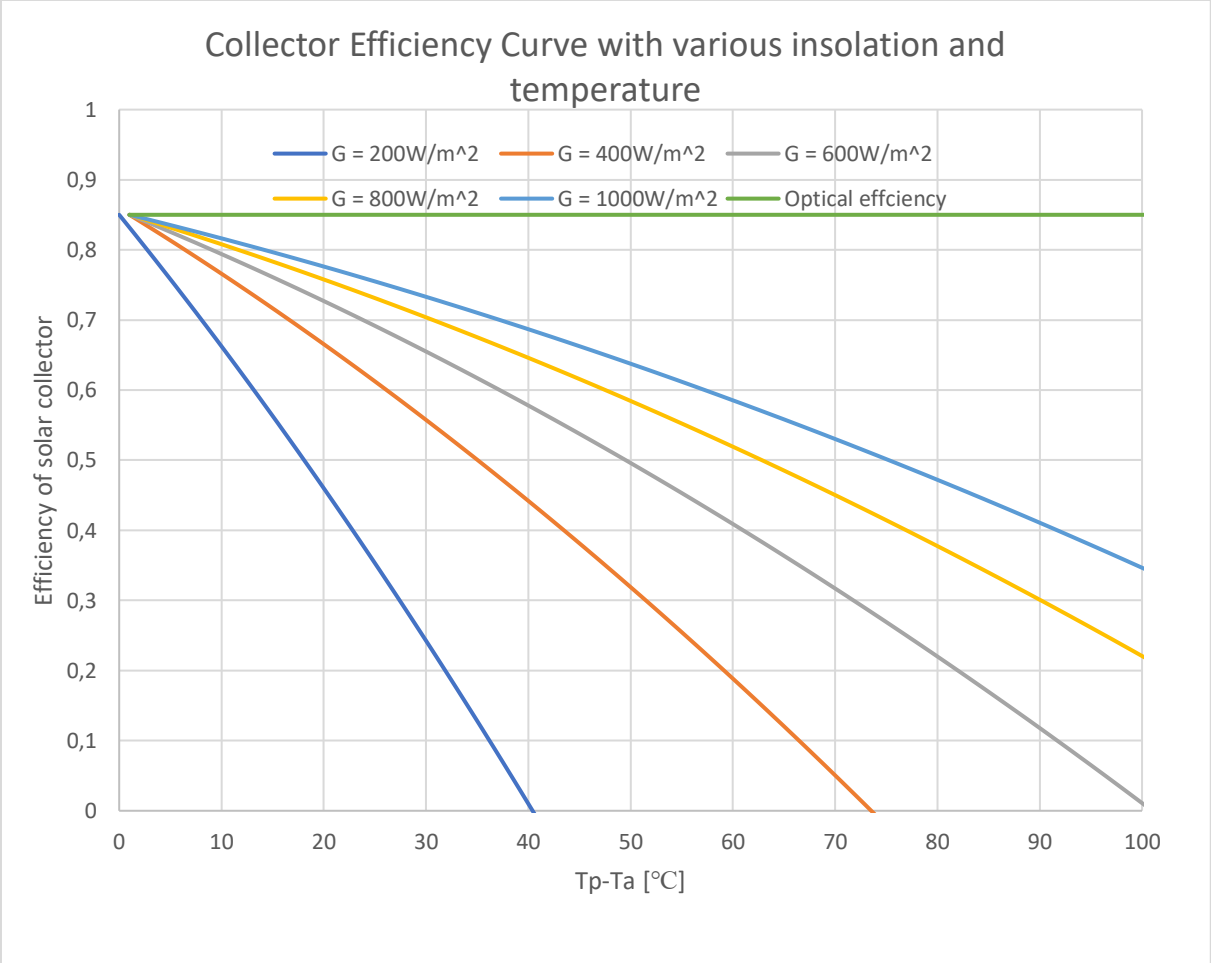

Figure 12: The figure reflects the efficiency of a flat plate solar collector and contains a lot of information. By demanding high average temperature from the solar collector, the T_p -T_a increases and the efficiency drop, this makes sense as the thermal losses to the surrounding increases when the temperature differences increases, this is true for all methods of heat transfer. E.g. In early spring on Svalbard, the irradiation on the collector surface is 200W/m^2 and the ambient temperature is -15℃, by demanding a 15℃ average temperature from the solar collector, the efficiency would be ≈ 25%. However, by lowering the demand to 5℃ average, the efficiency would rise to ≈ 50%. If the radiations intensity increases, the solar collector can collect higher temperatures with the same without lowering the efficiency. The loss and efficiency factors in this instance where set to a_1 = 3.6, a_2 = 0.015, η_0 = 85%, as a best fit to the Volker Quaschning article on Solar thermal water heating.(Quaschning, 2004)

The graphs indicate that higher temperature difference operated on the panel results in lower efficiency, and that higher radiative power can result in a higher output temperature at the same efficiency rate.

The power received on the sun collector plane can be calculated by using a simple analysis of the angles in the system drawn below.

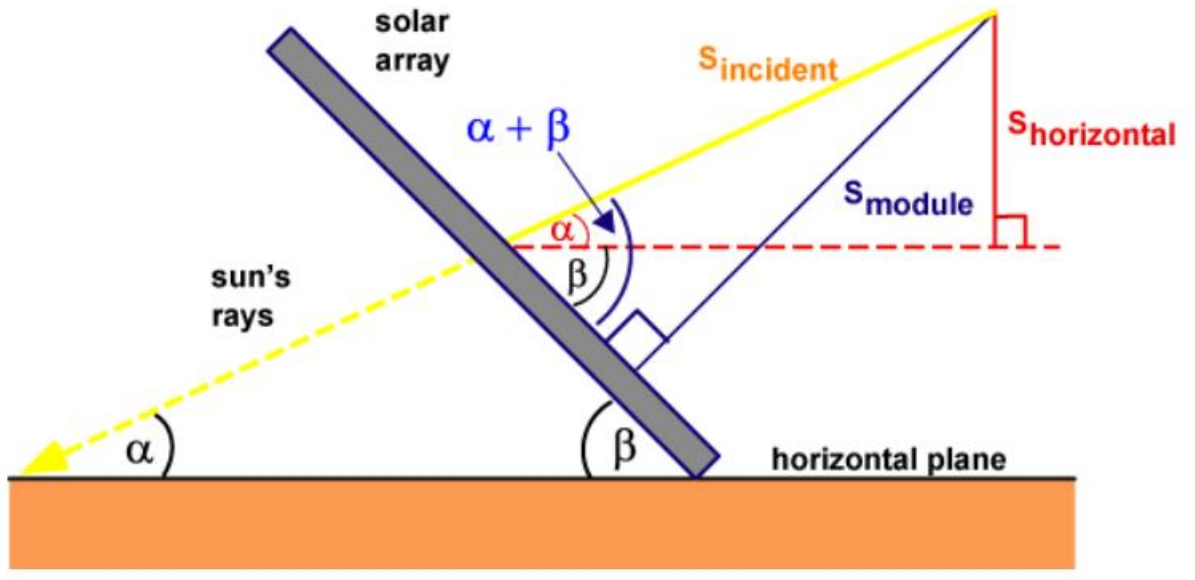

Figure 13: Illustrates the trigonometry of radiation to a plane. The figure is used to derive equation 16

The figure above illustrates that:

$$P_{sc} = P_{horiz} * \frac{\sin(\alpha + \beta)}{\sin(\alpha)} \quad (16)$$

There P_{sc} is the power incident on the solar collector plate, P_{horiz} is the power incident on the horizontal plane, α is the suns elevation angle, and β is the sun collector tilt.

The sun's energy gives rice to many of the renewable energy resources humans exploit today.

2.5 Photovoltaic cells

Photovoltaic cells are usually made of the semiconductor silicon. The silicon is doped with tiny amounts of phosphorus containing five free electrons and boron containing 3 free electrons. When these two impurities are stacked together they create a light sensitive PN-junction. Photons absorbed in this junction knocks out electrons causing a surplus of electrons on one side of the junction and a shortfall on the other. When these two sides are linked together by a conductor they construct a electricity current. (Tidwell. J. & Weir. T., 2006)

2.6 Wind power

When the sun radiates onto the earth surface, the earth absorbs power and emits heat. The heat is conducted into the air and triggers convection where hot air ascends, and cool air descends due to

mass differences caused by the temperature. Because these two phenomenon, happens at different localisations, high- and low-pressure system develops. The cold air descending will then blow near to the ground and replace the hot air ascending. The wind that travels between the pressure systems contains kinetic energy which can be converted into mechanical work to create electrical energy by using wind generators. The wind power is given by:

$$E_{kw} = \frac{1}{2} * u^3 * \rho * A_w \tag{17}$$

Where u is the wind speed, ρ is the density of the air and A_w is the area sweped by the windturbine.

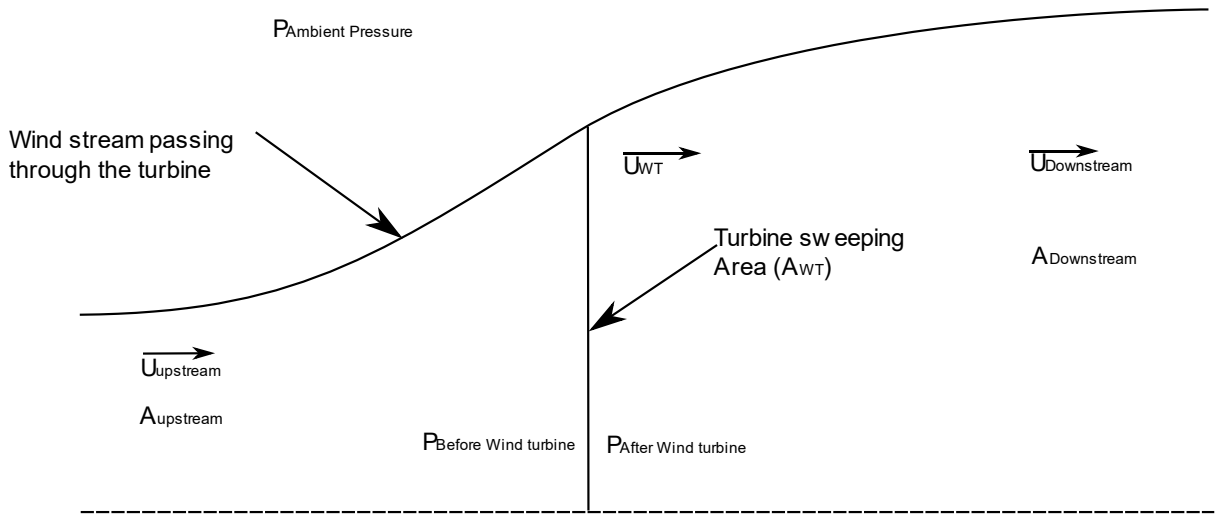

Figure 14: Shows an airstream through a windmill sweeping area. The air expands due to a reduction in pressure and speed to maintain the assumption of continuity.

However, there are some constraints to wind power. Betz law states that the maximum efficiency of a wind turbine is 59,3%. This constraint is also known as the maximum theoretical power coefficient for a wind turbine and provides the following equation:

$$E_{kw} = C_{tp} \frac{1}{2} * u^3 * \rho * A_w \tag{18}$$

Where C_{tp} is the theoretical power coefficient for wind turbines. This theory is derived from the continuity equation and Bernoulli's equation. (Tidwell. J. & Weir. T., 2006)

By knowing wind data from different heights, it is possible to numerically find the roughness length factor used to explain the wind profile in the area. The wind profile is described by this equation:

$$v_2 = \frac{v_1 \left(\ln \left(\frac{h_2}{z_0} \right) \right)}{\ln \left(\frac{h_1}{z_0} \right)} \tag{19}$$

Where v_2 is the wind in desired height or hub height of the wind turbine, v_1 is the wind at a known level, h_2 is the desired height or in most cases the hub height, h_1 is the height of the known wind measurement, and z_0 is the roughness length factor which is based on the surrounding terrain (Tidwell. J. & Weir. T., 2006).

When describing the wind variation over time the most used statistical model due to its good fit is the Weibull distribution. The distribution is given as:

$$f(u;\lambda,k) = \frac{k}{\lambda} * \left(\frac{u}{\lambda}\right)^{k-1} e^{-\left(\frac{u}{\lambda}\right)^{k}} \tag{20}$$

Where f is the likelihood of the wind speed, u is the wind speed, lambda is the average wind speed parameter and k is the frequency parameter of wind speeds, also known as the Weibull distribution factor.

Lambda is calculated by the gamma function:

$$\lambda = c\Gamma(1 + 1/k) \tag{21}$$

Where c is the Weibull wind speed factor and Γ is the standard integral generally referred to as the gamma function (Tidwell. J. & Weir. T., 2006).

In most cases, it is interesting to know how much downtime the wind turbine suffers due to instability in the wind speed. The time wind spends within a specific time interval can be calculated by the equation:

$$T_{interval} = e^{-\left(\frac{u_1}{U} * \Gamma\left(1+\frac{1}{k}\right)\right)^{k}} - e^{-\left(\frac{u_2}{U} * \Gamma\left(1+\frac{1}{k}\right)\right)^{k}} \tag{22}$$

Where u_1 is the lower windspeed limit, u_2 is the upper wind speed limit, U is the average wind speed, Γ represents the gamma function and k is the shape factor of the Weibull distribution/frequency parameter of wind speeds.

2.7 Microwave pyrolysis

Microwave assisted pyrolysis is a thermochemical energy conversion technology used to convert waste materials into energy. Pyrolysis in general describes a physical decomposition of hydrocarbon materials in absence of oxygen reactants (Company). The technology has developed rapidly the last few years and has shown several promising results brought together and presented by F. Motasemi and Muhammad T. Afzal (Motasemi & Afzal, 2013).

Microwaves reside within the electromagnetic spectrum. It is defined as wavelengths between the infrared and short radio radiation with a frequency of 1GHz - 300 GHz. Microwave pyrolysis is a

method used to break down an substance to its elemental constituents by heating it up to a point where microwaves can be used to further offset molecules to detach from the biomass (Company). This method uses lower temperatures, heats the material uniformly through the whole volume and can convert the waste material into oil products and gasses from the process with less energy usage than conventional pyrolysis (O'Toole & Grønlund, 2012).

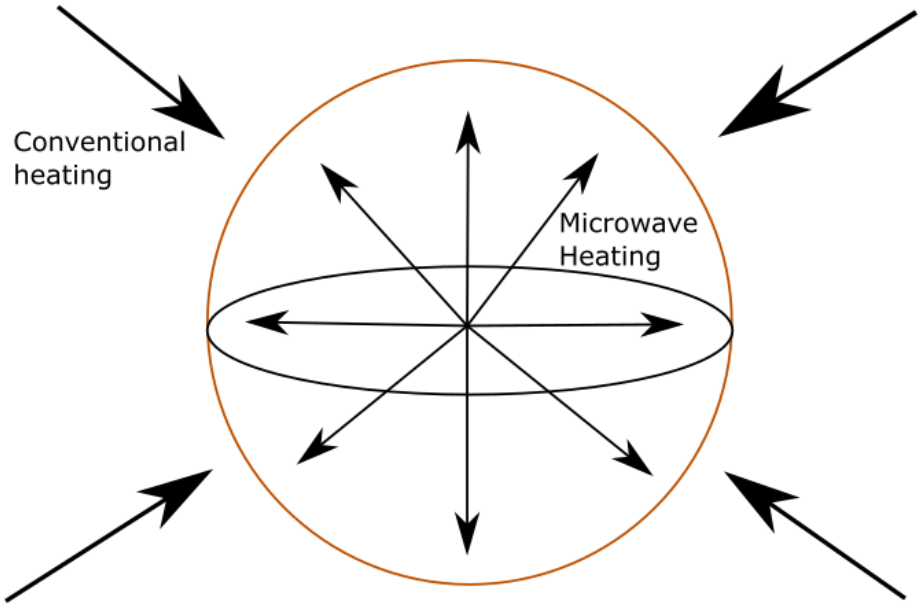

Figure 15. The heat distributes evenly through the volume when using microwaves, making it an effective option compared to conventional heating. Based on Micro Fuel AS presentation for Bioforsk.

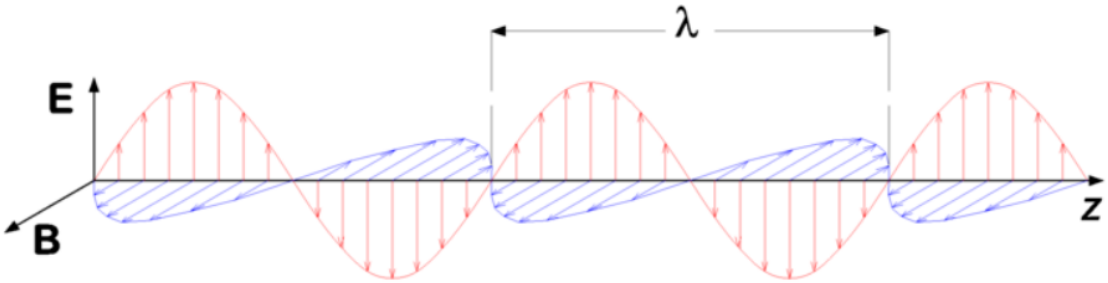

Figure 16. illustrates the two perpendicular components in electromagnetic radiation. B is the magnetic component and E the electric component Source: https://commons.wikimedia.org/wiki/File:Electromagnetic_wave.png

The electric component of the field can interact with materials, these materials can be classified in three different ways according to how they interact with microwaves. Firstly, the insulator which is a microwave transparent material (e.g. glass, quartz, etc.), secondly, the conductor which the microwaves reflect upon hitting (e.g. metals) and lastly, the absorber which are materials that can absorb the microwaves and turn it into heat (e.g. water, oils, carbon). The microwave absorber

materials are often called dielectric materials and microwave heating is called dielectric heating (Motasemi & Afzal, 2013).

In Norway, Scandinavian Biofuels AS started developing a microwave reactor in 2012 as a part of the EU: FP7 research project. A flow diagram illustrates the process.

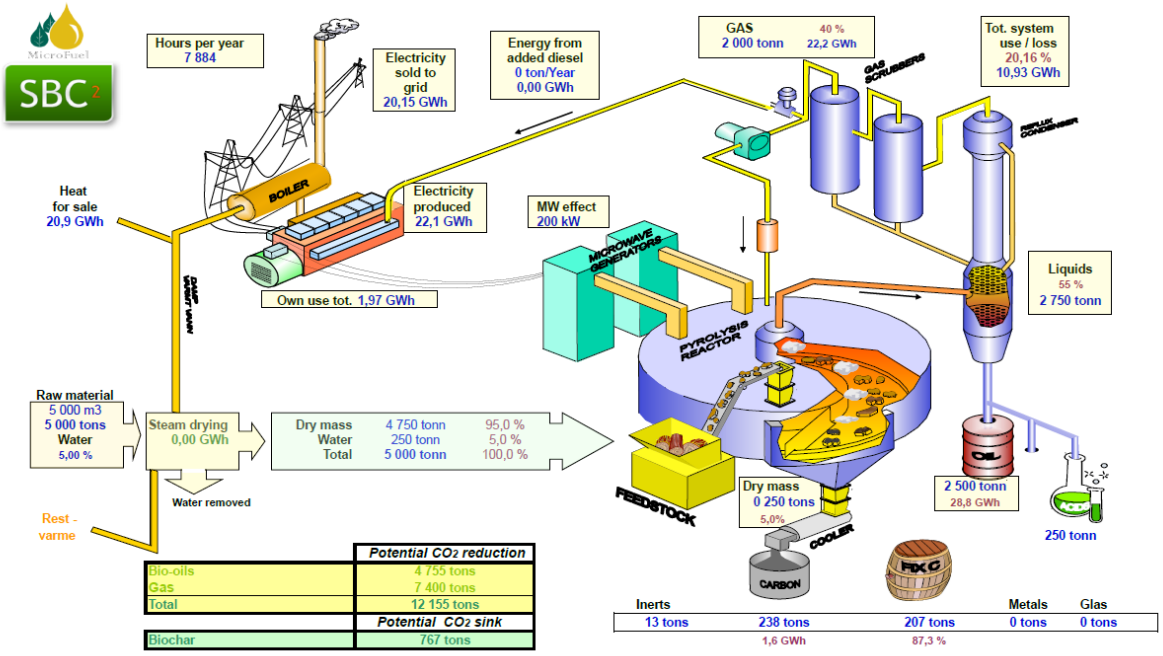

Figure 17: Illustrates a flow diagram for the Microwave assisted pyrolysis. In this case, 5000 ton of plastic waste is converted into gas and oil which are used for electricity generation.

The biomass gets shredded before it is feeded to the reactor. In the reactor the shredded biomass is exposed to microwave radiation for just a few second, enough to detach the volatile molecules from the biomass. The gasses are then processed in scrubbers where oil and gasses are distinguished, the oil is further processed a distillation tower to extract oil of different fragments and quality. The gasses are directly used for electricity generation or other mechanical work. By exploiting the gas to run a generator for the microwave generator, the process is self-sustainable.

In addition, biochar is produced, a product which has multiple applications in different industries (O'Toole & Grønlund, 2012). This whole system fits within a 40 feet container and are easy portable (Scandinavian Biofuel Company, n.d.).

2.8 Biogas reactor

A biogas reactor uses a biochemical reaction called anaerobic digestion. Anaerobic means in absence of oxygen. Certain anaerobic microorganisms have the ability to supply themselves with energy by reacting with carbonhydrate materials of type $C_cH_hO_o$. By doing so they can devide the material into

fully oxidised CO_2 and fully reduced CH_4 gas. Most biogas reactors/digesters are designed to favour the production of methane to carbon dioxide, however, the mix of these two gases are called biogas and has several uses e.g. power production, cooking and heat supply. One of the big advantages of bioreactors are that nutrients such as nitrogen compounds and phosphorus remain in the digestate, providing a valuable fertilizer for new crops. It can also utilize 60-90% of the dry matter heat of combustion energy and can obtain this from slurries up to 95% water. This essentially means that these reactors can utilize energy from high water containing materials, such as tomatoes and other vegetables which would never been beneficial treat thermochemically (Tidwell. J. & Weir. T., 2006).

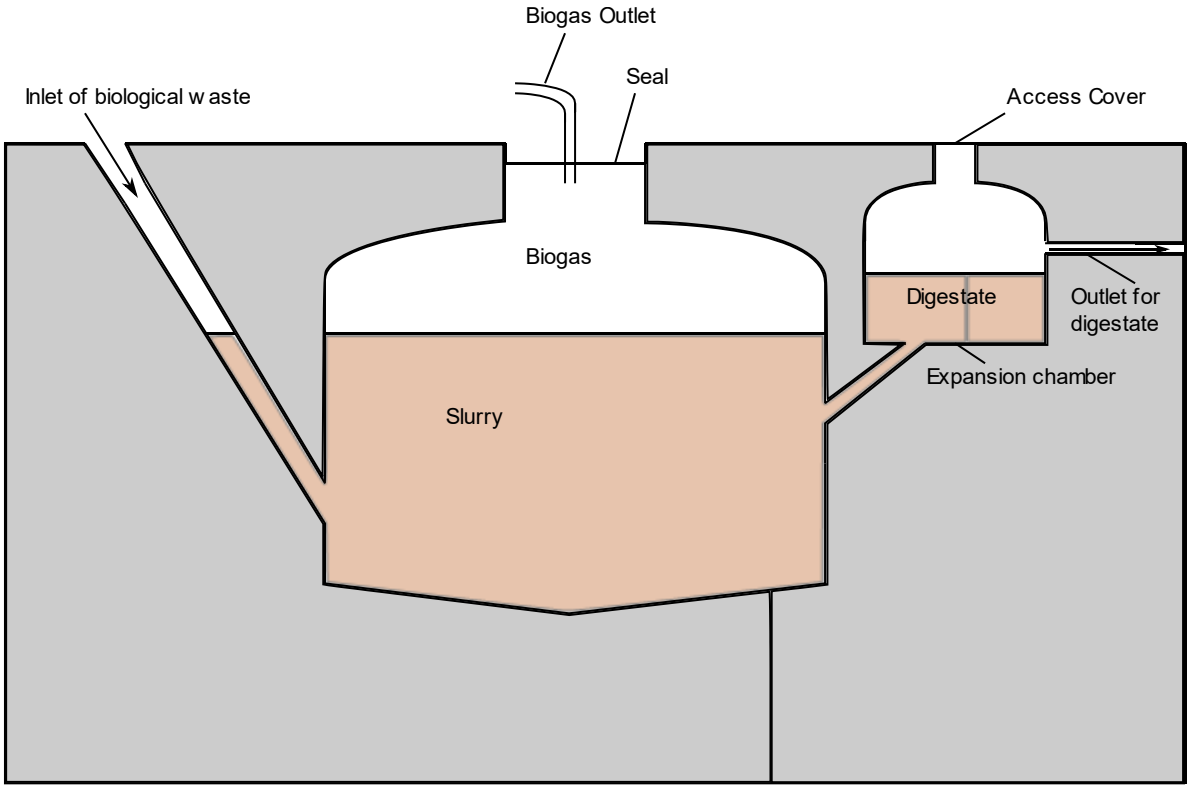

Figure 18: Illustrates a biogas digester. The anaerobic digestion takes place in the slurry. The digestate is used for fertilizers, the inlet for biological waste could e.g. be sewage systems, food processing residues, and rotten food.

The general chemical equation for anearbic digestion is:

$$C_xH_yO_z + \left(\frac{x - \frac{y}{4} - \frac{z}{2}}{2}\right) H_2O \rightarrow \frac{x}{2} - \frac{y}{8} + \frac{z}{4} CO_2 + \frac{x}{2} + \frac{y}{8} - \frac{z}{4} CH_4$$

This reaction is slightly exothermic, however, the energy released is so low it does not influence the temperature in the slurry. Depending on the carbohydrate molecule, the heat lost to the slurry averages only 10% of the dried heat of combustion figure, meaning that a biogas digester could have up to 90% conversion efficiency. However, this takes to long and a conversion of 60% is normal. In general,

there are three ranges of temperatures that favours different types of digestive bacteria where higher temperature means higher digestive tempo. The three types of bacteria are: psicrophilic around 20℃, mesophilic around 35℃ and thermophilic around 55℃ (Tidwell. J. & Weir. T., 2006).

The energy available from a biogas digester is given by:

$$E = \eta H_b V_b \tag{23}$$

Where η is the combustion efficiency of burners, boilers etc. H_b is the heat of combustion per unit volume of biogas at a given pressure and V_b is the volume of the biogas. However, the biogas contains CO_2 which will absorb the heat of combustion of methane. It is therefore useful to know the fraction of methane in the biogas to calculate the energy output of the biogas:

$$E = \eta H_m f_m V_b \tag{24}$$

Where H_m is the heat of combustion of methane and f_m is the fraction of methane.

The volume of extracted biogas from an input is given by:

$$V_b = cm_0 \tag{25}$$

Where c is the biogas yield per unit of dry mass and m_0 is the mass of a dry unit input

The volume of fluid in the digester is given as:

$$V_f = \frac{m_0}{\rho_m} \tag{26}$$

Where ρ_m is the density of dry matter in the fluid.

The total volume of the digester is then:

$$V_d = V_f t_r \tag{27}$$

Where t_r is the retention time in the digester.

2.9 Greenhouse

A greenhouse is a house designed to facilitate optimal growth condition for plants. Plants uses photosynthesis to convert water and CO_2 to sugar and starch. In addition, the plants need nutrition in form of minerals etc., and light to facilitate this chemical pathway. The main product of photosynthesis is sugar the plants can utilize to grow, however, oxygen from the water is a bi product caused by this chain of chemical reactions.

The process has two main stages. The first one is the light dependent stage where photons (light energy) is absorbed to produce ATP and NADPH from ADP and $NADP^+$ respectively. These molecules are then used in the light independent reaction cycle called the Celvin cycle. The Calvin cycle is where the sugar is produced by use of CO_2 and the products ATP, NADPH made in the light dependent stage.

2.10 Norwegian Standards

There are guidelines for calculating the energy performance of buildings in Norway called Norwegian standards (NS), in this instance, a further examination of the NS3031 standard is used to calculate the energy performance of buildings. The law, however, is given by the TEK 17 standards. In this thesis, a combination of the two has been used. In many ways, the new TEK 17 legislation makes a lot of the NS3031 standards obsolete as they are closing in on passive house standards regarding heat and ventilation losses. However, NS 3031 contains valuable equations and empirical discovered table values to calculate heat losses.

Total power demand for the building per degree Kelvin is given by NS3031 as:

$$H = H_D + H_U + H_g + H_V + H_{inf} \tag{28}$$

Where H is the total power demand, H_D is heat transmission through the building structure, H_U is heat transmission to unheated building parts, H_g is heat lost to the ground, H_V is heat lost through ventilation and H_{inf} is heat lost by infiltration.

Transmission losses are calculated by the equation:

$$H_D = \sum U_i A_i + \sum \Psi_k l_k + \Sigma \chi_j \tag{29}$$

Where U_i is the u-value of element i, A_i is the area of element i, Ψ_k is the thermal bridge value for thermal bridge k, calculated based on indoor measurements, l_k is the length of thermal bridge k, calculated based on indoor measurements, and χ are specific thermal bridges. $\sum \Psi_k l_k$ are tabled values.

Ventilation losses are calculated by the equation:

$$H_V = 0.33 * \dot{V} * (1 - \eta_T) \tag{30}$$

Where 0.33 is the heat capacity for air per volume, $\dot{V}$ is average ventilated air supply and η_T is the temperature efficiency of heat recovery.

Infiltration losses is calculated by equation:

$$H_{inf} = 0.33 * n_{inf} V \tag{31}$$

Where V is the heated volume, n_{inf} is the air substitution factor due to infiltration. n_{inf} is calculated by (Standard Norge, 2014):

$$n_{inf} = \frac{n_{50}e}{1 + \left(\frac{f}{e}\right) * \left(\frac{V_1 - V_2}{V n_{50}}\right)^2} \quad (32)$$

Where n_{50} is the air substitution factor given 50pa pressure difference inside versus outside, e is the terrain shielding coefficient tabled value in NS3031, f is a terrain shielding coefficient tabled in NS3031, V_1 is volume supplied air, V_2 is volume extracted air, and V is the total heated air volume.(Standard Norge, 2014).

In "Byggforsk" series no. 552.103 published by SINTEF is a simplified equation for computing energy consumption with the use of degree-day figures. The equation is provided as:

$$Q_t = 24h/day * H * G \quad (33)$$

Where Q_t is the total energy loss, H is the total power demand per Kelvin, and G is the degree day figure. The degree-day figure is the daily deviation between the outdoor mean temperature and indoor temperature, 17 degrees is used as a standard in Norway. (Standard Norge, 2014) (Byggforskserien, 1990)

According to NS 3031, heat supplements are calculated as:

$$Q_{HS} = Q_{sun} + Q_{int} \quad (34)$$

Where Q_{sun} is the energy supplied through the windows by the sun and Q_{int} is the internal energy provided by equation 35:

$$Q_{int} = \left(q_{light} + q_{equ} + q_{per} + q_{fan}\right) * A_{fl} \quad (35)$$

Where q_{light} is heat supplied by light sources, q_{equ} is heat supplied by various equipment, q_{per} is heat supplied by people, q_{fan} is heat supplied by the fans in the ventilation system, and A_{fl} is the total floor area. The heat supplied by fans in the ventilation are calculated as:

$$q_{fan} = 0.33 * \frac{V * \left((1 - \eta_T)\Delta\theta_1 + \Delta\theta_2 + \eta_T\Delta\theta_3\right)}{A_{fl}} \quad (36)$$

Where V is the average supply of air, η_T is the temperature efficiency of the heat exchanger, $\Delta\theta_{1,2,3}$ is the temperature increase over fans depending on the placement in the ventilation unit: $\Delta\theta_1$ is the air supply fan before ventilation unit, $\Delta\theta_2$ is the air supply fan after the ventilation unit and $\Delta\theta_3$ is the exhaust fan before the ventilation unit.

Yearly energy demand for air fans and heat distribution pumps are calculated as:

$$E_{fan} = \frac{V_{on} SFP_{on} t_{on} + V_{red} SFP_{red} t_{red}}{3600} \quad (37)$$

$$E_p = V_w SPP t_{dr} \quad (38)$$

Where E_{fan} is the energy demand for ventilation, V is the air supply, SFP is the specific fan power related to air supply, t equals time in hours, subscript "on" indicates during operation, subscript "red" indicates reduced supply outside operations. In case of CAV the $V_{red} SFP_{red} t_{red} = 0$. E_p is the energy demand for waterborne heat/cooling pumps, V_w is the amount of circulated water, SPP is the specific pump power, and t_{dr} is the time of operations in hours. The amount of circulated water in [L/s] is calculated as:

$$V_w = \frac{Q}{\Delta\theta C_p \rho} * 1000 \quad (39)$$

Where Q is the heat demand, $\Delta\theta$ is the heat difference in supplied and extracted water, C_p is the specific heat capacity to fluid, and ρ is the density of the fluid.

The electricity demand of the building is estimated by the equation:

$$E_{del,el} = E_{del,spes-el} + E_{del,er-el} + E_{del,hp-el} + E_{del,sol-el} + E_{del,C-el} \quad (40)$$

Where $E_{del,el}$ is the total electricity demand, $E_{del,spes-el}$ is the electricity for specific demands presented in equation 41, $E_{del,er-el}$ is electrical demand for electrical heating applications, $E_{del,hp-el}$ is the electrical demand for heat pump applications, $E_{del,sol-el}$ is the electrical demand for thermal sun energy systems, and $E_{del,C-el}$ is the electrical demand for cooling systems. In this thesis, the $E_{del,spes-el}$ are of interest and are provided by the equations:

$$E_{del,spes-el} = E_{spes}(1 - f_{El-sol}) + \frac{E_{spes} f_{El-sol}}{\eta_{El-sol}} \quad (41)$$

Where E_{spes} is provided by equation 42, f_{El-sol} is the share of electricity supplied by PV cells, and η_{El-sol} is the system efficiency of a PV system.

$$E_{spes} = E_{fan} + E_p + E_l + E_{eq} \quad (42)$$

Where E_{fan} is the electrical energy demand for fans, E_p is the electrical demand for heat system pumps, E_l is the electrical demand for lights, and E_{eq} is the electrical demand for technical equipment (Standard Norge, 2014). The energy consumption of the BTES will be compared to the already existing BTES in DLSC.

2.11 Geology

Geology is the study of the structure, evolution, and dynamics of the earth and its resources and how they have evolved through time. Underlying this definition is the study of rocks, sediments, and permafrost and all their abilities such as strength, heat capacity, permeability, and thermal diffusivity.

2.11.1 Bed rock heat storage

There are many different types of rock where each type has its unique heat capacity, strength, and permeability. There are three main categories with many of different subcategories; they are igneous, sedimentary and metamorphic.

Each type of rock has a distinctive ability to absorb heat. This ability is expressed through its specific heat capacity (C_v) and is unique for each type and geographical area in which the stone resides. Heat capacity is a measurement of how much energy a substance absorbs to rise one Kelvin. This capacity in coherence with the materials thermal conductivity and density is decisive for rocks ability to store energy.

Rocks thermal conductivity are mainly dependent on the internal structure. Porous stones have a higher thermal resistance/lower conductive ability. The increase in thermal resistance is because all natural pore filling substances have lower conductive abilities than rocks. Equation 43 illustrates how different saturations effect the conductive abilities of rocks. (Lee. K.S., 2013)

$$k_{eff} = nk_l + (1 - n)k_s \tag{43}$$

Where k_{eff} is the effective thermal conductivity, n is the share of liquid saturation, k_l is the conductivity of the liquid, and k_s is the conductivity of the solid rock.

Temperature has also proven to have an impact on the rock thermal conductivity, higher temperatures decreases the conductivity of the stone. In 1971 Kutas and Gordienko proposed the following empirical formula for estimating the thermal conductivity of sedimentary formations up 300°C, the equation has a presicion level of ±5%:

$$k_T = k_k - (k_k - 3.3)[\exp\left(0.725 * \frac{T - 20}{T + 130}\right) - 1] \tag{44}$$

Where k_T is the unknown desired conductivity, k_k is the known conductivity temperature and T is the temperature at the unknown state for conductivity. It should also be mentioned that sedimentary rocks have documented anisotropy ratios, as high as 2.5 horizontally to vertically. These ratios could be economically beneficial to BTES if the values are known, utilizing the information about anisotropy could mean fewer collectors in the storage without disrupting the total power output of the BTES.

Table 1: Thermal properties of different rock types measured in Russia. Source: (Eppelbaum. L et al., 2014)

Lithography	Density [kg/m³]	Thermal Diffusivity [mm²/s]	Thermal Conductivity [W/m²K]	Heat Capacity [J/kgK]
Dolomite	2750	100	2.1	802

Limestone	2700	96	2.2	851
Clayey limestone	2650	91	2.0	844
Argillite	2300	99	2.3	838
Siltstone	2550	108	2.3	795
Siltstone, Oil-bearing	2300	129	2.2	880
Clayey sandstone	2500	143	2.8	915
Sandstone fine grained	2550	72	3.4	844
Sandstone fine grained	2400	105	1.6	845
Sandstone Oil-bearing	2090	125	1.9	876
Sandstone Oil-saturated	2200	116	2.3	737
Sandstone Water saturated	2300	128	1.7	840
Sandstone average	2300	110	2.1	830

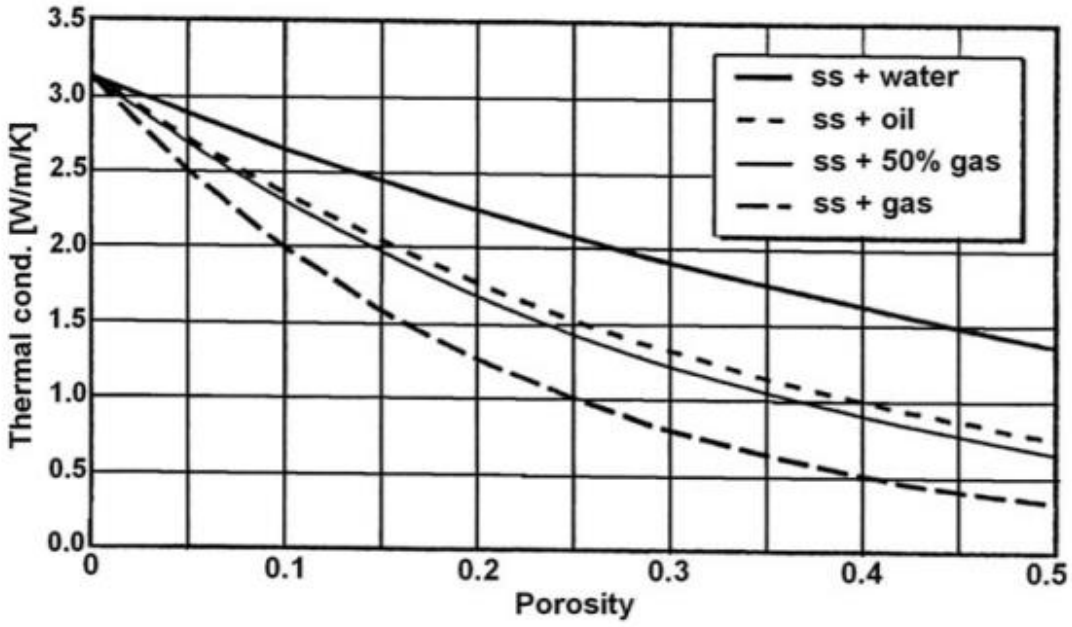

Figure 19: Illustrates how sandstones thermal conductivity changes with types of saturations. Source: (Eppelbaum. L et al., 2014)

2.8 Hydrogen production and storage

Most common production method for hydrogen today is by extraction from fossil fuels(Tidwell. J. & Weir. T., 2006). However, another cleaner way of producing hydrogen is electrolysis of water, and the most common and developed type of electrolysers is the alkaline type. The alkaline electrolysers are recognized by operating in an alkaline electrolyte solution (e.g. KOH, NaOH, etc). In the electrolyte is

an ion-permeable membrane used to separate the anode from the cathode. This membrane prevents the products from cathode and anode to mix, denying development of the explosive gas $H_2 + O_2$ and maintains a chemical stability and safety. It has some other uses as well, e.g. separates the anode and cathode, preventing short circuits etc.

$$Electrolyte: 4H_2O_{(aq)} \rightarrow 4H^+_{(aq)} + 4OH^-_{(aq)}$$

$$Cathode: 4H^+_{(aq)} + 4e^- \rightarrow 2H_{2(g)}$$

$$Anode: 4OH^- \rightarrow O_{2(g)} + 2H_2O_{(aq)} + 4e^-$$

$$Total: 2H_2O_{(aq)} \rightarrow O_{2(g)} + 2H_{2(g)}$$

By assessing the total chemical equation, it is possible to calculate the Gibbs free energy which reveals the amount of energy released or needed to make the reactants react:

$$\Delta G° = \Delta H° - T\Delta S° \tag{45}$$

$\Delta G°$ is the change Gibbs free energy, $\Delta H°$ is the change in enthalpy, T is the temperature, and $\Delta S°$ is the change in entropy. Enthalpy and entropy of the total chemical equation at standard conditions per mol given as:

Quantity	H_2O	H_2	$1/2O_2$	Change
Enthalpy [kJ/mol]	-285.83	0	0	ΔH = 285.83 kJ
Entropy [J/molK]	-69.91	130.68	0.5 x 205.14	$T\Delta S$ = 48.7 kJ

Figure 20: Tabled values for entropy and enthalpy. Source: https://www.engineeringtoolbox.com/standard-state-enthalpy-formation-definition-value-Gibbs-free-energy-entropy-molar-heat-capacity-d_1978.html

Gibbs free energy indicates that the amount of energy needed to decompose water to hydrogen and oxygen is 237.1 kJ/mol. However, these calculations are purely theoretical and do not account for resistances in the circuits, membranes and electrodes which are substantial values (Tidwell. J. & Weir. T., 2006). In addition, most electrolysers operate at higher temperature than the standard condition which increases the contribution of the entropy, lowering the amount of energy needed for a spontaneous reaction.

When converting the hydrogen back to electricity the Gibbs free energy equation is simply reversed. Since there is no intermediate combustion cycle, in other words no heat to work like conventional combustion engines, the fuel cell is not limited by the second law of thermodynamics stated in chapter 2.1. This means that in theory, fuel cells should be able to convert 100% of the chemical energy to electricity. However, this is not the case as there are several resistances within the fuel cell, e.g. dissolving $H_2 \rightarrow 2H^+$(catalysed), the electrolyte penetration resitance, etc. (Tidwell. J. & Weir. T.,

2006). Today Protone Exchange Membrane (PEM) fuel cells can operate at 50-60% efficiency, the remaining 40-50% turning into heat (Thangavelautham, 2017).

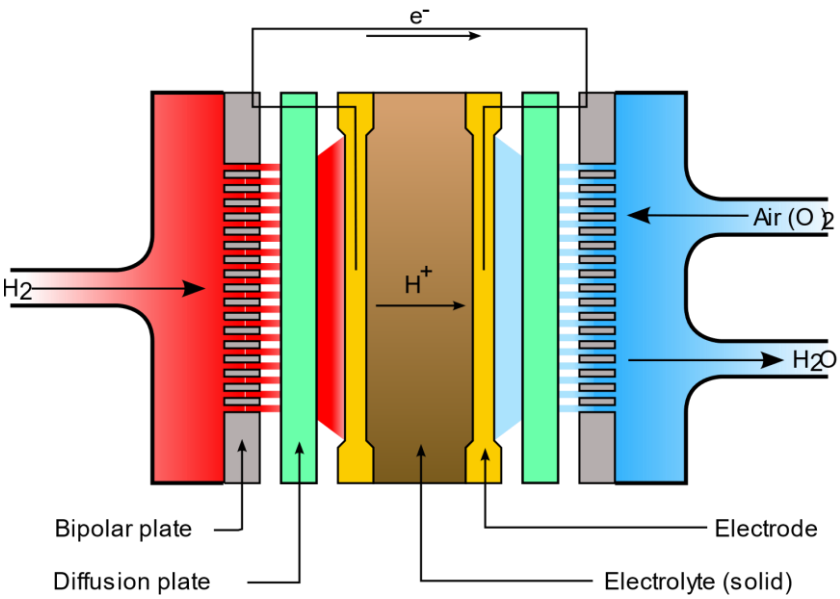

Figure 21: Illustrates the working mechanisms of a fuel cell. Chemical reactions are the same but reversed as stated earlier.

NEL is a global dedicated hydrogen company founded in Norway in 1927. Today they cover the entire value chain from hydrogen production technologies to manufacturing hydrogen fuelling stations.

NEL has developed module alkaline electrolysers which uses an aqueous KOH solution as an electrolyte. Alkaline electrolysers are a mature technology which allows remote operations of stationary applications.

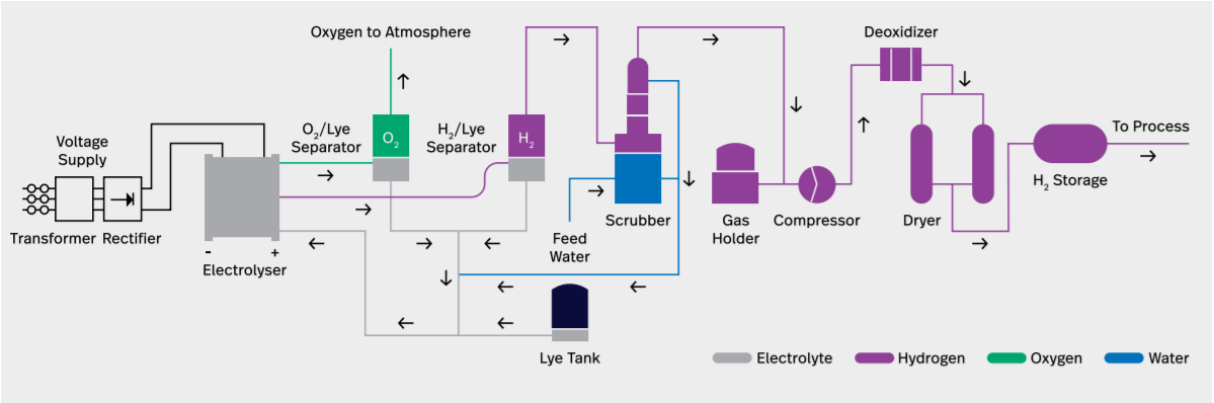

Figure 22: Process diagram for alkaline electrolyser. Source: NEL

Sited with some modifications from NEL brochure:

“The transformer and rectifier convert the AC voltage supply into DC current input. Keeping the same polarity on the electrodes always. The electrolyser is of the filter press type with bipolar electrodes separated by non-asbestos membranes. Hydrogen gas is generated at the cathode and the oxygen gas at the anode. This module consists of two gas separators and the electrolyte recirculation system. The

electrolyte is recovered in the separators, then chilled and recycled into the cell block. The scrubber has three primary functions:

• Remove residual traces of electrolyte

• Cool down the hydrogen

• Feed water tank

The gas holder is a buffer tank installed between the electrolyser and the compressor or the process at the site. If required, a compressor is installed to compress the gas from atmospheric pressure in the gas holder to the pressure required for the process or the storage vessel. Hydrogen generated in the electrolyser is very pure gas, saturated with water, and its oxygen content does not exceed 0.2%. If higher purity is required, the last molecules of oxygen can be removed by a catalytic reaction in a deoxidiser. The dryer will dry the gas to reach the suitable dew point. It consists of twin towers filled with a desiccant to absorb the water. The gas storage provides a backup solution or ensures the hydrogen make-up for batch applications with uneven gas consumption". (NEL, 2018)

There are many commercial developed systems in use today, so this thesis will only focus on energy storage with capacity to resolve peak loads on Longyearbyen's solar community. Hydrogen are a perfect storage in such an example as it is possible to expand the park to the power output needed.

Hydrogen has a high gravimetric energy density; however, the volumetric energy density is low which causes a challenge for storage. Metal hydride storage is hydrogen stored in the metal of a material. By doing so, it is possible to store hydrogen both safer, at low pressures, and with a higher energy density than compressed or liquidised hydrogen. However, the most likely cheaper option on a big scale energy storage would be compressed hydrogen. This issue will be further discussed in the discussion after dimensioning of the system and the results on peak load.

The molar volume of an ideal gas under standard temperature and pressure conditions, respectively one atmospheric pressure and 273,15K, is 22,4 L/mol. Because of the low density of hydrogen, it needs a high pressure or a significant volume of storage. The ideal gas law provides the amount of gas stored concerning the pressure, volume and temperature.

$$PV = nRT \tag{46}$$

Where P is the pressure, V is the system volume, n is the quantity of gas in mol, R is the ideal gas constant and T is the temperature.

If in some cases with extremely high pressure or low temperatures, it might be necessary or sensible to consider the van der Waals equation instead:

$$\left(P + \frac{an^2}{V^2}\right)(V - nb) = nR_sT \tag{47}$$

Where a and b are Van der Waals constants for the specific gas and R_s is the specific gas constant.

The reason why Van der Waals must be examined at high pressures is because the two Van der Waals constants account for the fact that the gas molecules interact with each other and possess a volume. These assessments are neglected in the ideal gas law. The constants a and b are specific to each gas. In high-pressure systems, the molecules have less free space which means they are interacting more with each other. Higher pressure means more uncertainty in the ideal gas law.

2.8 Thermal response test of the bedrock

Thermal response test is a method developed to determine the conductive capabilities of the bedrock storage and the thermal resistance in the energy well. Because of local variations, thermal response tests need to be performed on each site. The values determine different parameters such as energy loss through conductivity, the power output of the wells, the distance between the wells to avoid thermal short circuits and so on. The test is performed by circulating water with a constant heat source above ground. By measuring the volume flow and heat of the fluid in and out of the well, it is possible to calculate the amount of energy absorbed by the rock. (Gehlin, 2002)

2.9 Dimensioning of power systems/energy usage for the heated structure

This subject is vast and technologically challenging, consultants all over Norway have different approaches to how they calculate and restrain their system. However, Norsk Standard has published a guideline on how to calculate heat losses and electricity needs in buildings. In this thesis, the standard NS3031 has been used as a guideline for calculations. The reason for this approximation is that several of these heat losses are dependent on systems that need to be detailed by different engineering departments. Data which is too significant to retrieve for a master thesis.

3 Background and Technology

3.1 Structuring the Borehole Thermal Energy Storage

Heat loss through the BTES is calculated by Fourier's law of conducting (eq.1). Depending on the layers of rocks and sediments of the borehole, the heat losses and temperature gradient are almost linear proportional between the BTES and the surroundings. It is therefore sensible to construct the BTES in zones, keeping a hot centre and lower temperatures at the edge reduces the heat losses to the surroundings. The low temperature storage will deduct heat from the medium temperature storage and

the medium storage will deduct heat from the high temperature storage. Nevertheless, the heat is kept within the BTES and can still be utilized.

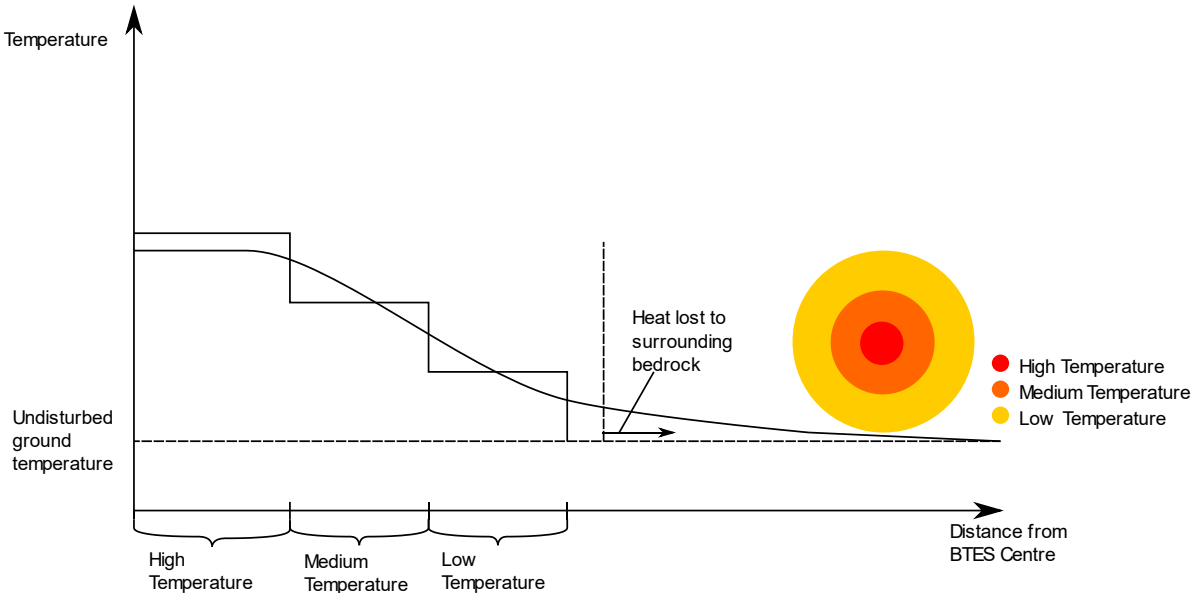

Figure 23: Illustrates the heat transfer in the energy well. By keeping a high temperature in centre of the BTES it can conduct heat to lower temperature zone within the BTES where it still can be utilized. Low temperatures in the outer rim is beneficial as ΔT to the surroundings is a low value. (cf. eq.1). Source: (Flatner, 2017) ,modified

Heat lost to surroundings is dependent on a volume to area ratio. Suppose the desired volume is found, it is then possible to minimise the surface area of the storage by a simple optimisation problem, however, these optimisation problems are slightly different depending on design. Assuming a cylindrically shaped heat storage with an isolated, top the optimum shape can be found by equation:

$$\frac{dA_{cyl}}{dr} = -\frac{2V_{cyl}}{r^2} + 2\pi r = 0 \tag{48}$$

And by assuming uninsulated top, the minimum area can be found by:

$$\frac{dA_{cyl}}{dr} = -\frac{2V_{cyl}}{r^2} + 4\pi r = 0 \tag{49}$$

Where A_{cyl} is the surface area of the uninsulated surface, V_{cyl} is the desired volume of the storage and r is the radius of the storage. When discussing heat storages, an often-used term is shape factor. The shape factor of a storage is given as a ratio of diameter to depth of the storage. In case of a insulated top the optimum shape factor would be equal two, and for an uninsulated top the optimum shape factor would be equal one.

3.2 Collectors

Transporting heat from sun collectors to the bedrock storage are done through energy wells (often called collectors) which work as an underground heat exchanger. In this thesis, the focus is on coaxial wells, a tube in tube system that consists of a water inflated flexible tube pressed towards the rock

foundation and hot water flowing down through the middle in an insulated tube. As the hot fluids float out in the outer tube, it rises and gives off heat to the lower temperatures in the rock storage through convective heat transfer. The heat is then absorbed and distributed in the rock by conductive heat transfer. The speed in which the heat distributes is therefore dependent on the wells resistance and the thermal conductivity of the rock(Gehlin, 2002).

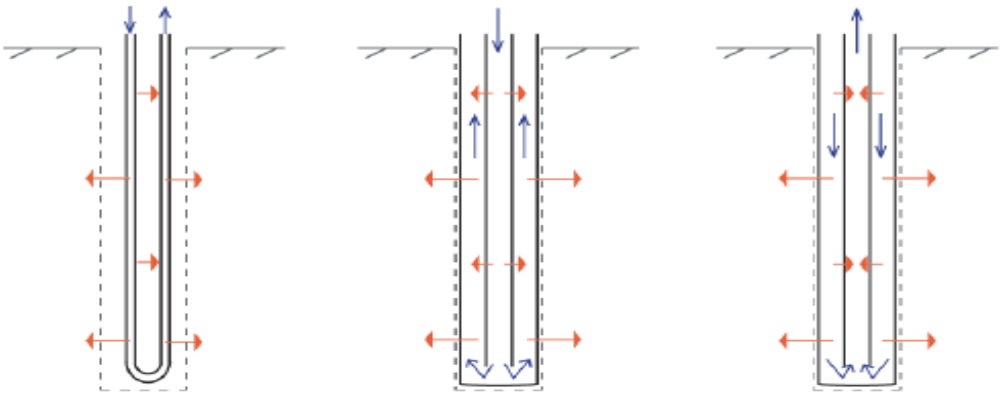

Figure 24: From left to right illustrates u-pipe and coaxial pipe heat exchangers. The blue arrows illustrate medium flow direction; the red arrows illustrate heat flow direction. All are during charging of the well. Source: (Flatner, 2017)

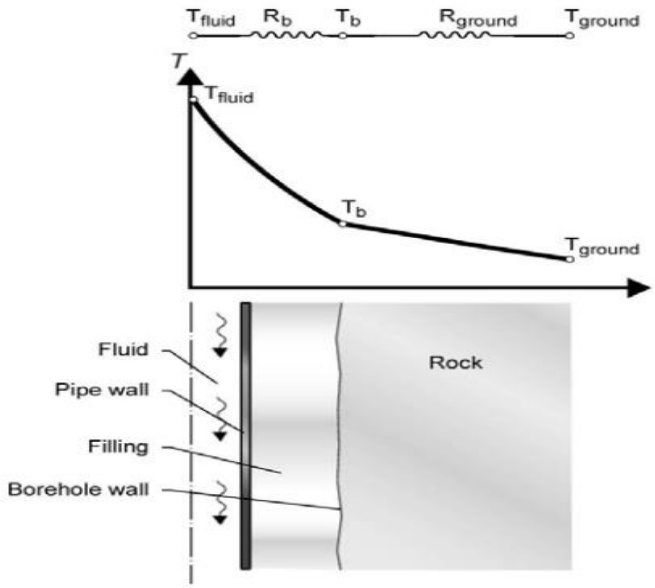

Figure 25: Shows the temperature gradients and the thermal resistances between the well and bedrock storage. Source: (Gehlin, 2002)

4 Method

4.1 Dimensions and assumptions related to the heated structure

Heat storage is the fundament for a sustainable society at Svalbard, and the size of this storage is dependent on how much of the society that needs energy. In general, the bigger the storage is, the

better, so depending on the result, a pipe grid for heat distribution should be considered if the dimensions allow it. By inspecting the relation between heat dissipation through the surface area compared to the volume increase and overall heat capacity of the storage, bigger storages will have higher capacity and lower losses. However, there exists an optimal trade-off between volume and area increase. By deciding the amplitude in which the temperature of storage is allowed to operate in it is possible to design the optimal shape factor by solving eq. 47 and 48.

When dimensioning the indoor heated area on Svalbard, the following assumption was made for conductive heat transfer:

South to north wall	100m	
East to west wall	300m	
Hight South wall	7m	
Hight North wall	15m	
Share of wall	80%	
Share of windows and doors	20%	
U-value wall	0.18 W/mK	Tek 17
U-value roof	0.13 W/mK	Tek 17
U-value doors and windows	0.8 W/mK	Tek 17
Normalized Thermal bridge value	0.07 W/mK	Tek 17
Volume of building	330000 m^3	

Following assumption were made for ventilation losses:

Preaccepted performance office area	15 m^3/per person	Tek 17
Pollution of air per person	26 m^3/h	Tek 17
Material pollution	3.6 m^3/h per area	Tek 17
Total ventilation demand	73000 m^3/h	
Airsubstitution per hour	0.48	
Temperature efficiency of heat dissipation	83%	Typical value ± 3% source: Magnus Kleven

It is also assumed that the ventilation always runs and has no reduced ventilation hours.

Following assumption were made for infiltration losses:

Leakage number at 50 Pascal	0.6	Tek 17

f-terrain coefficient	15	Table A.5 NS3031
e-terrain coefficient	0.1	Table B.6 NS3031
Volume air supply	73000 m^3/h	
Volume air extraction	73000 m^3/h	
Infiltration	0.06	Equation 32

The following assumptions were made for internal heat supplements:

Total solar factor g_u	0.4	Table E.2 NS3031
Irradiation intensity wall	644 kWh/m^2year	
Total Area window	1700 m^2	
F_s	0.9	E.2 NS3031
q_{light}	47 kWh/m^2year	Table A2 NS3031
q_{eq}	6 kWh/m^2year	Table A2 NS3031
q_{per}	5kWh/m^2year	Table A2 NS3031
q_{fan}	1.76 W/m^2	
Area	30000	m^2

The following assumtions were made for the electricity demand:

SFP factor	1.5 $kW/m^3/sec$	TEK 17
SPP factor	0.5kW/l/sec	Table I.1 NS3031
Lights	47 kWh/m^2year	Table A2 NS3031
Equipment	6 kWh/m^2year	Table A2 NS3031
Heated water	30kWh/m^2year	Table A2 NS3031

4.2 A safe supply of energy

The bedrock storage secures supply of low-quality heating. This storage will maintain a heat reserve adequate to supply the indoor society, and hopefully other buildings such as warehouses, old settlements or even a port of refuge if necessary.

The electrical energy supply is four- or five-fold with the microwave pyrolysis, wind power, PV, biodigester and hydrogen storage in combination with fuel cells. To secure safe energy supply there must exist some forms of independent energy combinations which are adequate to supply the a necessary load of electricity demand for an extended period of time.

The project looks at the possibility to store hydrogen gas in polyethene pipes. These pipes are cheap to produce, gastight and can be welded together to fit within big mining systems in Longyearbyen. However, the most common conventional type of storing hydrogen today are by pressurized hydrogen in steel tanks. (Halvorsen, 2018)

4.3 Energy storage for electricity

4.3.1 Waste material

For many years, waste have been either burned, dug down or deposited in Longyearbyen. Starting in 2007 the Longyearbyen community has sent their waste to the Norwegian mainland for treatment and recirculation. Waste could represent a significant energy contribution. In fact, Longyearbyen produced 1530 tons of waste in 2015, that is 700kg of waste per person. These numbers do neither consider that Svalbard food waste is flushed out into the sea nor that the biggest industries on the island manage their own transportation of waste, therefore, the amount would be considerable higher.

Adding to this is the local community commitment to keep a clean and healthy environment on the Island. Every year under the direction of the community council is a cleaning day of the coastline around Svalbard. The last two years these cleaning projects has brought in 81 tons of waste mostly plastic which contains aproximatly 4MWh/ton of electricity when pyrolysised using MAP.

4.3.2 Hydrogen Storage

4.4 Bedrock storage

The temperature of the bedrock storage must be decided in conjunction with the climate solar collectors operate in and the minimum required heat in the distribution network. Svalbard has a cold arctic climate which presents two main challenges, firstly, it is not possible to operate sun collectors at high temperatures without substantially lowering the efficiency, and secondly, the power output necessary to keep the construction at the desired temperature are high. Nevertheless, the irradiation received in Svalbard should be enough to maintain a decent temperature in the BTESs medium and low temperature zone. In addition, the MAP creates almost as much heat as electricity and generates its electricity from a gas turbine. (Kasin. K.I., 2018) These turbines operate with an exhaust temperature of 370-590℃ meaning that a desired high temperature from the MAP can be directed to the centre of the BTES.(Toolbox, n.d.)

4.5 Bedrock Storage simulation in MATLAB

MATLAB is a programming platform designed for engineers and scientists. In this thesis, the software was used to program a simple one-dimensional heat transfer problem to calculate heat dissipation from the storage. The script is presented in the Appendix.

When calculating the bedrock storage capacity, it was necessary first to detect the amount of energy effectively captured by the sun collectors. These amounts were then used to find the most volume to

area efficient cylindrical shape to effectively constrain heat losses which are linearly dependent on the surface area. To find the energy losses in the storage a simulation model in MATLAB was created. The model that simulates the one-dimensional heat equation were based on the one dimensional heat eqution provided as:

$$\frac{\partial T}{\partial t} = -k\frac{\partial^2 T}{\partial x^2} \tag{50}$$

Where T is the temperature equation with respect to time, x is the length, and k is the materials conductivity. The temperature equation, and the solution to the heat diffusion equation was derived from a simple analysis of the energy balance in the system (see figure 39).

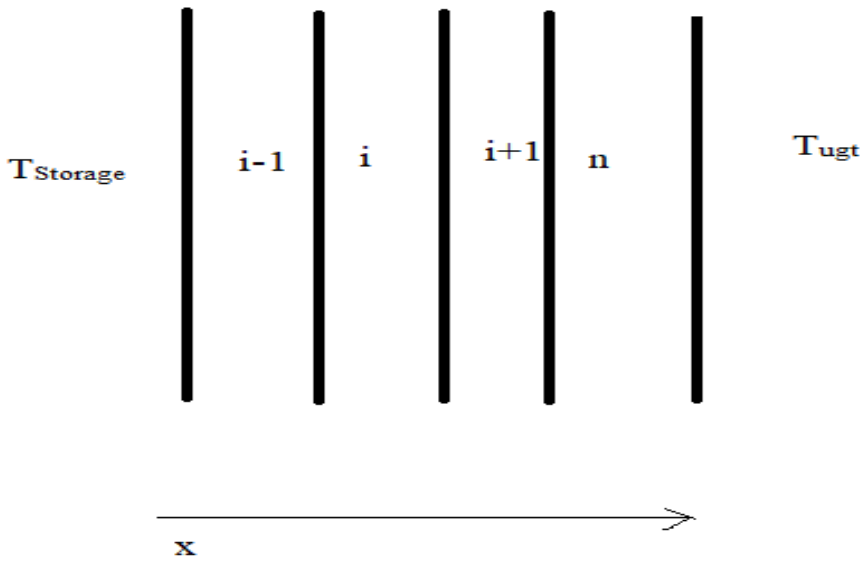

Figure 26: Shows an interpretation for the equation below. T_{ugt} is the temperature of the unaffected ground.

By numerically solving the equation:

$$\frac{dT_i}{dt} = \alpha\left[-\frac{T_i - T_{i-1}}{\Delta x^2} + \frac{T_{i+1} - T_i}{\Delta x^2}\right] \tag{51}$$

, where α is the thermal diffusivity of the material [$\alpha = \frac{k}{c_p \rho}$], and by use of forward Euler method as a simplification which states that:

$$T(t + \Delta t) \approx T(t) + \frac{dT}{dt}\Delta t \tag{52}$$

MATLAB can simulate a temperature gradient spreading out of from the storage through the surrounding ground. See appendix for MATLAB code.

4.6 Climatology Data from NASA and eklima

NASA provided the insolation datasets. These data are based on satellite data and has a resolution of 1x1 degree longitude and latitude (approximately 111x23km at N78°). NASA provided the same data for wind. Temperature, on the other hand, was supplied by eklima, a web portal which provides free access to the climate database of the Norwegian Meteorological Institute. These datasets were extracted from on sight instruments and have been quality checked by the Norwegian Meteorological Institute to ensure its credibility. The temperature is used when calculating the buildings heat loss as well as the efficiency of the sun collectors. Temperature is also of importance when calculating the efficiency of PV modules. However, these calculations are not of importance for this thesis as we can use existing data from Longyearbyen Airport

4.7 PVsyst and Excel

PVsyst is a software that can retrieve data in a 1x1 degree area from NASA and utilise those data to predict the locations insolation. The satellite data were used because of difficulties in finding real ground data from the location. Even though Svalbard airport has produced solar energy for 2016 and 2017 it is essential to use data over a larger timespan to rule out yearly fluctuations in solar radiation, temperature etc. However, the energy production retrieved from the technological supervisor of the Longyearbyen airport can, by comparing the 2016 and 2017 data with a climat normal year, be a good approximation to calculate future PV production.

PVsyst is a complex software, but like every other software, it is essential to be aware of the data put into the software to decipher the results. It was therefore found necessary to retrieve the datasets manually from NASA to do much of the work in Excel as an extra control. Excel is a spreadsheet software and added value to this thesis by being able to express big datasets figuratively and by statistical analysis. However, Excel is more sensible to human mistakes and can not do as detailed calculation as PVsyst.

PVsyst possesses a more flexible and advanced simulation method that can accommodate several situational analyses at the same time. e.g. shading from mountains, buildings specific calculated on an hourly basis to the suns orbit. It also accounts for mutual shadings from sun collectors etc.

4.8 Waste Datasets

When creating the waste datasets and the composition of combustible residual waste, it was sensible to compare the datasets with those from the Norwegian mainland. Another challenge where the actual efficiency of the microwave pyrolysis with respect to different waste materials. To calculate the potential electrical energy gain from waste, it was necessary to develop an uncertainty model that through Monte Carlo simulation comprehended uncertainties in quantities, energy potential, and waste composition of all waste materials. The model was run through a plug-in software in excel called

Oracle Crystal ball. The simulation presented cumulative distributions which gave a more intuitive presentation of the energy potential in all the waste materials.

When constructing the monte carlo simulation, the following assessments were made: uncertainties in water content for dielectric losses, heat of combustion for waste materials compared to laboratory results from Scandinavian biofuels, and uncertainties in material within certain classes of waste were made. E.g. wood has a heat of combustion 12% higher than paper, however, the wood will contain more water contributing to dielectric losses. In the simulation, wood only have 10% higher expected energy output and the percentile values vary more due to higher uncertainty. In textile, there are many various materials containing different amount of energy. Nylon and fleece are examples of high energy textile, while cotton is the opposite.

4.9 Biogas Reactor

When calculating the biogas output some assumptions where made. Based on an article published on NCBI (E. et al., 2015) it is assumed that a average human in high income countries produces 28g of dry feces per day. In Longyearbyen, that would be approximately 60 kg of dry human feces per day. The fluid volume would then be, based on equation 26, 1.2 m^3/day. Based on the cold climate at Svalbard it is assumed a retention time of 20 days in the digester, used to calculate the size of the digester. The yield of biogas per dry unit human feces and vegetables is assumed to equal 0.3 m^3/kg. Efficiency of a biogas generator is typically set at 25% (Tidwell. J. & Weir. T., 2006).

Water content of popular vegetables varies between 80-95% making them a better option for a bio digester rather than microwave assisted pyrolysis.

4.10 Wind

Wind datasets where downloaded from NASA (NASA, 2016). Both daily and monthly. These datasets contained wind speed 2, 10 and 50m above ground. Based on the 10 and 50m monthly values, the ground roughness factor where calculated with respect to equation 19. Further calculations show a monthly wind distribution which gives an idea of the production distortion over a year.

Further processing of data extended to discovering the Weibull distribution and the Weibull shape factor. These calculations were performed with the built-in software data analysis and problem solver in excel. The software's were applied to a developed spreadsheet containing equation 20 and 21. The Weibull distribution factor where calculated by using daily values over a time span of 34 years.

4.11 Incident solar power

In calculations of the incident solar power, datasets from NASA has been treated in both PVsyst and Excel. Excel provided a better overview of the dataset while PVsyst has built-in simulation methods which provides more accurate simulations of the total energy irradiance on a tilted plane.

4.12 Geology in Longyearbyen

Longyearbyen geology is dominated by two young chapters of earth history, the Cretaceous and Tertiary period are fixed on top of each other. The oldest, and most interesting period for this thesis is the early Cretaceous period (145-100million years ago) which constructs the fundamental layer in Longyearbyen area. The characteristic sediments of the area are green and grey successions of sandstone and mudstone (Hübner, 2012). By investigation of the Svalbard map, published by the Norwegian Polar Institute, it is evident that the bedrock of Longyearbyen consists of clastic sedimentary rocks, mainly sandstone (Institute, n.d.). Calculations of bed rock storage are therefore based on the thermal capabilities of the average sandstone presented in table 1.

5 Results

5.1 Heat loss calculations and energy demand for heated structure

Table 2: Shows the energy needed per year for heating the indoor area to 17 °C, the degree day figure is calculated on an average from 1981-2010 in Longyearbyen weather station.

Heat loss section	Heat loss number	Unit
Walls	1 267	W/K
Roof	3 912	W/K
Ground	-	W/K
Windows and doors	1 408	W/K
Thermal bridges	2 100	W/K
Infiltration	4 574	W/K
Ventilation	9 085	W/K
Total heat loss	22 346	W/K
Average Power output (dT=27)	603	kW
Max Power output (dT=57)	1 274	kW
Degree day figure 1981-2010 (17°C)	7 839	K*h
Total energy loss	4 204 136	kWh
Total internally generated heat	1 272 528	kWh
Total transmission heat sun	408038	kWh
Total energy needed from heat storage	2 523 570	kWh

The table provides an overview of the significant heat losses in the structure. Infiltration, ventilation and conduction through the roof are the most significant contributors to the heat loss. Notice that the ground value is not present. That is because the ground underneath the building will contain the heat

storage. By deliberately insulating this storage poorly, it would provide a negative value to the table above.

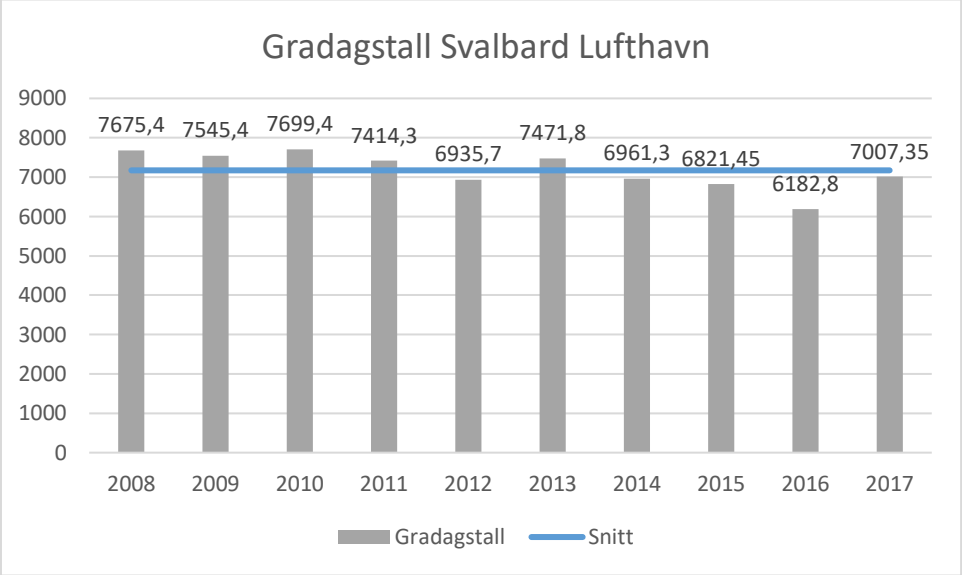

Figure 27: Shows daily degree figures from 2008 to 2017, Data downloaded from the Norwegian Meteorological Institute through eklima. Based on these figures, the degree day figure presented in table 2 may seem high, however, the table 2 value has a considerable longer timespan

The daily degree figure trends downwards which indicates a rise in the temperature of the last decade. However, this is just an observation as a timespan over nine years does not give any basis to forecast any further rise in temperature. Then again, a report released by the Norwegian Meteorological Institute forecasts different pollution scenarios impact on Svalbard, all of which anticipates a rise in temperature(Isaksen, 2017).

5.2 Electrical energy demand for heated structure

The electrical demand on the house has been calculated based on NS3031 and are presented in table 3

Table 3: Presents the total electrical energy demand for the heated structure, it also provides information where the energy is used

Energydemand	**Amount**	**Unit**
Fans	584000	kWh
Pumps	106 649	kWh
Light	1410000	kWh
Equipment	180000	kWh
Heated water	900000	kWh
Total	3.18	GWh

Table 3 presents the required electrical energy supply to run the heated construction. These values are based on the following assumptions. Fans are calculated with an SFP factor of 1.5 kW/(m^3/s). Pumps are calculated with the assumption of waterborne floor heating, dT = 6°C. Based on equation 39 and table I.3 circulated water amount was found to be 24.35 l/s. All NS3031 tables presented an uptime on the circulation pumps of 5300 hours. In this case it is assumed 8760, constant circulation of heat as the building is located in the arctic with 365 heating days. Lights are assumed after the hotel standards, this represents a relatively high energy cost. Equipment and heated water are calculated after hotel standards. The total should represent an overestimate of the needed total.

5.3 Wind Power

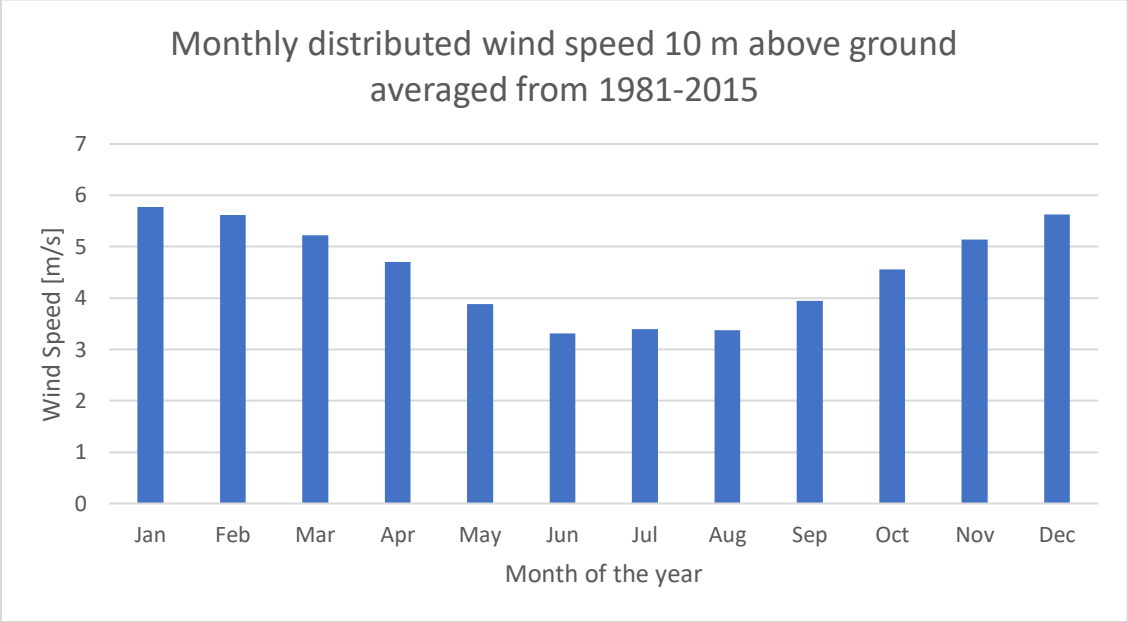

Figure 28: Graphs the monthly distribution of the wind speed 10 m above ground. This distribution is based on NASA satellite data from 1981-2015

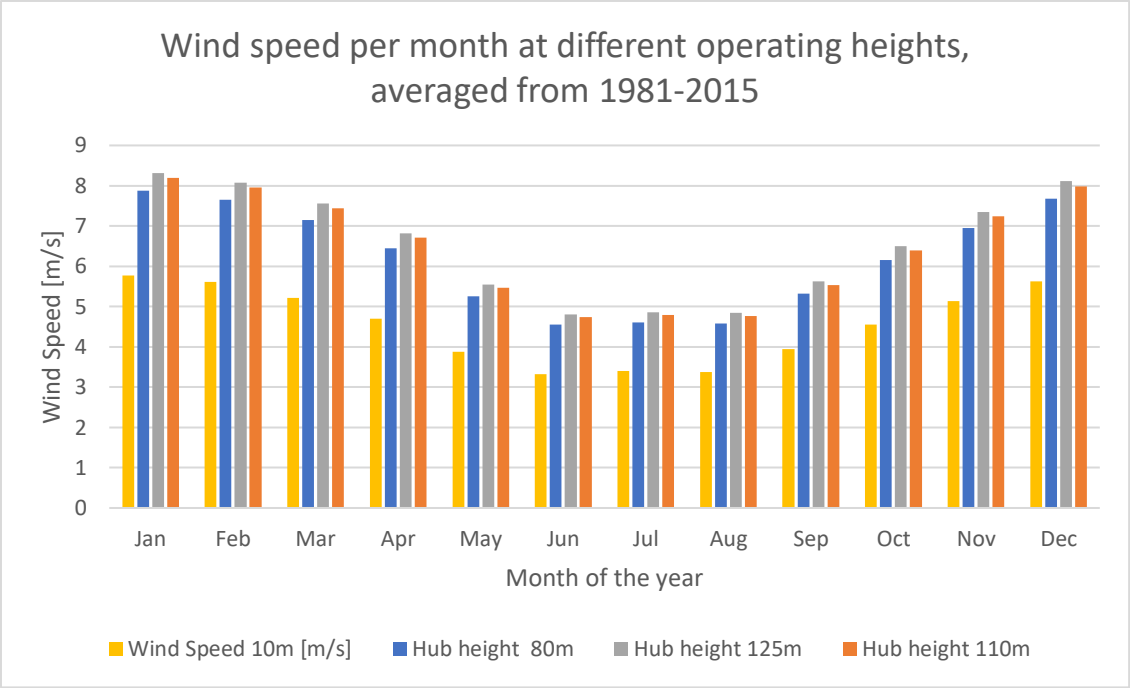

Figure 29: illustrates the monthly distribution of the wind speed at hub heights, in this case, 80, 110 and 125m above ground. This distribution is derived from NASA's satellite data from 1981-2015. The ground roughness coefficient z_0 is numerically calculated to be 0.03 in the area based on the 10 and 50m data collected from the satellite data.

By use of the logarithmic equation 19 to profile the wind, the wind distribution at different hub heights is shown in the figure above. The figure reflects that the average wind is distributed ideally compared to when the energy is needed for electrical applications such as electric lights, warm water heating and other household application that need high-quality electrical energy. An interesting observation is that the distribution can be observed like a normal distribution.

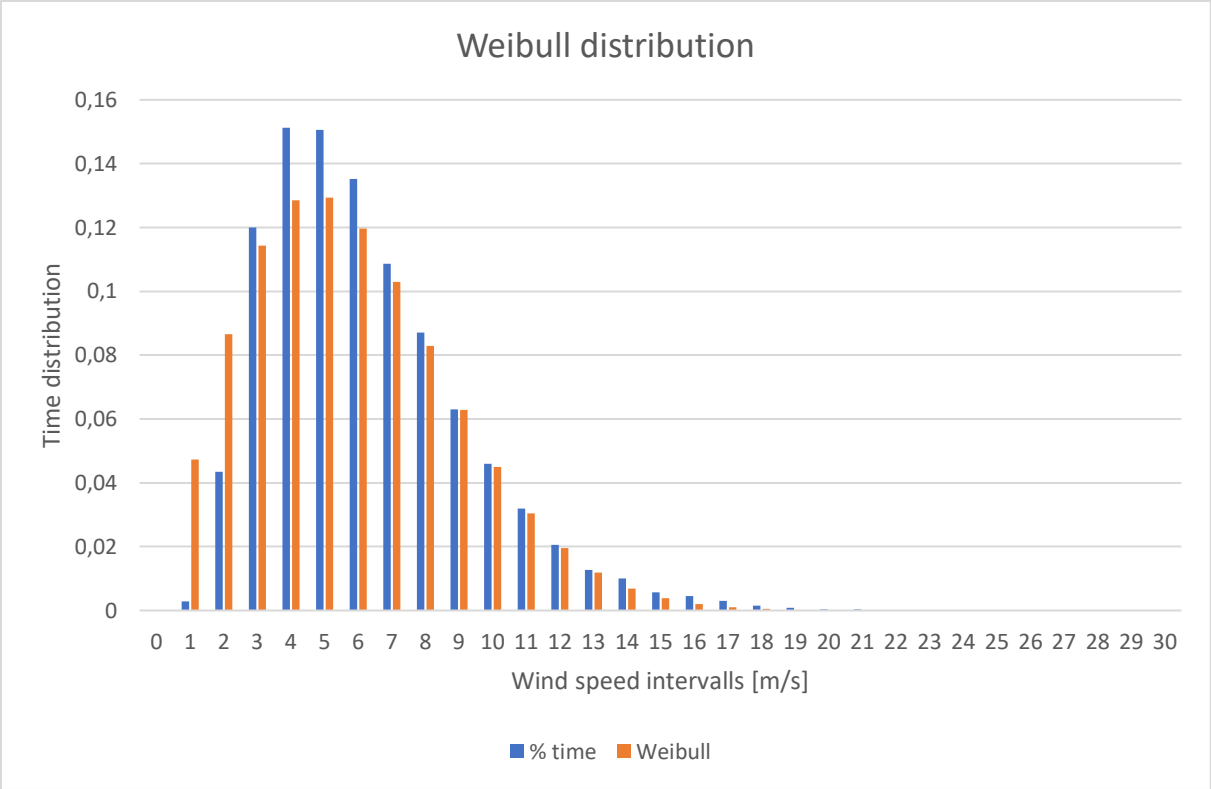

Figure 30: Shows the original data and the best fit Weibull distribution. These data were used to calculate the Weibull shape factor. Coincidentally this k factor equalled 1.98 ≈ 2, fitting the AEP curve from Vestas well (fig.31), meaning the average expected production presented in the curve could be used.

Weibull distribution does not overlap 100% with the measured data. However, figure 30 points to a good consistancy between the real data and the Weibull distribution curve. The Weibull distribution can be used to calculate how much of the time is spent within the production limits by equation 22. By inspecting the wind turbine brochure delivered by Vestas it is evident that the cut-in speed and cut-out speed are respectively 3m/s and 21m/s (Vestas, 2017). The time spent within these limits are 63% of the total 8760 hours. However, this number is based on the Weibull distribution which according to figure 19 overestimates wind frequency below 3m/s.

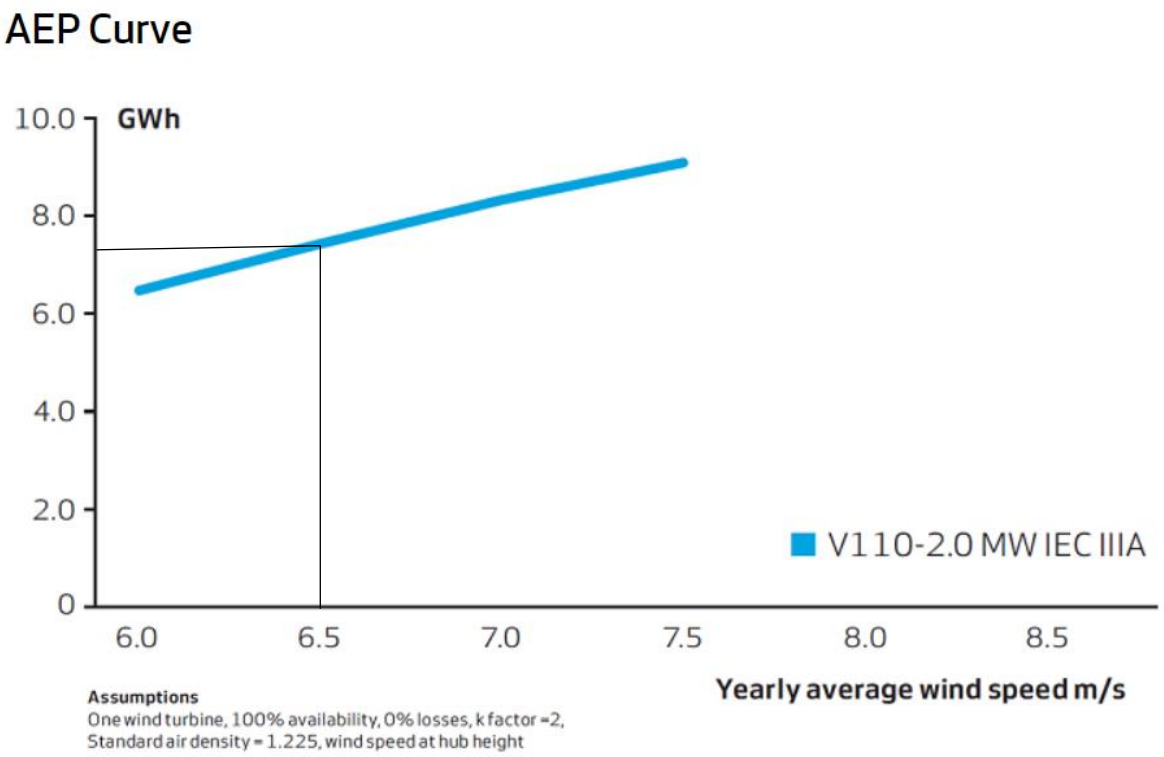

Figure 31: Sample wind turbine (Vestas V110-2.0MW IEC IIIA). The graph represents a yearly production based on the yearly average wind speed at hub height under the conditions listed above. No downtime, zero losses and a k factor equal 2. The air density is somewhat higher as Svalbard resides in an arctic region, the cold climate makes a higher air density.

According to figure 10 and table below, it could be argued that the expected yearly production could be as high as 7,5 GWh per 2 MW installed, this equals a production factor of 42,8%.

5.4 Photovoltaic cells

Based on Svalbard Airport production results it can be calculated that the approximated yearly electricity production of wall mounted PV cells are approximately 0.2GWh per year. 1 kWP ≈ 5m^2 of PV cells. A total possible area on the south wall is 2100, however, calculating windows etc it might be 1800 m^2 of PV meaning a possible kWP mounted is approximately 360kWP.

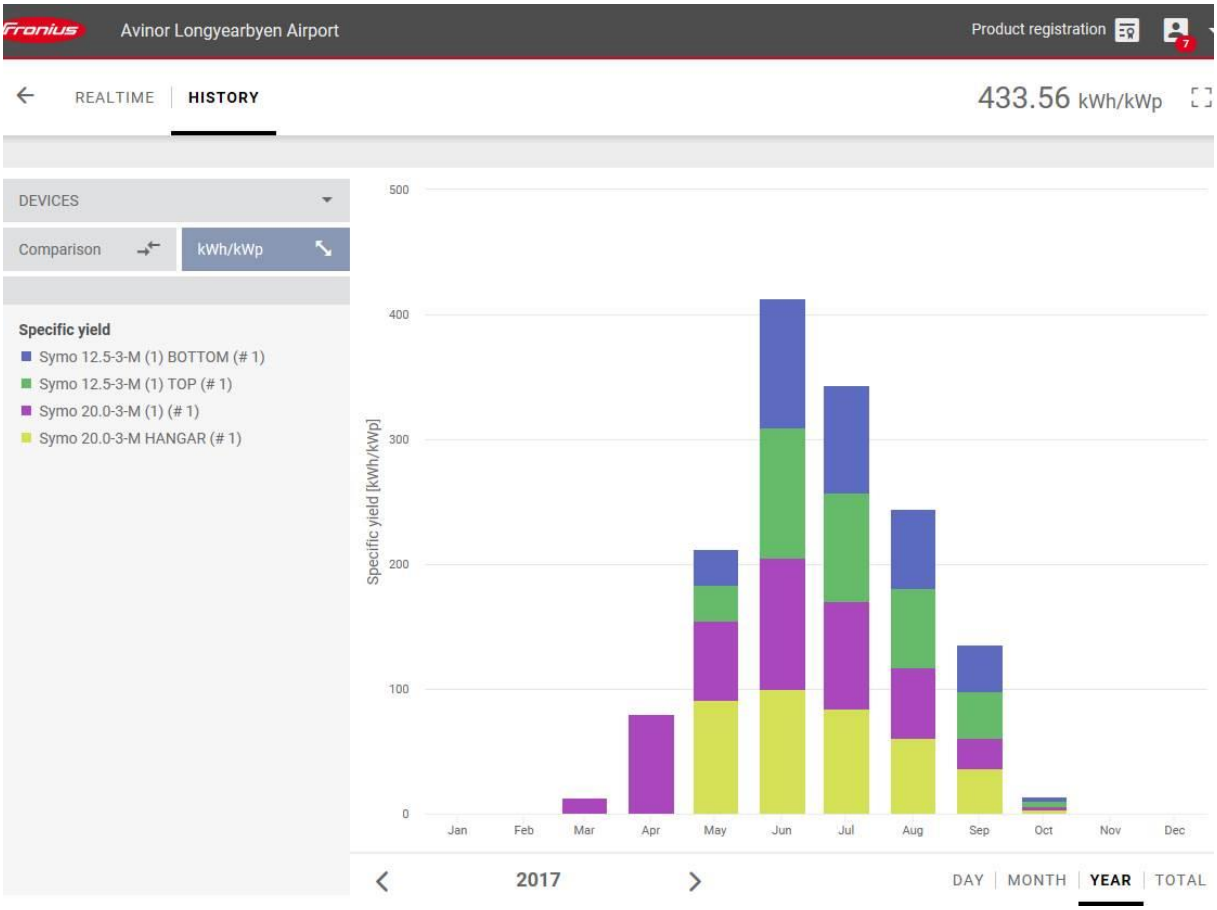

Figure 32: PV production at Avinor Longyearbyen Airport. The figure illustrates a production of 433.56 kWh/kWp.

5.5 Microwave Assisted Pyrolysis of Waste

Table 4: Distribution of waste [kg] in Longyearbyen. (Rasmussen. R.D., 2017), modified

Fraction	2009	2010	2011	2012	2013	2014	2015
Paper	88 210	61 500	106 446	85 411	64 539	28 140	18 710
Cardboard	73 540	68 840	69 682	65 220	62 541	74 940	74 275
Glass	78 440	81 260	83 320	81 420	108 820	75 721	84 052
Aluminium	13 960	14 300	22 235	13 340	12 530	12 310	17 200
Metals	182 490	158 000	169 280	183 140	131 580	133 630	163 010
Gypsum /concrete	252 241	91 180	102 390	111 240	59 940	82 140	85 062
Wood	395 771	66 800	392 126	289 120	396 020	369 790	314 650
E-waste	45 456	33 469	49 899	53 639	44 411	20 000	64 140
Hazardous waste	68 494	60 449	46 100	74 445	43 982	47 550	56 087
Landfill	151 728	93 520	75 410	22 140	12 520	27 070	17 380

Combustible residual waste	1 341 186	1 157 630	745 984	757 740	816 187	817 900	637 256
Sum Landfill	482 409	265 960	261 120	214 800	181 280	184 931	186 494
Sum Recycled	2 209 107	1 620 988	1 601 752	1 522 055	1 571 790	1 504 260	1 345 328
Sum waste	2 691 516	1 886 948	1 862 872	1 736 855	1 753 070	1 689 191	1 531 822
Population	2 017	1 966	2 063	2 090	2 043	2 118	2 189
Waste per person	1 334	960	903	831	858	798	700

Table 5 were collected from the waste management report delivered by Asplan Viak to Longyearbyen community council (Rasmussen. R.D., 2017). However, the value sum landfill submitted in 2010 has been modified due to a deviation in the calculation from all other years.

Table 5 only presents the amount of waste processed by Longyearbyen Community Council. Larger industries such as Store Norske, COOP, and LNS arrange for their own disposal and treatment of waste. Given this information, it is evident that the amount of waste on the island is considerably higher than what table 5 indicates.

Table 5: From Scandinavian Biofuels published documentation on the microwave assisted pyrolysis. The table reflects the maximum electrical energy extraction from waste materials of five microwave pyrloisis machines in series.(Scandinavian Biofuel Company, n.d.)

Feedstock	**Rice straw**	**Bagasse**	**Coconut**	**Plastic**	**Car tires**
Capacity/yr	27 778 tons	28 409 tons	25 000 tons	25 000 tons	25 000 tons
Water content	20 %	20 %	15 %	5 %	1 %
Net capacity/yr	25 000 tons	25 000 tons	25 000 tons	25 000 tons	20 000 tons
Output Oil	13 250 tons	16 250 tons	17 500 tons	12 500 tons	5 600 tons
Output Gas	3 500 tons	3 250 tons	3 250 tons	10 000 tons	3 000 tons
Output Carbon	8 250 tons	5 500 tons	4 250 tons	1 240 tons	11 000 tons
Electricity output	32.4 GWh	39 GWh	38.5 GWh	103.4 GWh	44.5 GWh
Electricity use	3.79 GWh	3.79 GWh	3.79 GWh	3.79 GWh	4.57 GWh

Electricity sales	28.66 GWH	35.17 GWh	34.74 GWh	99.65 GWh	39.89 GWh
Payback/yrs	2.9 Years	2.6 years	2.1 years	1.4 years	2.2 years

Table 5 and 6 is challenging to link together and gives rise to a discussion when trying estimate the total energy potential of the waste on the island.

Table 6 indicates that the capacity of this machine is adequate and can generate energy for several households or bigger industries if necessary. By setting up a Monte Carlo simulation with use of the software Crystal Ball in excel, it is possible to generate data of uncertainties around how much energy it is possible to extract from different waste materials. However, this result is an approximation based on the method described in the second paragraph of 4.8.

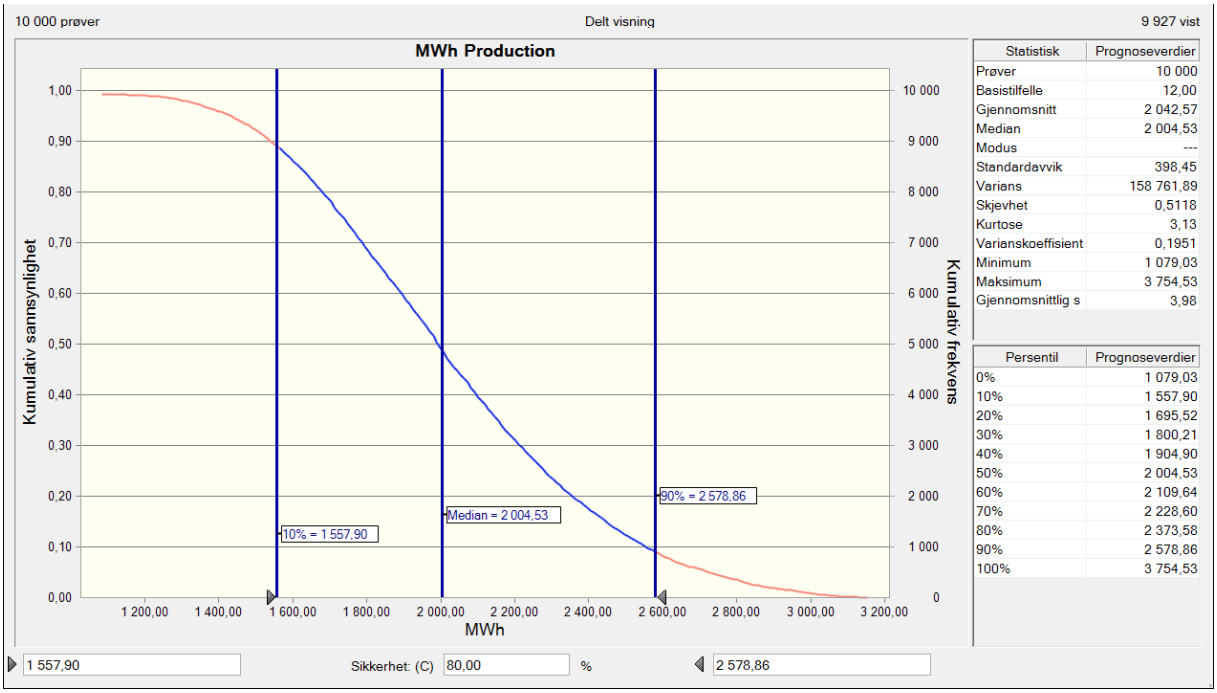

Figure 33: Results from the Monte Carlo simulation. Results are presented in MWh

The figure above shows results from the Monte Carlo simulation. The 10-percentile value represents the lower production estimate. The figure can be interpreted as if it is 80% likely to produce a number in between then 10- and 90-percentile mark, and it is a 10% chance the microwave pyrolysis will produce more or less than the 90- and 10-percentile mark, respectively. It is expected that the pyrolysis will supply 2GWh of electricity per year.

In addition to the electrical production, the MAP produces about the same amount of heat energy which can be supplied to the BTES.

Table 6: Overview of the garbage collected in the seashore from 2015-2017

Litter type	Total amount [kg]	Share
Plastic/polystyrene pieces (unindentifiable)	47790	59 %
Nets and pieces of nets	5670	7 %
Caps/lids	4050	5 %
Strapping band	3240	4 %
String and chord	2430	3 %
Industrial packaging	2430	3 %
Small plastic bags	1620	2 %
Glass bottles	1620	2 %
Plastic food bottles and containers	810	1 %
Plastic Crisp/sweet packets and lolly sticks	810	1 %
Rope (Dimaeter>1cm)	810	1 %
Plastic shotgun cartridges	810	1 %
Cotton Bud sticks	810	1 %
Other items	8100	10 %
Total	81000	100 %

The plastic/polystyrene pieces could in theory supply 95 MWh/year alone based on test results supplied by Scandinavian Biofuels ref. table 6. Note that these numbers are not considered in the Monte Carlo simulation.

5.6 Biogas Reactor

Table 7: Based on a few assumptions the biogas reactor can produce approximately 49MWh of heat per year or 12MWh of electricity. In addition, the digester produces fertilizer containing essential products like nitrogen and phosphorus.

Biogas Reactor		
Dry feces/person	0.03	kg/person*day
Population Longyearbyen	2200	Persons
Dry feces tot	62	Kg
Tot vegetables	100	kg/day
Average water content	1	
Total dry vegetables per day	20	kg/day
Biogas generation per unit dry mass (c)	0.3	m^3/kg
Biogas energy	33	MJ/m^3

V_b	24	m^3/day
Efficiency boiler	60 %	
Efficiency electrical generator	25 %	
Energy (heat)	485	MJ
Energy (heat)	135	kWh/dag
Energy yearly (heat)	49	MWh
Energy electricity	121	MJ
Energy electricity	34	kWh/dag
Energy electricity yearly	12	MWh

A biogas reactor of these production numbers would need a volume of approximately 40m^3. That is based on a retention time of 20 days and a dry matter concentration of 5%. However, this presents only an example, by scaling these numbers the bioreactor could handle more waste, and this option of converting biomass could be particularly interesting when assessing an indoor fish farm and greenhouse.

5.7 Sun power

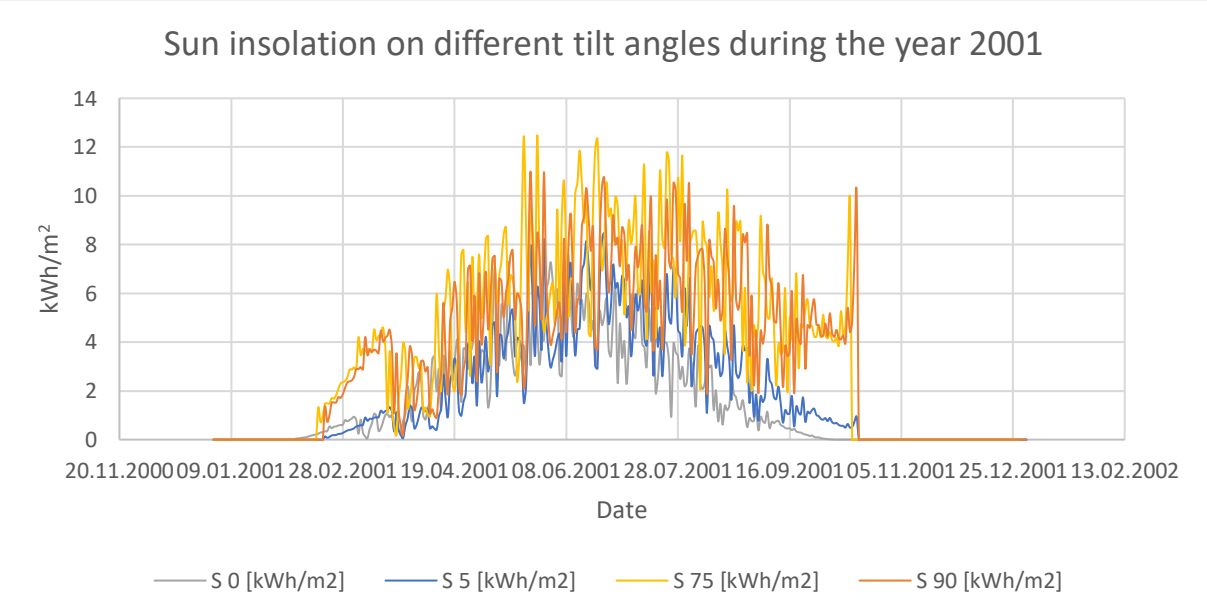

Figure 34: A simplified model from excel which shows irradiation on tilted planes. This model does not incorporate the orientation of the solar collector in its calculations.

Figure 35 is based on equation 9, 10 and 15 and gives a good approximation compared to the PVsyst model represented in figure 36. By computing the area under the graph, it is evident that it is a good approximation accurate within ± 3.5% on angles 75° and 90° however it underestimates 30 %

radiation on the 5° and 0° angles. These values are based on a selection of 10 years. 1981, 1982, 1983, 1991, 1992, 1993, 2001, 2002, 2004 and 2005.

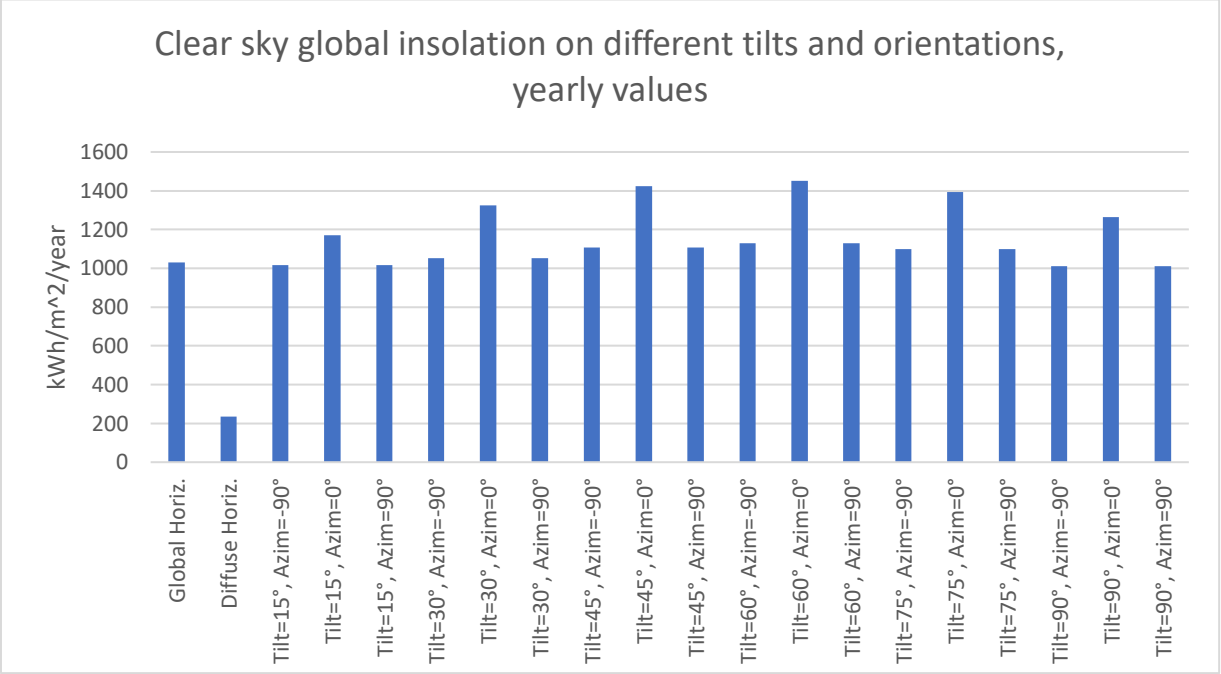

Figure 35: The figure shows, as expected, that a tilt below the latitude degree (60 degrees) is the most sun absorbing. That is because of no winter sun, and the optimal tilt is therefore adjusted for the summer half. However, the result could be misleading if several rows of collectors are mounted due mutual shading. The values represent a climate normal year in PVsyst.

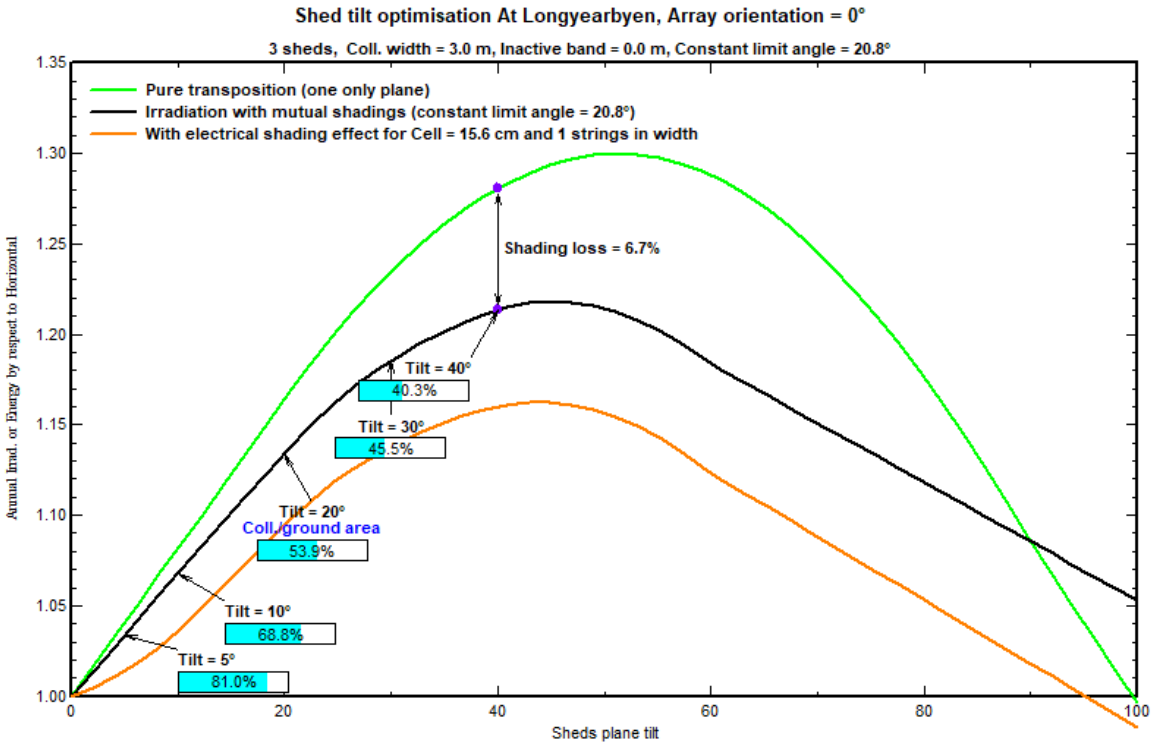

Figure 36: Shows optimal tilt for multiple collector surfaces.

By making use of the software PVsyst, it is possible to receive feedback on how much loss is caused by mutual shading between the solar collectors. This feedback can be obtained by use of the optimisation tool built into the software. Green graph shows the optimal tilt for one shed, black graph corrects for shading losses, and the percentages shows the sun collector to ground area. However, the tilt on the roof is approximately 5°, meaning that there is a 5° offset value. The 45° angle will therefore only experience the 40° mutual shading loss.

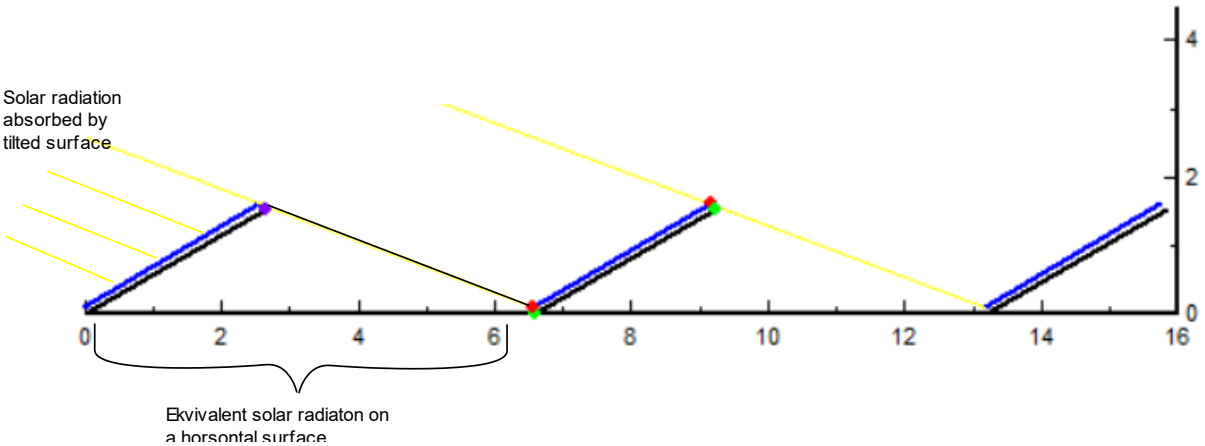

Figure 37: Illustrates that a tilted surface absorbs more radiation per m^2 than a flat collector.

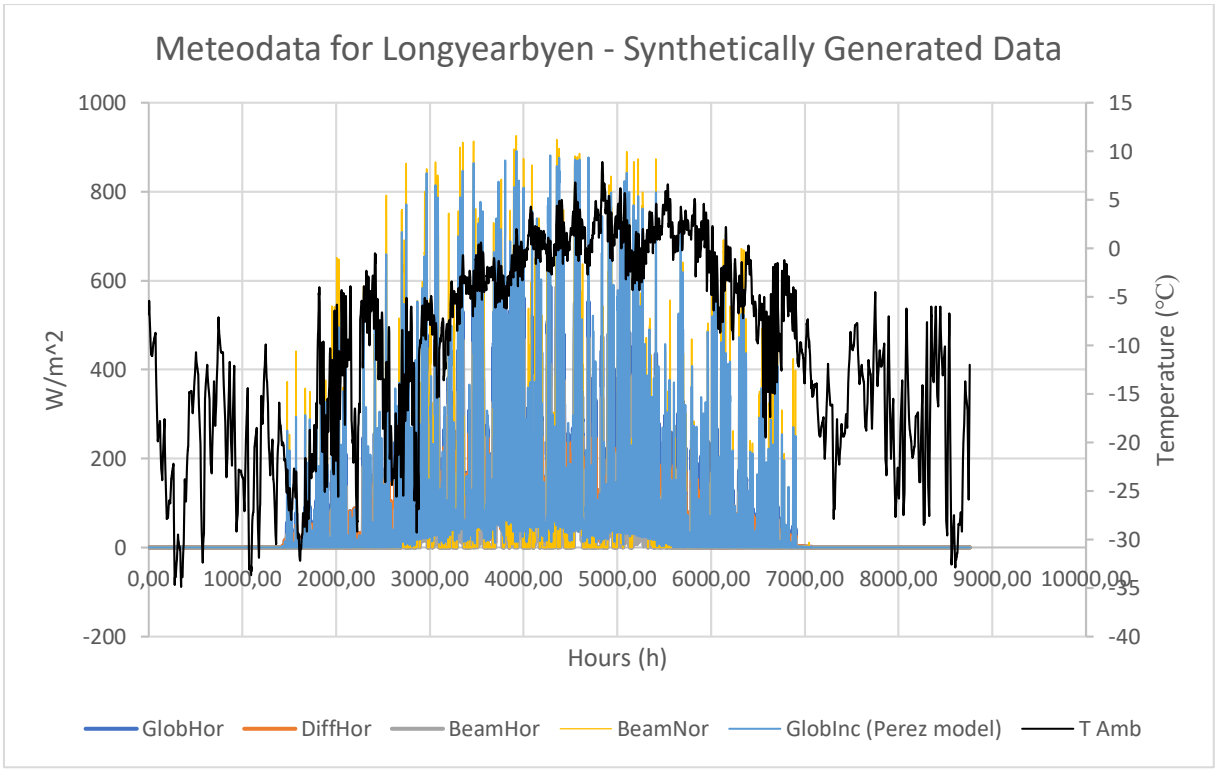

Figure 38: Shows irradiation on a 30° tilted plane compared to tracking and horizontal irradiation. Temperature is plotted on the right axis.

Synthetically generated data shows a “normal” year based on the dataset from NASA. The temperature is plotted to get an idea of when production is possible. The figure compares to the Volker-Quashning curve in table below.

Table 8: Shows how efficient the sun collectors are at different operating temperatures and the total energy collected.

Tilt	Azimuth	Global irradiation sun collector plane [kWh/m2]	T out sun collector	Energy collected to energy storage [kWh/m2]	Efficiency
5	0	624	10	369	59 %
			20	270	43 %
			30	194	31 %
45	0	747	10	477	64 %
			20	390	52 %
			30	320	43 %
90	0	644	10	405	63 %
			20	332	51 %
			30	272	42 %
T out sun collector	Roof Collector Area/ Ground Area	Wall Collector Area/ Wall Area	Roof Area	Wall Area	Tot energy collected
10	1	NR	30000	NR	11.1
20					8.1
30					5.8
10	0.4	NR	30000	NR	5.8
20					4.7
30					3.9
10	NR	1	NR	2100	0.8
20					0.7
30					0.6

5.8 Heat storage

When heat is applied to the permafrost ground, it will thaw and creates a talik. Talik is a melted area surrounded by permafrost and will expand as long as the storage is supplied with heat.

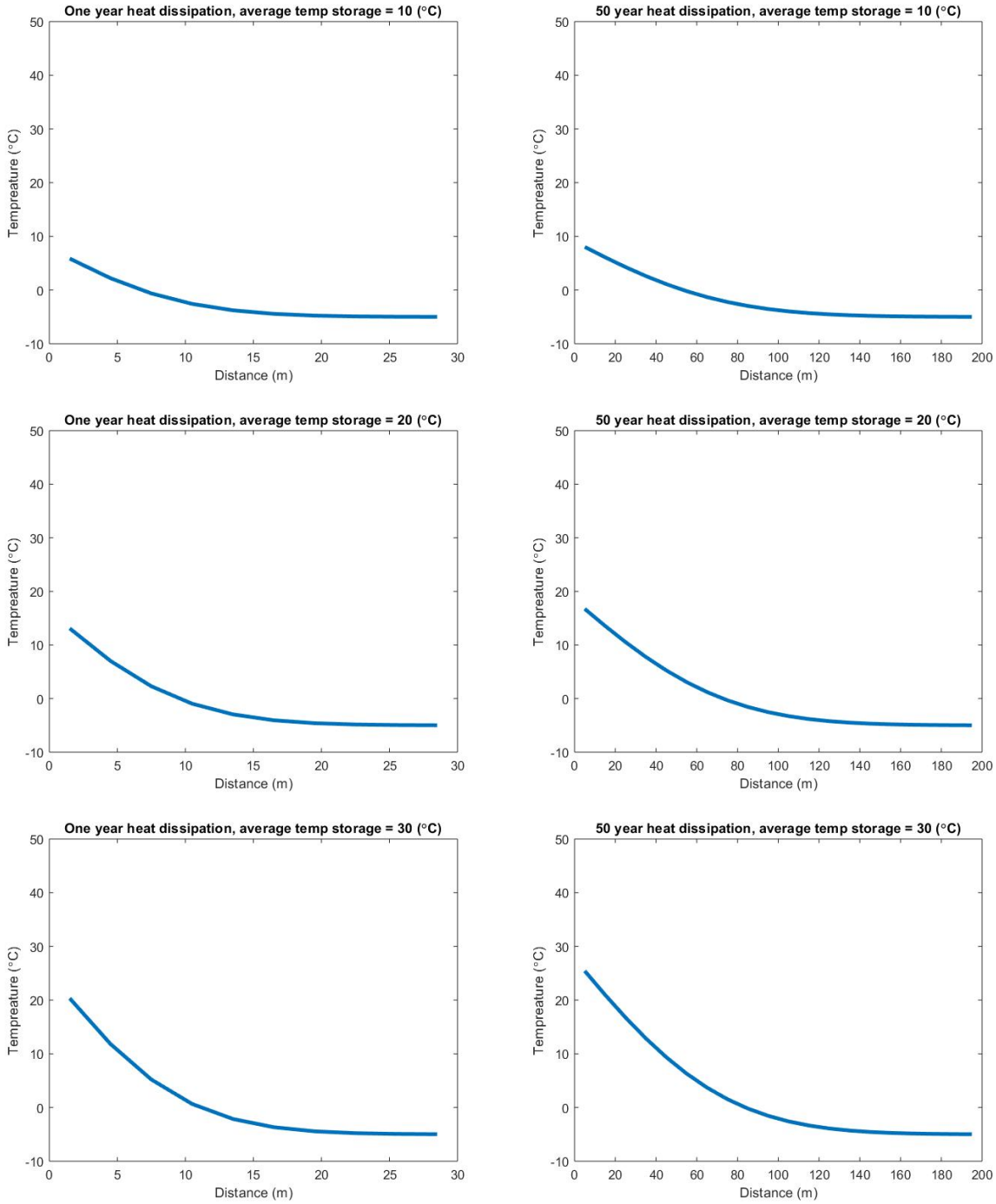

Figure 39: Shows a MATLAB simulation of the heat dissipating from storage. Left hand side shows one-year dissipation; the right-hand side shows 50year/one solar collector lifetime dissipation. The average temperature of the outer rim of the storage from top down are 10, 20 and 30℃

The figure shows temperature gradient from the last well and outwards during the first year on the left-hand side and for one solar collector lifetime of 50 years on the right-hand side. The following assumptions is made for this simulation: Thermal conductivity = 2.1 W/(m*K), density storage = 2300 kg/m^2, heat capacity = 830 J/(kg*K), unaffected ground temperature = -5°C, average temperature of storage wall is changing from 10 to 30°C in a 10°C interval. Interesting to notice is that a 50-year period creates an 80m talik from the edge of the borehole. By altering the model in figure 39 for a

comparison over a 10 year period with the study from Underground Energy, it is evident that the models correspond very well, 35 vs 40m talik were created in the two different models. (Underground Energy, n.d.).

Equation 1 and 2 provides the power output of the well. A schematic of the thermal resistance in the energy well appears in figure 25.

Table 9: Power output per energy well based on the distance between wells.

Distance between boreholes [m]	10.00	8.00	6.00	4.00
Diameter boreholes [m]	0.06	0.06	0.06	0.06
k storage [W/m*K]	2.00	2.00	2.00	2.00
h [W/m^2*K]	50.00	50.00	50.00	50.00
Rcond	0.35	0.33	0.31	0.28
Rconv	0.05	0.05	0.05	0.05
∆T Between bedrock and collector	20.00	20.00	20.00	20.00
Power output (W/m)	49.38	51.65	54.89	60.22

Table 10:Table below shows the increase in number of wells if the volume is optimized with respect to heat loss. The power output and meter of wells is the same for the two storages.

Radius heat storage	**Distance between boreholes [m]**	**Depth**	**Number of wells**	**Total Length of pipes**	**Tot Power output (KW) dT=10**	**Tot Power output (KW) dT=20**	**Tot Power output (KW) dT=30**
63	4	63	992	62512	1882	3765	5647
63	6	63	441	27783	763	1525	2288
63	8	63	248	15628	404	807	1211
63	10	63	159	10002	247	494	741
50	4	100	625	62500	5647	3765	5647
50	6	100	278	27778	2288	1525	2288
50	8	100	156	15625	1211	807	1211
50	10	100	100	10000	741	494	741

Table 11: Different sizes illustrates the variation in total heat capacity of the BTES. The oscillations in the heat storage are based on the heat demand from table 2. In reality this will be higher with heat losses.

Radius	Depth	Area [1000 m2]	Volume [1000 m3]	Heat capacity Granite [kWh/m^{3}K]	MWh/K	Amplitude [K]
30	100	25	282	0.5	159	15.7
40	100	35	502	0.5	245	8.8
50	100	47	785	0.5	384	5.7
60	100	60	1 130	0.5	552	3.9
70	100	74	1 539	0.5	752	2.9
80	100	90	2 010	0.5	983	2.2

Table x indicates that a sensible size for the storage is 785x10^3 m^3, but it also indicates that a smaller storage could be adequate assuming the heat is not used elsewhere. However, by selecting a 785x10^3 m^3 storage it opens up other opportunities, e.g. heating of biogas re

actor, compression of hydrogen and connecting more houses and industry to the BTES as the society expands. It also enables more freedom for architects to create.

Assuming the only use of energy is heating the contruction to 17 degrees, this would cause an average fluctuation in temperature around 5-6 Kelvin meaning that a sensible operating temperature in the park could lie around 30-25°C. However, higher temperatures add more value as it provides freedom to heating option and can be used to heat water, compress hydrogen, etc.

Based on DLSC annual reports 2011-2012, 2012-2013 and 2013-2014, the following heat loss calculations were conducted:

Year	Heat delivered [kWh]	Heat extracted [kWh]	Heat loss to surroundings [kWh]	BTES efficiency	Loss per surface area [kWh/m^2]
11-12	699361	250722	448639	36 %	89
12-13	712833	363000	349833	51 %	70
13-14	683167	381250	301917	56 %	60
Average	698454	331657	366796	47 %	73

The BTES storage of DLSC has a volume of 35600m^3 and a surface area of 5000m^2. By scaling the average performances for DLSC it can be found that the efficiency of SLSC BTES is approximately 80%. These figures corresponds well with figure 8 in the report from IEA-SHC, 2014. (Bruce. S. & McClenahan. D, 2014)

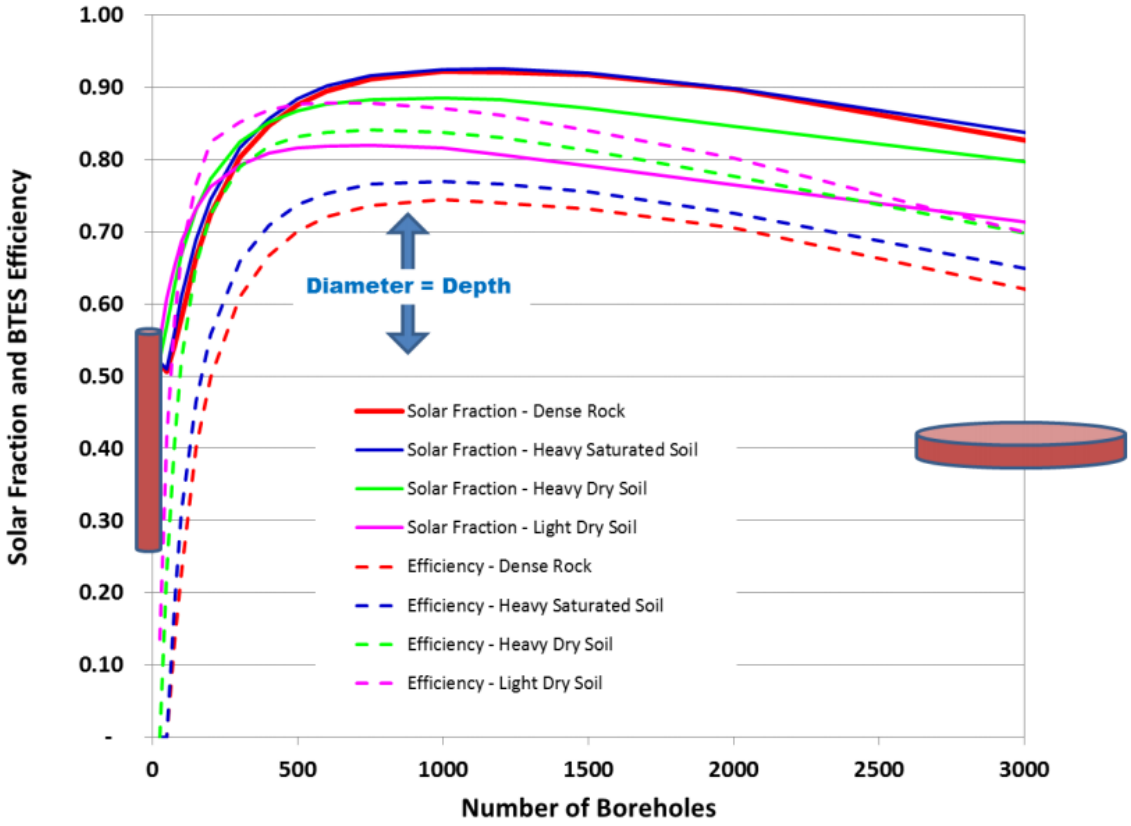

Figure 40: This figure simulates the Solar fraction and BTES efficiency of a storage containing a constant total of 60000m collectors in different geological conditions. Compared to the Svalbard geology, this would be somewhere in between heavy saturated and heavy dry soil. That is approximately twice as big as the one planned on Svalbard. However, the tendency of increased efficiency of the BTES storage (dotted lines) is obvious compared to a BTES on DLSC size displayed in figure 41. (Bruce. S. & McClenahan. D, 2014)

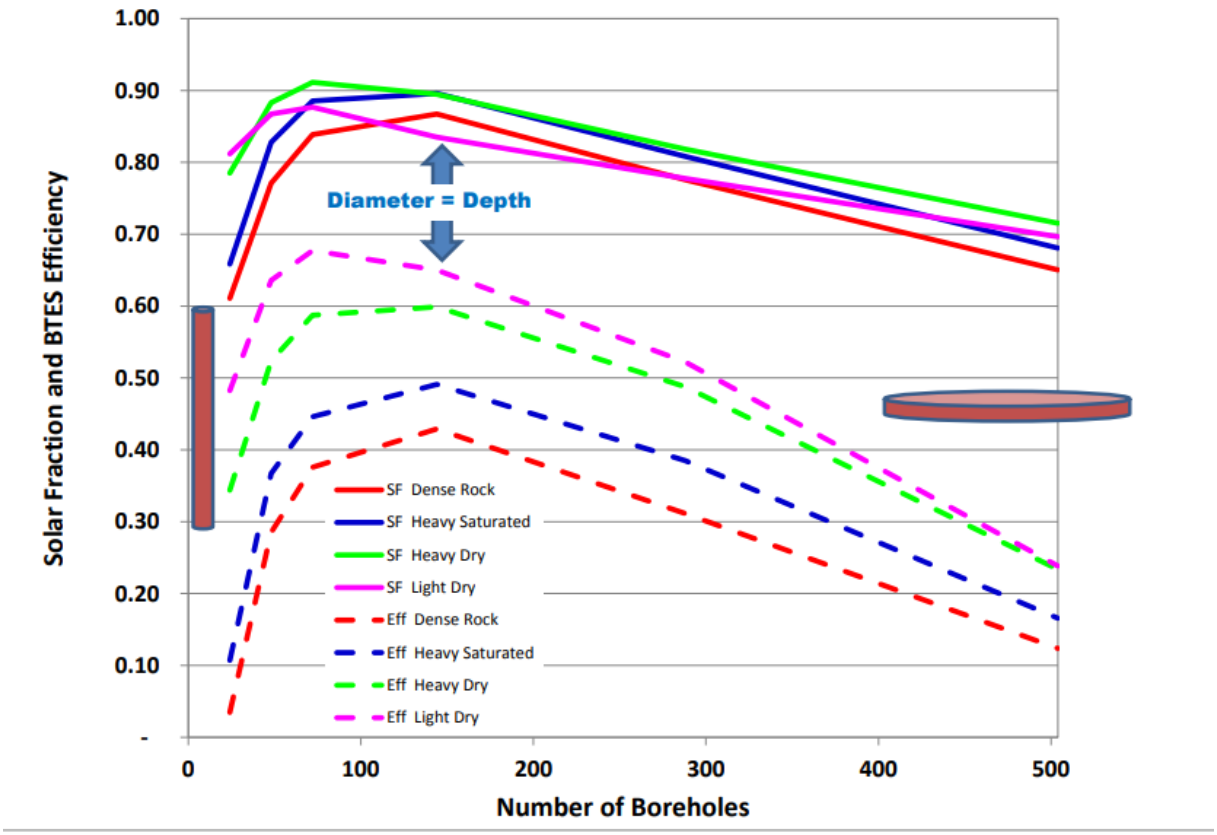

Figure 41: Illsutrates a signinficant lower BTES efficiency in a DLSC size BTES. (Bruce. S. & McClenahan. D, 2014)

5.9 Hydrogen

NEL produces module water electrolysers for hydrogen production. These modules can be connected to meet the demand of hydrogen. Assessing the situation at Svalbard, this construction will demand approximately 3-10 GWh per year of electricity. Assuming worst case scenario where both MWP and wind holt production simultaneously for a month, the energy stored in hydrogen should be able to supply the demand the electricity demand for the building. In such an event, the hydrogen storage should be able to supply approximately $\frac{6}{12}$ = 0.5 GWh of electricity. To be able to do so with a PEMFC efficiency of 50%, the storage needs to contain 1 GWh (Thangavelautham, 2017).

By the ideal gas law (eq. 30), the production results supplied by NEL, and assuming $1Nm^3$ is presented under the industry standards of 0 °C and 1atm condition, it is evident by the ideal gas law that $1Nm^3$ contains 44.6 mol of hydrogen gas which equals 2.9 kWh (ref. eq. 30) (Halvorsen, 2018). According to the ideal gas law this demands a volume of 1750 m^3 on a 200bar pressure level. However, even though hydrogen gas molecules are small, the pressure and dimensions are substantial at 200 bar and 1 GWh. It is therefore necessary to examine the van der Waals equation. The result from van der waals

equation shows that the same amount of energy at the same pressure should not demand more volume than approximately 1500 m^3 at 200bar and 4℃.

Assuming the pressurisation adds 10% the electricity needed for the process (Halvorsen, 2018), conversion rate of the electrolyser are 60% and PEMFC are 50%, a total cost in energy of producing these amounts of hydrogen would be approximately 3.7 GWh (NEL, 2018).

6 Discussion

6.1 Results and Quality assessment

6.1.1 Indoor heated area

The main subject of the thesis is to decide whether it is feasible for an indoor heated area to maintain a constant temperature purely on solar energy. However, the question is immensely more complicated as there are binding legislation and guidelines to follow. In this thesis, an example calculation has been performed in accordance with TEK 17 and NS3031 standards. TEK 17 and NS3031 provides a free scope for assumptions which gives rise to uncertainties. In TEK 17 there are strict regulations towards U-values of walls and windows, these values already equal passive house standards and are challenging to achieve, meaning that these minimum standards have been set as a basis for further calculations and will most likely not improve. In other aspects, however, e.g. ventilation, it is assumed preaccepted values for office building as these values are the most similar to the intended use of the indoor area.

The heat loss calculations are an approximation based on NS3031. It does not contain detailed simulations in Simien of, e.g. ventilation, heating from the sun, pumps, electrical lights and so on. Consequently, the precision level of the heat loss calculations is limited. The reason for this is the unknown use of the building. The assumptions used from NS 3031 has therefore been picked in a way that does not benefit this project. E.g. NS3031 states that if no further simulations are made, variable air ventilation (VAV) regulated by CO_2 -level or presence, can reduce the air supply by about 20%. In calculations, it is assumed constant air ventilation (CAV) to not underestimate heat losses through ventilation.

Total heat loss figure of 4.2 GWh per year are based on the heating degree days of 7839Kh. Of the 4.2GWh approximately 1.7GWh is supplied by equipment, people and solar radiation through windows. The figures are meant purely as an illustration on the basis that the decided use of the hall would greatly influence these numbers.

One of the most significant flaws of the thesis is how the heat, received from the sun, people, ventilation fans, lights, other electrical equipment, are distributed over the year. Again, these values are extremely dependent on how the hall is utilized, consequently, cooling calculations have not been

considered. In hindsight, an illustrative calculation of the cooling should have been made. It was not anticipated that it might be necessary with cooling in the arctic. However, cooling in the arctic area is not a problem, but it shifts the energy balance as it is necessary to dispose of energy

The heat loss of the hall is an essential result for deciding the operating temperature of the energy storage. A massive storage means lower fluctuations in temperature which promotes lower fluctuations in the power output per litre medium flowing through the collectors. Calculations of the maximum power output required are based on an ambient temperature of -40°C while the average power output is based on the yearly average temperature in Longyearbyen of -10°C. The maximum power output of P = 1273kW might be over-dimensioned as the temperature very seldom falls below -40°C, however, the coldest recorded temperature in Longyearbyen is -46°C(Toppe, 2009). As an observation, by lowering the minimum accepted temperature of the hall to 10 degrees, it lowers the maximum power output to approximately 1100kW. Either way, by choosing a collector spacing of 6m the total collector length would be 28000m which in would comfortably accommodate the maximum power output. However, a thermal response test to build a simulation model is necessary to dimension the collector spacing to a technological economically optimum.

In the event of building the park it should also be considered as an energy storage for new and existing industries and houses. The power demand of these additions should be included when assessing the collector spacing and size of the BTES

6.1.2 Energy capture from the sun

Table 6 holds information about the total energy delivered from the collector plane to the storage each year at a presumed temperature average in the sun collectors. The results are a good approximation to the real energy capture in an average year. Though, it could be somewhat higher or lower yield on the yearly total. Energy collected in the early spring/summer would be captured at lower temperatures when the heat storage is drained causing the sun collector efficiency to rise, while the energy captured in the late summer, autumn, would not be able to obtain high enough temperature to be stored in the BTES.

However, collected energy could also be directly utilized if not warm enough to store. By doing so, this fraction of the collected solar energy will not suffer from the losses of the BTES.

6.1.3 Thermal Storage

Size of thermal storage is decisive for the temperature fluctuation in the waterborne heat system. The indoor area needs, in theory, an average heat supply of 2.5GWh per year. By having cylindrical shaped storage containing 785 398 m^3 of rock (sandstone), the fluctuation in the thermal storage would approximately be 5-6 Kelvin. However, this number is based on the storage receiving and extracting 2.5 GWh per year. In practice, the storage will receive on an average 5.8GWh and leak some of that energy to the surrounding rock by conductive heat transfer. On the basis of 80% BTES efficiency on

Svalbard this signalises a heat energy buffer of 2GWh per year. In addition, the MAP would supply high temperature to the centre of the park, approximately the same amount as generated electrical energy. Based on the Monte Carlo simulation this would be in the area 1.5-2.5 GWh per year making a total of approximately 8GWh per year. With a BTES efficiency of 80% it creates a surplus of 3.9 GWh of heat which could supply industry or other households. However, it is also an indication that the sun collectors should be run harder on the temperature output. A trade off of lowering the efficiency to get higher quality heat can be done.

In Svalbard, the storage operates in permafrost which means there is no groundwater causing convective heat losses in the ground. This situation makes the behaviour of the BTES predictable as it loses energy uniformly around the storage surface.

In calculations of the depleted temperature level of the BTES there are some uncertainties connected to heat systems. Floor heating is a system that is easy to regulate and can operate on low temperatures due to its ability to cover large surface areas. Radiators and fan convectors on the other hand radiates more power per unit area and are practical to use towards outer walls.as they prevent air pressed towards the wall to cool and create a draft caused by natural convection. According to NS3031:2014 a floor heating system usually operates on a $\Delta T \approx 6K$ while radiators or fan convectors operate on a $\Delta T \approx 30K$. (Standard Norge, 2014) This means that floor heating would effectively lower the depleted temperature limit of the BTES.

By building SLSC on top of the BTES the insulation don not need to be tight. By building insulated skirts on the construction the leakage will create a basement with a constant temperature of e.g. 25-30°C. If the flooring of the SLSC is poorly insulated on purpose, the basement convection will create a natural floor heating with no circulating water. This possibility has not been thoroughly examined, so the contribution of this conscious heat leakage is uncertain.

6.1.4 Collectors

A thermal response test will contain vital information about the local geology, the importance of this information lies in the values of thermal conductivity and thermal capacity. The thermal capacity is necessary when deciding the operating temperatures as it directly influences the temperature fluctuations in the storage. The heat conductivity directly influences the power absorbance and output of the wells. It also delivers information about the thermal energy dissipation from the storage. My calculations based on the BTES information of DLSC anticipates a heat loss to the surroundings around 20%.

6.1.5 Wind

According to the methodology used to make the wind speed calculations developed by NASA, the wind speed has an R^2 equal to 0.55 and an RMSE equal to 1.6 compared to measured data from ground stations(Stackhouse, 2017). R^2 is a value that ranges from zero to one and states how good the

model is on predicting values, RMSE is the square root of the residual data meaning that the RMSE can be interpreted as the standard deviation of the unexplained variance which in this case has the unit [m/s]. The uncertainty in these data could therefore be decisive for the energy production (see figure 31 vestas). When assessing the data provided by Vestas, it would be beneficial to develop a sensitivity and statistical analysis to comprehend the risk of under-projecting the production. If the risk analysis shows insufficient, it would be necessary with a better basis of data. On the other hand, such a data collection would take several years to retrieve. A further report on the uncertainty around wind projection would most likely be able to present an uncertainty adequate for decisionmakers in this instance. By inspecting the wind turbine brochure delivered by vestas it is evident that the cut-in speed and cut-out speed are respectively 3m/s and 21m/s. The time spent within these limits are 63% of the total 8760 hours. However, this number is based on the Weibull distribution which according to figure 30 overestimates wind frequency below 3m/s.

This thesis proves that it is highly likely that a wind farm in Longyearbyen has an excellent yield. Calculations done on the V110-2.0MW IEC IIIA shows a potential power factor of almost 42%, in comparison, Norway's biggest wind farm has a yield around 30%. Newer de-icing technologies involving drones will make it possible to operate these applications in arctic climates with low costs. These drones can also inspect and do simple repairs on windmills, cutting cost of workforce and hours(Løvik, 2017). Griff Aviation is currently working on drones with lift capacities more than adequate to de-ice windmills in start-up operations(Holand, 2018). Vestas windmills deliver windmill with ice detection and de-icing systems and can operate in climates down to minus 30 degrees Celsius.

The primary challenge with wind is the instability of supply and storage of energy. Like many other renewable energy sources, it is very dependent on the power and energy balance. In a small community like Longyearbyen, there are small changes in power demand and no ability to distribute the power production to other districts where the demand is high. A presentation made for SINTEF by "Longyear energiverk" in 2017, presents the power and energy demand for a typical February month. Data shows that the power demand for electricity seldom exceeds 7.5 MW(Røkenes, 2017). However, a shift in the business at Svalbard points to more tourism, and a report released by the Norwegian Coastal Administration displays a 124% increase in passenger traffic from 2005 to 2015 and a further 10% increase by September 2016. The report reveals that this increase is due to bigger cruise vessels visiting the harbour, which presents a yet unknown challenge. To create a parallel, it could be interesting to learn from Geiranger- and Nærøyfjorden which struggles with a problematically high concentration of pollution due to electricity generation aboard cruise vessels. A way to get rid of the problem is by connecting vessels to onshore power. However, such a solution with high demands and stable power output might not be feasible in a small society like Longyearbyen.

6.1.6 Waste

Electric energy generetion from waste would be an improvement to the current waste treatment in Longyearbyen. The report by Asplan Viak presents a thorough investigation of the different waste materials found on Svalbard and shipped to Norway mainland for further treatment. A report from regular households on the mainland, which contained pick analysis of combustible residual waste, made it possible to develop an approximation to the composition of the combustible residual waste on Svalbard with some adaptation.(Mepex, 2013) However, adaptation and insufficient data on the total amount of waste creates an uncertainty to the result. In the Monte Carlo simulation, this report has tried to capture the uncertainty.

The energy output from different materials is presented on Scandinavian Biofuel homesite. These outputs are presented in table 6 and contain laboratory tests results of different materials. However, by comparison of the tabled calorific values of the waste compositions to the values of the test materials, an uncertainty model has been developed in a Monte Carlo simulation. This method presents an approach to the real energy output but serves a high degree of uncertainty to the microwave pyrolysis production. Pyrolysis processes take place at high temperature, meaning start-up costs regarding energy could be high. These costs are not taken into consideration when the results are presented.

Electricity generation of the microwave pyrolysis is dependent on the amount of waste supplied to the system. It is a flexible system regarding regulating the power output which makes it a practical power supply for a small community with limited possibilities reroute electricity to other locations with higher demands. (Kasin. K.I., 2018)

Longyearbyen society arranges a cleaning project each year where they collect litter on the seashore around the island. Operating engineer for renovation and environment Karine Hauan, claims in an email that these project has brought in 81 tons of garbage between 2015 and 2017(Hauan, 2018). In the same email, a litter analysis provides detailed information about the fractions of the waste listed in table 7.

Some of the most exciting parts of the microwave pyrolysis are the residual waste left over after the process. This waste material is called bio-carbon and has several features. In the central Amazonas, there is a soil called Terra Preta or black earth which has proven to be very fertile. Reason for this is the microscopic structure in the bio-carbon produced, it contains tiny air pockets that improves the aeration of the soil, harbours fungi and increases the water absorption. These structures are also very resistant and break down slowly, causing this “fertilizer” to exist for a longer time than any other fertilizers. This is interesting at Svalbard, as newer technologies evolve the agricultural possibilities expand and today they grow vegetables in Svalbard using artificial lights and heat when the sun is not present. One of the critical challenges is to find quality fertilizers and soil to grow in, and today most of the biomasses are flushed into the sea.(*How To Garden In The Arctic _ Mach _ NBC News*, 2018).

By use of a biogas reactors, it is possible to utilize human manure, crops and food waste to create biogas for electrical production, one of the advantages of doing this instead of pyrolysis is the capture of nitrogen, and potassium residing in food waste (could excist in MAP bichar as well but not been investigated). These mineral resources are mined to create artificial fertilizers and improve the growth rate and quality of the plants, as the plants absorb these minerals and pass them on the humans, it is important to reuse this resource in the new harvest instead of squandering the minerals. However, this gain of harvesting minerals will come at some expense of the electrical output from the pyrolysis.

6.1.7 Hydrogen

Hydrogen as an energy carrier at Svalbard is an interesting proposition which were proposed by Sintef some time ago. Hydrogen is a very flexible energy carrier, it is easy to transport and has uses both in transport and in stationary applications. Hydrogen has some similarities with the world's most important energy source today, oil. It can be stored for longer periods of time, the energy can be extracted when it is needed, and it is easy to fuel vehicles on the move. It has some disadvantages compared to oil, mainly that it is in gas form and sensitive to temperature changes, it demands a lot of energy to pressurize to compromise for its low volumetric energy density and its high pressure causes a danger to the local environment and people operating the facilities.

However, it is an energy carrier that can be made of the earths most abundant resource, water. By electrolysis of water hydrogen can be made with zero emission, provided that the energy input to overcome the spontaneous reaction barrier is delivered by a renewable energy resource.

In Svalbard there are several mining systems stretching in beneath thousands of tons with rock. During this thesis, the opportunity of storing hydrogen in PE pipes stretching in thorough these systems has been investigated through PE suppliers. However, there are some issues concerning this. Polyethylene pipes are not necessarily diffusion tight and there are none gas approved PE gas pipes of dimensions more than

6.2 Society contribution

6.2.1 Indoor heated area

An indoor heated area at Svalbard could have several contributions to Svalbard. First thought of such a contribution was a safe living area for the avalanche-prone households. An indoor community with four-story houses on the north wall and two-story houses on the south wall so every household would have access to daylight and fresh air. In the middle, it could have industry, e.g. tourist travel agents, shops, research facilities etc. It could have an indoor climbing park on the north wall or even a soccer field in the middle. All these features in a hall that holds constant 17°C all year around. Maybe even 20 in the summer when the sun shines through the windows. These offers would make Svalbard more attractive for families as the society would offer leisure activities for kids and families, and work possibilities for adults.

The previous paragraph paints a picture which also ensures a safe haven in the Arctic. As more and more cruise ships arrive at Svalbard with thousands of passengers, it is crucial to have a port of refuge in case of ground striking, ship fire, collisions and so on. A heated indoor area would provide the most critical necessity in short notice even in an arctic climate. One of the most untested and unfinished safety equipment are survival suits capable of providing necessary warmth and comforts in such an inhospitable climate as Svalbard. A report by SAREX (Search And Rescue Exercise) was presented to the Norwegian Government 3.May 2018, finding it insufficient with survival suits in the arctic. (Salater, 2018) A 30000m^2 heated hall would provide a substantial contribution in securing the safety of both the population and tourists alike.

As Svalbard is a small community, an indoor society of these dimensions may seem redundant. However, only a portion of the hall needs to paint the picture described in the first paragraph of this section. By dividing the structure, it could be interesting to pursue different research topics in Svalbard, e.g. aquaculture and agriculture.

By extracting the oxygen from the pyrolysis, electrolysis and the greenhouse, farming fish indoors could be an interesting use of the heated structure. This thought is dependent on the West Spitsbergen Current supplying "Adventfjord" with the necessary temperature to farm fish. The temperture from the sea is crutial in this instance as an indoor fish farm producing 250-ton fish per year would require 18m^3/min of water to remove the ammonium content. (Wangel. C.A, 2017) Heating these amounts of water is not feasible for the society at Svalbard. E.g. for every 1°C rise in temperature the 18m^3 of water would demand 21 kWh worth of energy per minute. Supplying these amounts of energy would require a power output of 1200kW. However, a 250-ton production clearly indicates export of fish from Svalbard. To supply the recommended demand of fish to Longyearbyen a yearly production of 30 tons fish per year would be adequate. Farming fish has a low feed conversion ratio of approximately one, this represent an advantage for a society dependent on import. Conversion rate of one means that 30 tons of feed for would roughly produce 30 tons of fish. From an energy perspective, it makes more sense to transport high energy dry feed than finished products containing water.

The biggest challenge for salmon fish farms is fish lice. These parasites prey on the slime, blood and skin of the fish. Infected fish can, if not treated, develop open wounds which exposes them to infections. Untreated fish can in worst case scenarios die of the damages caused by this parasite directly and indirectly. Cold waters however lower the population and growth of fish lice, it also lower the chance of lice larva infecting the fish, in fact, the report published by the Norwegian Veterinary Institute reported insignificantly low values of fish lice in the most northern part of Norway. (Hjeltnes. B et al., 2017) Unfortunately, the Atlantic salmons optimum growing condition are the same as for the lice. However, documentation of feeding salmon has been documented as low as 0°C and a further research of this topic is advised. (Statkraft Grøner AS, n.d.)

Aquaculture presents opportunities to new and ongoing research like Marbank. Marbank is marine biobank research gathering biological material round Svalbard and the Barents Sea. This research aspires to find new genes, molecules or organisms with features that could be beneficial for the society, and have potential for commercial development. (Institute of Marine Research, 2012)

Fish farms would also contribute to biogas energy production. Fish heads, intestines and digested waste materials are all contributors to the bio digester.

The construction also presents a research opportunity for big scale indoor agriculture. growth far north in combination with bio digester treatment and bioreactor treatment of human manure and food waste. If this deems possible, it could cut cost and pollution of expensive transport of food. Most vegetables have a water content of 70% and upwards. Transporting vegetables to Svalbard is therefore inefficient from an energy perspective.

Pollution connected to food transport is difficult to determine for sure, in statistical analysis from "Port of Longyearbyen" it is evident that the cargo vessels called to port approximately every 5^{th} day in 2017. Unfortunately, there are no statistics on the amount of food and waste transported to and from the island so to quantify the cost and CO_2 emission savings is a challenge and requires expertise and overview of the society. Getting information about these matters from people in possession of this knowledge has proven to be difficult. However, statistics on eaten vegetables per person on the mainland is transperent and the Norwegian Directorate of Health claim, that each Norwegian eats 81kg of vegetables each year, not included fruit, berries and potatoes.

One of the world's biggest challenges today is humanitarian crisis spread across the world. In 2017, there were 65.6 million forcibly displaced people worldwide, 22.5 million of these were refugees and only a total of 189300 refugees were resettled, that is less than 1% (Agency, 2017). The refugee camps often struggle with insufficient funds in terms of water quality, food, sanitation and housing. Safe housing with adequate housing conditions is one of the most elemental needs and protects against sicknesses (Sight, n.d.).

A structure like the one presented in this thesis could provide a ventilated refugee city, placed in the more sparsely populated areas of the world. These areas are often located far north. Here it would be possible seek refugee both from war, persecution, natural disasters and from sicknesses like malaria, cholera, etc. dominating in the warm climates of the world (Organisation, n.d.). Creating an indoor self-sustainable society could in other ways help refugees by making use of land that is too remote for necessary utilities to reach. This thought is worth to pursue by a socioeconomic research.

7 Conclusion

The calculations deem the construction possible. The results of the BTES in combination with solar collectors and MAP are uplifting as it displays a surplus of 2.9 GWh of heat. However, some of this

heat must be traded for electrical generation for this project to be 100% self-sustainable. New calculations for the electrics should be made in more detail as the margins are small for errors in the calculations. NS standards does not apply very well for this construction and a more detailed calculation example should be constructed if the project moves forward.

8 Sources

Agency, T. U. R. (2017). *Figures at a Glance*. Available at: http://www.unhcr.org/figures-at-a-glance.html (accessed: 24.05.2018).

Barr, S. (2018). *Svalbard*. Available at: https://snl.no/Svalbard (accessed: 01.03.2018).

Borgnakke, C. S. R. E. (2009). *Fundementals of Thermodynamics*. 8. ed. University of Michigan John Wiley & Sons Singapore

Bowden. S. & Honsberg. C. (n.d.-a). *Solar Radiation in Space*. Available at: http://pveducation.org/pvcdrom/properties-of-sunlight/the-sun (accessed: 02.02.2018).

Bowden. S. & Honsberg. C. (n.d.-b). *The Sun*. Available at: http://pveducation.org/pvcdrom/properties-of-sunlight/the-sun (accessed: 02.02.2018).

Bowden. S. & Honsberg. C. (n.d.-c). *Terrestrial Solar Radiation*. Available at: http://pveducation.org/pvcdrom/properties-of-sunlight/the-sun (accessed: 02.02.2018).

Bruce. S. & McClenahan. D. (2014). *Task 45 Large Systems, Seasonal Borehole Thermal Energy Storage*. Report from IEA-SHC 10/2014. Available at: https://www.iea-shc.org/data/sites/1/publications/IEA-SHC-T45.B.3.1-TECH-Seasonal-storages-Borehole-Guidelines.pdf (accessed: 25.05.2018).

Byggforskserien. (1990). *Oppvarming av boliger. Energiforbruk og kostnader*. Available at: https://byggforsk.no/dokument/519/oppvarming_av_boliger_energiforbruk_og_kostnader (accessed: 11.04.2018).

Cengel, Y. A. G., A. J. . (2005). *Heat and Mass Transfer*. Fifth ed. New York: McGraw-Hill Education.

Company, S. B. *Advanced and sustainable biofuels* (accessed: 10.04.2018).

Damkås. J. (2017). *Longyearbyen lokalstyre og beredskapsansvar*. Available at: https://www.lokalstyre.no/skredfare-og-evakuering.400839.no.html (accessed: 02.02.2018).

Drake, G. W. F. (2017). *Thermodynamics* (accessed: 12.02.2018).

E., C., Jefferson, B., Parker, A. & Rose, C. (2015). The Characterization of Feces and Urine: A Revieew of the Literature to Inform Advanced Treatment Technology. *Taylor & Francis*, 45 (17): 1827-1879. doi: 10.1080/10643389.2014.1000761.

Eppelbaum. L, Kutasov. I & Pilchin, A. (2014). *Applied Geothermics*: Springer.

Flatner, E. (2017). Sesonglagring av solvarme i termisk borrehullslager - vurdering av sentrale systemkomponenters ytelse.

Garathun. M.G. (2014, 11. February). Oslos nye praktgate hviler på 1100 påler. *Teknisk Ukeblad*. Available at: https://www.nmbu.no/om/biblioteket/skrive/referanseverktoy/endnote-stil-materoppgaver (accessed: 24.05.2018).

Gehlin, S. (2002). *Thermal Response Test Method Development and Evaluation*. Doctoral Thesis. Luleå: Luleå University of Technology.

Halvorsen, B. G. (2018). *Masteroppgave NMBU* (Email to Bjørn Gregert Halvorsen 28.05.2018).

Hannus, M. (2016). *Skredfarekartlegging utvalgte områder på Svalbard*. Report by NVE: NVE (accessed: 01.02.2018).

Hauan, K. (2018). *Sluttrapport for tokt, Prosjekt Isfjorden 2017* (E-mail to Karine Hauan 01.05.2018).

Hjeltnes. B, Bang-Jensen. B, Bømo. G, Haukaas, A. & Walde. C.S. (2017). *Fiskehelserapporten 2017*: Norwegian Veterinary Institute.

Holand, P. H. (2018). *Personal communication with boardmember Phillip Johan Hofset Holand Griff Aviation* (16.04.2018).

Honsberg, C. B., S. (2018). *Solar Radiation at the Earth's Surface*. Available at: http://pveducation.org/pvcdrom/properties-of-sunlight/solar-radiation-at-the-earths-surface (accessed: 26.03.18).

How To Garden In The Arctic _ Mach _ NBC News. (2018). vimeo: NBC news. Available at: https://vimeo.com/254602275 (accessed: 06.04.2018).

Hübner, C., Jochmann, M., Piepjohn, K. & Stange, R. (2012). *The Geology og Longyearbyen*. Available at: https://folk.uio.no/hanakrem/svalex/Papers_and_extended_abstracts/Jochmann-Longyearbyen-eng.pdf (accessed: 26.05.2018).

Institute, N. P. (n.d.). *Svalbardkartet*: Norwegian Polar Institute.

Institute of Marine Research. (2012). *Marbank*. Available at: http://www.imr.no/marbank/en (accessed: 01.06.2018).

Isaksen, K., Frøland E.J., Dobler, A., Benestad, R., Haugen J.E., & Mezghani, A.

. (2017). *Klimascenarioer for Longyearbyen-området, Svalbard*. Modell og klimaanalyse. Available at: https://www.met.no/publikasjoner/met-report/_/attachment/download/8932a8b1-

17b4-4567-8559-ed4b78d61aee:6fe02353a8212c195f00bd59dc5b2baaa6c4118c/2017-10-METreport_Statsbygg-Svalbard_final.pdf (accessed: 16.04.2018).

Kasin. K.I. (2018). *Masteroppgave NMBU med interesse for Mikrobølge assistert pyrolyse (Kjell-Ivar Kasin)* (E-mail to Kjell Ivar Kasin 29.05.2018).

Landrø, M., Mikkelsen, O.A., & Jaedicke, C. (2017). *Gjennomgang og evaluering av skredhendelsen i Longyearbyen 21.02.2017*. Rapport nr 31-2017. Available at: http://publikasjoner.nve.no/rapport/2017/rapport2017_31.pdf (accessed: 10.05.2018).

Lee. K.S. (2013). *Underground thermal energy storage*: Springer, London.

Løvik, H. (2017, 4. December). Halverte tid og antall personer: Statoil inspiserte 264 turbinblader på 20 dager. *Teknisk ukeblad*. Available at: https://www.tu.no/artikler/halverte-tid-og-antall-personer-inspiserte-264-turbinblader-pa-20-dager/413326 (accessed: 05.04.2018).

Mepex. (2013). *Avfallsplan for Bærum*.

Motasemi, F. & Afzal, M. T. (2013). A review on the microwave-assisted pyrolysis technique. *Renewable and Sustainable Energy Reviews*, 28: 317-330. doi: https://doi.org/10.1016/j.rser.2013.08.008.

NASA. (2016). *NASA Prediction Of Worldwide Energy Resources*. Available at: https://power.larc.nasa.gov/new/ (accessed: 14.02.2018).

NEL. (2018). *The World's Most Efficientand Reliable Electrolysers*. Available at: http://nelhydrogen.com/assets/uploads/2016/05/Nel-Electrolysers-Brochure-2018-PD-0600-0125-Web.pdf.

O'Toole, A. & Grønlund, A. (2012). *Produksjon av 2. generasjons- biodrivstoff via termokjemiske prosesser. Kunnskapsstatus, kostnader, og potensial for klimagassreduksjon i Norge*: Bioforsk.

Olje- og energidepartementet. (2018). *Utredning om energiforsyningen på Svalbard*. web: Minestry of Petroleum and Energy. Available at: https://www.regjeringen.no/no/aktuelt/utredning-om-energiforsyningen-pa-svalbard/id2587059/ (accessed: 30.01.2018).

Organisation, W. H. (n.d.). *Areas affected by cholera epidemics*. Available at: http://www.who.int/gho/epidemic_diseases/cholera/epidemics/en/ (accessed: 26.05.2018).

Prop. 1 S (2017-2018). *Svalbardbudsjettet*: Justis- og beredskapsdepartementet. Available at: https://www.regjeringen.no/no/dokumenter/prop.-1-s-sva-20172018/id2574190/sec1?q=snsk#match_0 (accessed: 15.02.2018).

Prop. 129 S (2016-2017). *Tilleggsbevilgninger og omprioriteringer i statsbudsjettet 2017* Oslo: Minestry of Petroleum and Energy.

Quaschning, V. (2004). *Solar thermal water heating*. Available at: https://www.volker-quaschning.de/articles/fundamentals4/index.php (accessed: 03.03.2018).

Rasmussen. R.D. (2017). *Avfallsplan Longyearbyen 2017-2020*. Tønsberg: Asplan Viak.

Røkenes, K. R. (ed.) (2017). *Fremtidens energiforsyning i Longyearbyen, Svalbard, June 12-13, 2017*. Svalbard: SINTEF.

Salater, R. (2018). *Så lenge klarte anna å overleve 79 grafer nord*. TV2. Available at: https://www.tv2.no/a/9852994/.

Scandinavian Biofuel Company. (n.d.). *Microwave Assisted Pyrolysis for waste treatment and renewable energy*. Available at: http://www.sbiofuel.com/presentation.html.

Sight, U. f. (n.d.). *Module 3: Food, Water, Sanitation, and Housing in Refugee Camps*. Available at: http://www.uniteforsight.org/refugee-health/module3 (accessed: 26.05.2018).

Stackhouse, P. W., Jr., Zhang, T., Westberg. D., Barnett, A.J., Bristow, T. & Hoell, J.M. (2017). *Power Methodology (Data Parameters, Sources & Validation)*. Booz Allen Hamilton, Norfolk, VA: NASA Langley Research Center. Available at: https://power.larc.nasa.gov/new/files/POWER_Data_v8_methodology.pdf (accessed: 17.04.2018).

Standard Norge. (2014). *NS 3031:2014 Beregning av byningers energiytelse*. Available at: http://www.standard.no/no/Nettbutikk/produktkatalogen/Produktpresentasjon/?ProductID=434722 (accessed: 12.02.2018).

Statkraft Grøner AS. (n.d.). *Laks og temperatur - en literaturgjennomgang*. Suldalslågen-Miljørapport. Available at: https://www.statkraft.no/globalassets/old-contains-the-old-folder-structure/documents/no/13---laks-og-temperatur--en-litteraturgjennomgang_tcm10-4208.pdf (accessed: 25.05.2018).

Thangavelautham, J., Strawser, D.D. & Dubowsky, S. (2017). *The Design of Long-Life, High-Efficiency PEM Fuel Cell Power Supplies for Low Power Sensor Networks*. Available at: https://arxiv.org/pdf/1705.10785.pdf.

The Norwegian Water Resources and Energy Directorate. (n.d.). *NVE faresoner*: The Norwegian Water Resources and Energy Directorate.

Tidwell. J. & Weir. T. (2006). *Renewable Energy Resources* 2nd ed. 2 Park Square, Milton Park, Abingdon, Oxon OX14 4RN: Taylor & Francis.

Tipler, P. A. M., G. (1996). *Physics For Scientists and Engineers*. 6th ed. New York: W.H. Freeman and Company.

Toolbox, E. (n.d.). *Fuels Exhaust Temperatures*. Available at: https://www.engineeringtoolbox.com/fuels-exhaust-temperatures-d_168.html.

Toppe, R. (2009). *Iskaldt på Svalbard*. Available at: https://www.tv2.no/a/2496606/ (accessed: 29.04.2018).

Underground Energy. (n.d.). *Diamond Mine BTES Prefeasibility Study*. Available at: http://underground-energy.com/case-study/btes-prefeasibility-study/ (accessed: 28.05.2018).

Vestas. (2017). *2 MW Platform*. Available at: http://nozebra.ipapercms.dk/Vestas/Communication/Productbrochure/2MWbrochure/2MWProductBrochure/?page=1 (accessed: 05.02.2018).

Wangel. C.A. (2017, 24. February). Det problematisk ved lukkede oppdrettsanlegg. *Kyst.no*. Available at: https://www.kyst.no/article/det-problematiske-ved-lukkede-oppdrettsanlegg/ (accessed: 02.06.2018).

9 Appendix

```
L = 200; %Distance from last known temperature in storage
n = 20; %Number of nodes
T0 = -5; % degree celsius, initial temperature of the ground
T1s = 10; %konst temp outer rim of heat storage
T2s = -5; %konst temp permafrost/unnaffected ground temperature

dx= L/n; %Thickness per node
k = 2.1 % thermal conductivity heat storage W/(m*K))
rho = 2300 % density heat storage (kg/m3()
cp = 830/3600 % heat capacity storage (Wh/(kg*K))790J/kg*K
alpha = k/(rho*cp) ; %Thermal diffusivety = k/(rho*heat capacity)

t_final = 24*365*50; %timeline end
dt=1000; %time interval

x=dx/2:dx:L-dx/2;

T=ones(n,1)*T0;

dTdt = zeros(n,1);

t = 0:dt:t_final;

for j = 1:length(t)
    for i = 2:n-1 %only midle nodes, no boarder nodes
        dTdt(i) = alpha*(-(T(i)-T(i-1))/dx^2+(T(i+1)-T(i))/dx^2);
    end
    dTdt(1) = alpha*(-(T(1)-T1s)/dx^2+(T(1+1)-T(1))/dx^2) %boardernode 1
    dTdt(n) = alpha*(-(T(n)-T(n-1))/dx^2+(T2s-T(n))/dx^2) %boardernode n
    T = T+dTdt*dt;

    figure(1)
    plot(x,T, 'Linewidth', 3)
    axis ([0 L -10 50])
    title('50 year heat dissipation, average temp storage = 10 (\circC)')
    xlabel('Distance (m)')
    ylabel('Tempreature (\circC)')

end
```

Norges miljø- og biovitenskapelige universitet
Noregs miljø- og biovitskapelege universitet
Norwegian University of Life Sciences

Postboks 5003
NO-1432 Ås
Norway